THE APPLICATIONS OF THE GI METHOD TO INCORPORATION OF MANY BODY EFFECTS IN METALS; THE BAND STRUCTURE AND RESOLUTION OF SEVERAL ANOMALOUS PROPERTIES OF LITHIUM METAL

Thesis by

Patricia Marie O'Keefe

In Partial Fulfillment of the Requirements

For the Degree of

Doctor of Philosophy

California Institute of Technology

Pasadena, California

1971

(Submitted August 5, 1970)

ACKNOWLEDGMENTS

My graduate career has been deeply enriched by my association with Dr. William A. Goddard III and the members of his research group. Dr. Goddard's suggestion of this project and his helpful advice, encouragement, and patience have been of untold value throughout the course of this research. I wish to express my appreciation to members of his research group for many stimulating discussions and assistance in numerous problems. I am very grateful to the International Business Machines Corporation for financial support through an IBM Fellowship and to the U. S. Government for a National Defense Education Act Fellowship.

ABSTRACT

A new approach to studying the electronic energy band structure on solids has been developed and calculations are reported for lithium metal. This framework, the GI method, leads to one-electron orbitals which in general are singly occupied, have no orthogonality constraints, are no longer required to have the full symmetry of the system, and lead to a description which is valid at all internuclear distances. Yet they still retain an independent particle interpretation.

In the application to solids, similar considerations apply. It is found that, for the alkalis, the resulting one-electron conduction orbitals can be taken to be Bloch functions for a smaller symmetry group than the bcc symmetry of the lattice. Thus, the resulting Brillouin zone (BZ) is smaller than that in Hartree-Fock (HF), and gaps can occur at the Fermi surface where none were previously permitted. For lithium these gaps are found to be sufficiently small so that many of the expected properties are not significantly affected and the resulting Fermi surface is found to be quite spherical in good agreement with, for example, position annihilation results. However, for such properties as the high field transverse magnetoresistance, the soft X-ray emission spectrum, the optical absorption spectrum, the thermoelectric power, and the Hall coefficient, striking alterations in the description are obtained which lead to an appealing explanation of many of the anomalous properties of the alkalis, and seem to be in at least qualitative agreement with the experimental observations. The Mott paradox

is also resolved; the metal is found to change continuously from a conductor to an insulator as the system is dilated.

TABLE OF CONTENTS

I. A NEW APPROACH TO ENERGY BAND CALCULATIONS ON METALS AND APPLICATION TO LITHIUM METAL

A. INTRODUCTION

In the past, the Hartree-Fock (HF) method[1] has been the basic framework for calculations of electronic energy bands in metals. However, many of the experimental properties of even the simplest metals, the alkalis, appear to be inexplicable within the context of this model.

This research was undertaken in the wake of a major extension and generalization of the HF method as applied to atoms and molecules. The GI method[2,3] while quite similar in basic structure to the HF formalism makes use of a more general operator than the antisymmetrizer. The G_i^γ operator when applied to a product of one electron spacial and spin orbitals produces a wavefunction which simultaneously satisfies Pauli's Principle and is an eigenfunction of S^2 so that it automatically possesses the correct total spin symmetry. Since in HF this latter criterion has to be independently satisfied, somewhat artifactual constraints on the resulting wavefunction (and hence on the orbitals) are necessary. That is, the orbitals are

required to be doubly occupied. No such restriction is imposed in the GI method, and all orbitals are singly occupied. Variational optimization then always leads to a lower energy than that obtained in HF. Other differences also result in the form of the orbitals which are discussed in more detail in Parts II and III.

It became clear that the same orbital restrictions which caused difficulties in the description of atoms and molecules within the HF framework could also be the key to some of the conceptual problems in the application of the theory to the band structure of solids. It was realized that use of the G_i^γ operator for constructing many electron wavefunctions in a solid could in the case of body-centered cubic (bcc) structures lead to singly occupied orbitals which had a periodicity smaller than that of the lattice. This in turn would lead to qualitative changes in the band structure of the alkalis, since gaps could now occur where none were previously permitted. We will consider in detail the theory behind this approach and the results of calculations on lithium metal.

In Sections B and C we will see how the HF and GI methods differ. In Section D a method for replacing the core electrons by ab initio pseudopotentials is described. Section E deals with the application of the GI method to band calculations in solids and Section F treats the resulting GI band structure for lithium metal and the properties obtained from this description.

B. The Hartree-Fock Method

We seek to describe a good approximation to the solutions of the exact many electron Hamiltonian[4]

$$\mathcal{H} = \sum_{i=1}^{N} \left[-\tfrac{1}{2} \nabla_i^2 + V(\underset{\sim}{r}_i) \right] + \sum_{i>j}^{N} \frac{1}{r_{ij}} \tag{1}$$

where $V(\underset{\sim}{r}_i)$ is the electrostatic potential seen by electron i at $\underset{\sim}{r}$ due to all the nuclei. Since this Hamiltonian commutes with the total spin and total spin projection ($\hat{S}^2$ and $\hat{S}_z$), we can take our approximate solution also to be eigenfunctions of these spin operators. In addition our solution must satisfy the Pauli Exclusion Principle (that is, it must be antisymmetric under the exchange of two electrons). But these formalistic restrictions dictate no specific form to the wavefunction expansion. Physically we want an expansion which would lead to separation of the Hamiltonian into one particle type Hamiltonians for which the solutions are mathematically tractable and for which the eigenstates can be given an independent particle interpretation. With this set of criterion we are led, in the Hartree-Fock (HF) method, to the wavefunction expansion.

$$\psi_{HF}(1, 2, \cdots, N) = \sqrt{N!}\ \mathcal{A}\Phi\chi \tag{2}$$

where $\mathcal{A}$ is the antisymmetrizer, $\mathcal{A} = \frac{1}{N!} \sum \zeta_\tau \hat{\tau}$ (here the sum is over all N! permutations, and ζ_τ is the parity of the transposition). The spacial part of this function is taken to be a product of one particle functions:

$$\Phi(1, 2, \cdots, N) = \varphi_1(1)\,\varphi_2(2)\cdots\varphi_n(n)\,\varphi_1(n+1)\cdots\varphi_n(N) \qquad (3)$$

where the φ_i are a set of doubly occupied orthogonal functions, and the spin part is given by

$$\chi(1, 2, \cdots, N) = \alpha(1)\alpha(2)\cdots\alpha(n)\beta(n+1)\cdots\beta(N), \qquad (4)$$

a product of spin functions $\alpha(i)$, $\beta(i)$ such that $\hat{s}_z\,\alpha(i) = \frac{1}{2}\,\alpha(i)$ and $\hat{s}_z\,\beta(i) = -\frac{1}{2}\,\beta(i)$. The orbitals ϕ in (3) are then optimized by applying the variation principle, that is by requiring that $E = \langle\psi_{HF}|\mathcal{H}|\psi_{HF}\rangle / \langle\psi_{HF}|\psi_{HF}\rangle$ be stationary under first order changes in the orbitals (with the restriction that the orbitals remain orthonormal). This leads to a set of simultaneous equations for the one-electron orbitals

$$H^{HF}\,\varphi_i = \mathcal{E}_i\,\varphi_i, \quad i = 1, N \qquad (5)$$

where H^{HF} is a nonlocal one-electron operator involving the solutions to (1). It is this result which leads to an independent particle interpretation for the φ_i's since H^{HF} is composed of all one-electron interactions for any electron i and the best average of the field due to the rest of the electrons in the system. Such a one particle description is crucial not only to a meaningful description of atomic and molecular properties but also to our understanding of metals in terms of energy bands, Fermi surfaces, and electronic properties.

However this approach has several attendant difficulties. (These are considered at greater length in Part III.) We know that

for the HF wavefunction to have the correct spin symmetry the orbitals must be doubly occupied. But for say, a diatomic molecule, as the nuclei are pulled apart the bonding orbital must remain doubly occupied, and the wavefunction cannot describe the dissociated atoms in their ground state. This spurious behavior also causes difficulties in calculations on solids, since such properties as the cohesive energy depend on the difference in energy between the equilibrium lattice configuration and the dissociation limit (which is incorrectly described).

Another problem in treating solids is that the conduction orbitals must have nodes in the vicinity of each lattice site, in order that they be orthogonal to the core orbitals. Since the core electrons are tightly bound, it would be desirable to replace them with an effective field, but the nodes in the conduction orbitals mean that the resulting potential must have singularities at these points if the lowest solutions are to be the conduction orbitals. With these restrictions, there seems to be no way to obtain unique local potentials to describe the core interaction.

Finally HF orbitals must be symmetry functions for the full symmetric group of the system. This is true for the core orbitals as well as the conduction orbitals in a metal. Thus, one can never obtain localized orbitals as a solution to the HF equations. A transformation to more localized orbitals, e. g., Wannier functions, can be made, but these resulting functions are not solutions of the original one-electron Hamiltonians and hence do not lead to an independent particle interpretation.

We will now discuss a generalization of the HF method and see how these difficulties can be overcome.

C. THE GI METHOD

It is clear that the major difficulties encountered in the HF approach result from the use of a single Slater determinant which imposes unnecessarily stringent restrictions on the one-electron orbitals. It has been shown that it is possible to construct a more general operator, the Group Operator,[2] G_i^γ, which when operated on any many-electron wavefunction both guarantees that Pauli's principle is satisfied and that the resulting wavefunction is an eigenstate of the total spin operator. The operator is mathematically tractable in that it utilizes Wigner projection operators constructed from Young's orthogonal representation[5] for the symmetric group $\mathcal{S}_N$. The spin coupling is then explicitly demonstrated in terms of Young's tableaux.[5] The superscript γ is determined by the total spin projection $\hat{S}$ and implies a specific Young shape of one or two columns and i represents one of the several possible independent spin coupling schemes (corresponding to a standard tableau or a particular way of coupling the individual electron spins) for a given choice of $\hat{S}$ and $\hat{M}_S$. In this representation i can assume any integer value from 1 to f^γ designating which of the f^γ standard spin functions (or tableau) is being considered. The operator is then defined as

$$G_i^\gamma \equiv \sum_{r=1}^{f^\gamma} \zeta_{\sigma_{ir}} O_{ri}^\gamma \omega_{\overline{ri}}^{\overline{r}} \tag{6}$$

where O_{ri}^γ is a specific linear combination of permutations of the electronic spacial coordinates,

$$O_{ri}^\gamma = \frac{f^\gamma}{N!} \sum_{\tau \in \mathcal{S}_N} U_{ri}^\gamma(\tau)\tau, \tag{7}$$

$\underset{\sim}{U}^\gamma(\tau)$ are matrices for the γ irreducible representation of $\mathcal{S}_N$. $\omega_{\overline{ri}}^{\overline{\gamma}}$ is a corresponding sum operating on the spin coordinates, and $\zeta_{\sigma_{ir}}$ is the parity of the permutation σ_{ir}.

Rather than going into the properties of these operators and the resulting general form of the Hamiltonian equations (which are thoroughly described elsewhere), we will consider some general features of the method.

In practice, although the actual equations are more complicated than those encountered in HF, the method of solution is quite similar. Since the Hamiltonian commutes with all spin functions, the total energy expression reduces to

$$E = \frac{\langle G_i^\gamma \Phi\chi | \mathcal{H} | G_i^\gamma \Phi\chi \rangle}{\langle G_i^\gamma \Phi\chi | G_i^\gamma \Phi\chi \rangle} = \frac{\langle \Phi | \mathcal{H} | O_{ii} \Phi \rangle}{\langle \Phi | O_{ii} \Phi \rangle} \tag{8}$$

where all the spin terms have been eliminated and only the spacial part of the wavefunction need be considered. The energy is

required to be stationary under any first order variation in the orbitals, from which a set of N simultaneous equations is obtained (for an N electron system) of the form

$$h_j \phi_j = \mathcal{E}_j \phi_j \tag{9}$$

where

$$h_j = -\tfrac{1}{2} \nabla^2 + U_j. \tag{10}$$

Here U_j is a complicated nonlocal potential[3] containing the nuclear electrostatic potential and the average potential due to the remaining N-1 electrons. The orbital ϕ_j can be interpreted as the eigenstate of an electron moving in the average field due to the other N-1 electrons, therefore yielding an independent particle interpretation. It is this feature which lends credence and utility to this method and justifies the additional labor required in these calculations.

We have said that the G_i^γ operator yields functions which have the correct spin symmetry. It is then a restriction to take the orbitals to be doubly occupied, and variational optimization always leads to singly occupied orbitals. Since these orbitals satisfy different one-electron Hamiltonians (10), they need not be symmetry functions for the full symmetric group of the system, and in general have a reduced symmetry. Also this means that there are no orthogonality constraints between orbitals which satisfy different one-particle Hamiltonians. We will see in the next section how these new nodeless orbitals can be used to obtain unique

ab initio pseudopotentials to replace core electrons.

Of the various independent ways of coupling the individual spins, two are found to be particularly important.[6] i = 1, generally referred to as the G1 method, corresponds to strong pair-wise coupling of the spins, and is equivalent to a generalized valence bond description.[7] The other type of coupling which is thought to be important for the conduction electrons in metals is i = f (the GF method).[3] Here one set of electrons is coupled to maximum spin, then the remaining set is coupled to maximum spin and these sets are coupled together to minimum spin. These two means of coupling spins are found to be the dominant ones in describing atoms and molecules, and as we will see in Section E, must both be considered when treating metals.

D. PSEUDOPOTENTIAL FORMALISM

Recently there has been broad progress in the replacement of atomic cores by pseudopotentials in describing molecules and solids. In particular numerous approaches to describing such effective interactions have evolved, resulting in varying degrees of success in describing the electronic structure and properties of systems.

The general theory encompasses methods of arriving at a pseudo-Schoedinger equation

$$-\tfrac{1}{2}\nabla^2\varphi + V^{ps}(r)\varphi = \mathcal{E}\varphi \qquad (11)$$

replacing the nonlocal potential by a weak local term resulting in a description valid within the nearly free electron (nfe) model in a solid. Thus, within the HF framework V^{ps} incorporates terms[8] which effectively orthogonalize the valence orbitals to the core, therefore eliminating the oscillatory character of the HF valence orbital in that region. In this approach the effective potential is nonlocal, nonunique, and not necessarily Hermitian.[9a] Alternatively, use can be made of atomic spectroscopic levels[9b] to define effective potentials useful in a solid. However, the formulation of these potentials is arbitrary with choices dictated for optimum applicability to a specific property description.

However, it has been shown that there is a simpler, nonarbitrary, and ab initio method for obtaining such pseudopotentials.[10] The G1 method characteristically yields nodeless atomic valence orbitals which retain an independent particle interpretation. Thus it is possible to use this self-consistent orbital directly, together with its orbital energy to solve for the effective local potential in which this electron moves, simply by replacing the nonlocal $U_i(r)$ in (10) by

$$V^{eff}(r) = \frac{(\mathcal{E} + \frac{1}{2}\nabla^2)\,\phi}{\phi} \quad . \tag{12}$$

There is no problem with singularities since the orbital is nodeless. This pseudopotential $V^{eff}(r)$ is Hermitian, local, weak, derivable from ab initio calculations, and in turn yields the same eigenstates as does the correct nonlocal potential.

Now we know that the Li core orbitals for LiH and Li_2 are essentially unchanged from the atom.[11] The same has been found true for boron and carbon compounds and we would hope that in general the tight inner electron orbitals would be little changed by valence electron bonding. A test of the validity of using such pseudopotentials for replacing the core electrons has been applied to the excited states of Li atom, to LiH, Li_2[11] and BH,[12] as well as to the ground and excited states of LiH[13] and C_2H_4[14] using the potentials derived from atomic G1 calculations and the results were compared to full ab initio calculations on these systems. For Li the effective potentials obtained for the atomic 2^2S and 2^2P states were found to be quite different, while the 2^2P, 3^2D and subsequent states yielded quite comparable potentials. These are shown in Fig. 1.

Of course one criterion which must be satisfied for an effective potential to be useful is that it must be able to reproduce not only the ground state but also the excited states of the system. When the $V_{2s}^{eff}(r)$ potential was used to calculate the ns excited states of the Li atom, the resulting energy levels were found to be in good agreement with experiment.[11] However, this same potential gave very poor results for np and nd states.[11] Nevertheless, when the potential derived from the 2^2P state was used, the excited np states were well described.[11] The same was true for the nd state using the V_{3d}^{eff} potential.[11]

These potentials were then used for replacing the Li cores in molecules and it was found that use of an angular momentum

dependent pseudopotential $V^{eff}(r) = V_\ell(r)|\ell\rangle\langle\ell|$, where V_ℓ for $\ell \geq 1$ was replaced by V_{2p}, quite accurately reproduced the valence eigenstates of LiH and Li_2.[11] In addition such properties as the dipole moments and electric field gradients calculated using these eigenfunctions were in good agreement with those from ab initio calculations.[11]

One further feature of these pseudopotentials which is crucial for any application to solids concerns the behavior of excited states. To this end the excited states of the LiH molecule were calculated using both the two-electron pseudopotential description and the full four electrons. For the lowest excited states of $^1\Sigma^+$, $^3\Sigma$, $^1\Pi$, and $^3\Pi$ symmetry, the energies obtained from the two methods were in excellent agreement.[12]

Thus, such effective potentials might be used to replace the field due to the core electrons in band structure calculations. Lastly to establish their applicability to metals and to make a direct comparison of this method with past approaches based on OPW, quantum defect, and other methods, HF calculations on the band structure of body centered cubic (bcc) lithium metal were carried out.[15] Simple plane wave expansions of the conduction orbitals were found to converge rapidly and a band structure quite similar to those derived from other well-accepted HF methods was obtained. Hence the use of such angular-momentum-dependent Hermitian pseudopotentials determined from ab initio atomic calculations would seem to be well justified for large molecules and solids.

E. APPLICATION OF THE GI METHOD TO METALS

We wish to construct a many-electron wavefunction satisfying the total Hamiltonian for the metal from a product of one electron orbitals within the GI framework. Based on the optimum spin coupling appropriate to various atomic and molecular systems, we expect[16] that the important coupling for the core electrons (which are tightly bound to their respective nuclei and are little affected by the conduction electrons) is G1 since this corresponds to a strong valence bond type pair bond. On the other hand, the conduction electrons are expected to be delocalized throughout the lattice with a minimum of pair-wise coupling and hence should be GF coupled (strong pair-wise coupling would result in a highly correlated solid). Then the tableau[5] for this system is as given in Fig. 2 where electrons m+1 through m+n are coupled to give maximum spin, and m+n+1 through m+2n likewise, and the resultant pair is coupled to give a total singlet state. The core electrons are of course all coupled in pairs to give a singlet state. This description then yields a total singlet wavefunction. Since the core orbitals are tight, localized, atomic-like states, far removed in energy from the conduction states, and should be little changed in going from an atom to a molecule to a solid, it is no restriction to replace those electrons with a nonlocal potential operator representing the average field seen by an electron due to these electrons centered at each of the nuclei. Since the G1 valence orbital for the lowest state of any symmetry in the atom is nodeless, except at r=o for $\ell \neq o$, we showed in Section D that the use of an

effective potential derived from this orbital could justifiably be used to replace the nonlocal potential terms representing the interaction with the core, not only to obtain eigenfunctions equivalent to those obtained from ab initio calculations on the atom but also for bigger molecular system and solids. Hence we assume that we can replace these core electrons by an effective potential and consider only the conduction electrons. Doing this we obtain for our many-electron wavefunction:

$$\psi(r) = G_f^{\gamma} [\varphi^a_{k_1}(r)\ \varphi^a_{k_2}(r)\cdots\phi^a_{k_n}(r)\ \varphi^b_{k_{n+1}}(r)\ \phi^b_{k_{n+2}}(r)$$

$$\cdots\varphi^b_{k_{2n}}(r)\alpha_1\alpha_2\cdots\alpha_n\beta_{n+1}\beta_{n+2}\cdots\beta_{2n}] \qquad (13)$$

where 2n is the total number of conduction electrons and k_i is the wave vector of the one electron states. The many electron Hamiltonian in the Born Oppenheimer approximation can be written as

$$\mathcal{H} = \sum_i [-\tfrac{1}{2}\nabla_i^2 + U_i(\underset{\sim}{r}) + \sum_{j<i}\frac{1}{r_{ij}}] \qquad (14)$$

where the sum is over all electrons, $U_i(\underset{\sim}{r})$ is the nonlocal potential due to the ion cores, and the last term is the electron-electron interaction energy.

Variational optimization of the GF orbitals leads to a pair of one particle Hamiltonians, one for each of the two sets of orbitals associated with the two columns (disregarding the core electrons) in the tableau in Fig. 2. We will refer to the set associated with the left column as the a orbitals and that with the right the b

orbitals. The one-particle Hamiltonian operator for which this set of a orbitals is a solution is

$$h_a = -\tfrac{1}{2}\nabla^2 + U_a(\underset{\sim}{r}). \tag{15a}$$

Here $U_a(\underset{\sim}{r})$ is a nonlocal potential which includes the interaction of an a electron i with all the remaining conduction electrons and the cores. An analogous Hamiltonian for the b orbitals is given by

$$h_b = -\tfrac{1}{2}\nabla^2 + U_b(\underset{\sim}{r}). \tag{15b}$$

Since all of the a electrons are solutions of this Hermitian operator h_a, it is no restriction to take these orbitals to be orthogonal among themselves and similarly for the b orbitals.

It is appropriate at this point to discuss the symmetry restrictions which apply to these orbitals. In H_2 and other homonuclear diatomics,[3] square H_4,[16] and hexagonal H_6[6] the optimum orbitals are found to have a symmetry lower than that of the total system. Even so the total many-electron wavefunction has the correct spatial symmetry. Since these allowed reductions in symmetry lead to more stable molecular descriptions, it is necessary to investigate and classify the permissable symmetry properties of orbitals for a bcc metal in a framework in which there are two sets of linearly independent functions instead of one doubly occupied set (as in HF).

One normally assumes that the appropriate basis vectors must be Bloch functions[17] for the symmetry group of the system. However, proof of Bloch's theorem[18] for a set of states explicitly assumes that the states spanning the space are normalized and orthogonal, and hence that the matrix representations of the lattice

translations both commute and are unitary. Under these conditions a unitary transformation of these matrices can be found which diagonalizes them and hence a translation cannot mix these states. This clearly holds in the case of HF states where the orbitals are doubly occupied and orthogonal.

However, we have seen that while each of our sets of orbitals, $\underline{a}$ and $\underline{b}$, is comprised of orthogonal vectors, the sets need not themselves be necessarily the same nor orthogonal. There is a theorem in group theory[19] which states that given a vector space Ψ which is invariant under a group $\mathscr{S}_N$ of transformations then the vector space Ψ must be either irreducible and contain no invariant subspace or it must be reducible into a sum of orthogonal invariant subspaces.

The first case corresponds to the condition that all the vectors in Ψ, i.e., all $|\phi\rangle$, must be invariant under the complete set of translations generating the lattice (by which we say they must be symmetry functions). In this case, all of these $|\phi\rangle$ can be taken to be doubly occupied and orthogonal and we return to the HF description, or the $|\phi\rangle$ must all be singly occupied and orthogonal which would lead to a very high excited state description.

However, we have seen that in the GF framework, the set of $|\phi_a\rangle$ can be taken to be orthogonal and also the set of $|\phi_b\rangle$ but no further condition is imposed on these vectors or on the relation of $|\phi_a\rangle$ to $|\phi_b\rangle$. We will consider for example the bcc lattice. It now remains to be shown that the second condition of

the theorem applies, namely that the space group of the bcc lattice is reducible into a sum of two orthogonal subspaces. If this can be shown we need merely take the set $|\phi_a\rangle$ to be basis vectors spanning one of these subspaces and $|\phi_b\rangle$ as basis vectors for the other, provided the operators h_a and h_b commute with the elements of these subgroups, and the requisite symmetry properties are obtained. In fact the space group for the bcc lattice clearly contains the simple cubic translation group as a subgroup. That is, the lattice is reducible into two interpenetrating simple cubic sublattices. Hence, if we consider some lattice point in the crystal, the eight points at the corners of the cube surrounding it belong to the other sublattice.

Now we know that we can take our set $|\phi_a\rangle$ to transform according to the irreducible representations for the simple cubic (sc) subgroup since h_a has less than the total symmetry and commutes with the sc subgroup. Then for any simple cubic (sc) translation $\hat{R}_{sc}$,

$$\hat{R}_{sc}\,\phi_{ka}(\underset{\sim}{r}) = \phi_{ka}(\underset{\sim}{r}+\underset{\sim}{R}_{sc}) = e^{i\underset{\sim}{k}\cdot\underset{\sim}{R}}\,\phi_{ka}(\underset{\sim}{r}) \tag{16}$$

so that Bloch's theorem applies to this vector subspace. Thus this vector space $|\phi_a\rangle$ is invariant under simple cubic translations. Consider now a translation from an $\underline{a}$ site to any $\underline{b}$ site, $\hat{R}_{ab}$, which does not commute with h_a. In order that the many electron wavefunction have the correct total symmetry, it must be true that $\hat{R}_{ab}\phi_{\underset{\sim}{k}a} = \sum_{k'} c_{k'}\,\phi_{\underset{\sim}{k}'b}$, $\hat{R}_{ab}\phi_{\underset{\sim}{k}b} = \sum_{\underset{\sim}{k}'} c_{\underset{\sim}{k}'}\,\phi_{\underset{\sim}{k}'a}$. But we can only mix functions of the same symmetry (i. e., $\underset{\sim}{k}$-vector) and hence

$$\hat{R}_{ab}\,\phi_{\underset{\sim}{k}a}(\underset{\sim}{r}) = \phi_{\underset{\sim}{k}a}(\underset{\sim}{r}+\underset{\sim}{R}_{ab}) = e^{i\underset{\sim}{k}\cdot\underset{\sim}{R}_{ab}}\,\phi_{\underset{\sim}{k}b}(\underset{\sim}{r})\ . \tag{17}$$

We see that this operation takes an a orbital into a phase factor times the b orbital for the same $\underset{\sim}{k}$-vector (and so the many-electron wavefunction is still a symmetry function for the full symmetric group of the system). Therefore these two sets of orbitals are equivalent, but spacially removed from each other by the set of translations relating these simple cubic substructures. This means that the eigenvalue solutions of these equations 15(a) and (b) will be the same and it suffices to consider only one of these sets.

In this description since we need to consider only the a orbitals which form symmetry orbitals for the simple cubic group, then the primitive unit cell is a simple cube of twice the volume of the corresponding HF cell. Thus the BZ is also a simple cube inscribed within the HF dodecahedral BZ and occupying half its volume. If the system we are considering has one electron per lattice site (as in the alkalis), the Fermi surface must occupy the same volume as this cubic BZ and hence must intersect it.

We have seen that the potential due to the core electrons can rigorously be replaced by a weak effective potential obtained from ab initio calculations on the atom. Because this potential is weak and the orbitals are nodeless in the core region, expanding the orbitals in simple plane waves should lead to rapid convergence. We take

$$\phi^{a}_{\underset{\sim}{k}}(\underset{\sim}{r}) = \sum_{j} c_j(\underset{\sim}{k})\, e^{i(\underset{\sim}{k} + \underset{\sim}{K}_j)\cdot \underset{\sim}{r}} \tag{18}$$

where $\phi^{a}_{\underset{\sim}{k}}$ is a Bloch function for the simple cubic (sc) sublattice of a sites. Thus the $\underset{\sim}{K}_j$ are reciprocal lattice vectors spanning the cubic substructure and $\underset{\sim}{k}$ is the wave vector. We want to solve a Schroedinger equation in which the one-electron Hamiltonian is

$$h^a = -\tfrac{1}{2}\nabla^2 + \sum_i V_a^{eff}(|\underset{\sim}{r} - \underset{\sim}{R}_i|) \tag{19}$$

Here $\underset{\sim}{R}_i$ are the a-site ion center coordinates and we consider here only a-site potentials. Then (18) and (19) give

$$h^a \phi_k^a(r) = -\tfrac{1}{2}\nabla^2 \sum_j c_j(\underset{\sim}{k})\, e^{i(\underset{\sim}{k}+\underset{\sim}{K}_j)\cdot \underset{\sim}{r}}$$

$$+ \sum_i V_a^{eff}(|\underset{\sim}{r} - \underset{\sim}{R}_i|) \sum_j c_j(\underset{\sim}{k})\, e^{i(\underset{\sim}{k}+\underset{\sim}{K}_j)\cdot \underset{\sim}{r}} . \tag{20}$$

Now the Hamiltonian matrix elements are obtained by multiplying through with $e^{-i(\underset{\sim}{k}+\underset{\sim}{K}_m)\cdot \underset{\sim}{R}}$ and integrating over the crystal,

$$\langle \underset{\sim}{k} + \underset{\sim}{K}_m | h^a | \phi_k^a \rangle = N\Omega_0\, \delta_{jm}\, c_j(\underset{\sim}{k}) \frac{|\underset{\sim}{k}+\underset{\sim}{K}_j|^2}{2}$$

$$+ \sum_i e^{i(\underset{\sim}{K}_j - \underset{\sim}{K}_m)\cdot \underset{\sim}{R}_i} \sum_j c_j(\underset{\sim}{k}) \times$$

$$\langle \underset{\sim}{k} + \underset{\sim}{K}_m | V_a^{eff}(r) | \underset{\sim}{k} + \underset{\sim}{K}_j \rangle_{crystal} \tag{21}$$

where Ω_0 is the volume of a sc unit cell and N is the number of sc cells. Note that the structure factor $\sum_i e^{i(\underset{\sim}{K}_j - \underset{\sim}{K}_m)\cdot \underset{\sim}{R}_i}$ sums to just N since each element in the sum in 1. We now make the Wigner Seitz approximation to account for the self-term due to the a-orbital we are considering and also to correct for exchange and correlation. (We discuss this approximation in more detail in Appendix 2.) Thus the potential is taken to extend to the simple cubic cell boundary and is zero outside. Hence the integral reduces to one over the sc cell and we obtain

$$\sum_j \left[\frac{c_j(\underset{\sim}{k}) - \epsilon(\underset{\sim}{k})}{2} (\underset{\sim}{k} + \underset{\sim}{K}_j)^2 \delta_{jm} + \frac{c_j(\underset{\sim}{k})}{\Omega_o} V_a(\underset{\sim}{K}_m \underset{\sim}{K}_j \underset{\sim}{k}) \right] = 0 \qquad (22)$$

where

$$V_a(\underset{\sim}{K}_m \underset{\sim}{K}_j \underset{\sim}{k}) = \langle \underset{\sim}{k} + \underset{\sim}{K}_m | V_a^{eff} | \underset{\sim}{k} + \underset{\sim}{K}_j \rangle_{\Omega_o} . \qquad (23)$$

Now we will consider the form for V_a^{eff}. We saw in section D that V_a^{eff} can be written

$$V_a^{eff}(r) = \sum_\ell V_\ell^a(r) |\ell\rangle \langle\ell|$$

where $V_\ell^a(r)$ is the effective ion core potential for the symmetry state ℓ of the atom and $|\ell\rangle\langle\ell|$ is the angular momentum projection operator. In lithium we saw that we can take $V_p(r)$ to be the effective potential for all ℓ, $\ell \geq 1$ so that

$$\sum_\ell V_\ell^a(r) |\ell\rangle \langle\ell| = V_s(r) |s\rangle \langle s| + V_p(r) \sum_{\ell \neq 0} |\ell\rangle \langle\ell| \qquad (24)$$

which, using the closure relation, becomes

$$\sum_\ell V_\ell^a(r) |\ell\rangle \langle\ell| = V_p(r) + [V_s(r) - V_p(r)] |s\rangle \langle s| . \qquad (25)$$

Thus

$$V_a(\underset{\sim}{K}_m \underset{\sim}{K}_j \underset{\sim}{k}) = V_p(\underset{\sim}{K}_j - \underset{\sim}{K}_m) +$$

$$\int_{\Omega_o} e^{-i(\underset{\sim}{k} + \underset{\sim}{K}_m) \cdot \underset{\sim}{r}} [V_s(r) - V_p(r)] \frac{\sin(|\underset{\sim}{k} + \underset{\sim}{K}_j| r)}{|\underset{\sim}{k} + \underset{\sim}{K}_j| r} d\underset{\sim}{r} \qquad (26)$$

where

$$V_p(\underset{\sim}{K}_j - \underset{\sim}{K}_m) = \int_{\Omega_0} V_p(r)\, e^{i(\underset{\sim}{K}_j - \underset{\sim}{K}_m)\cdot \underset{\sim}{r}}\, d\underset{\sim}{r} \ . \tag{27}$$

We note here that all integrations over surfaces in these equations are carried out exactly over the cubic cell. We tested the approximation of replacing the integrations over a simple cube or a bcc Wigner Seitz cell by an equivalent volume sphere. Using the spherical approximation we found that the Fourier components for the correct surface was a smooth function of $\underset{\sim}{k}$ whereas the spherical approximation led to spurious oscillations in the components. Comparisons of Fourier coefficients with empirically derived form factors and a more complete discussion of this behavior are given in Appendix 1.

Thus, inserting (26) into (22) we have only to solve the matrix equation (22) as a function of $\underset{\sim}{k}$ to obtain the band structure.

However, for treating high symmetry points in the BZ, that is, points which transform predominantly as some pure symmetry

type, or equivalently whose cubic harmonic expansion is dominated by the first spherical harmonic, we have found that by using the local potential appropriate to that symmetry type and similarly symmetrizing the orbital expansion (thus treating the potential as purely local), yields eigenvalues generally well within 1% of the correct value, even for high lying states. In Table 3 in section F (1) we will see that the error involved in this approximation is small. This amounts to assuming that a state such as M_1 mixes in little d character and is predominantly s-like. In this case the appropriate matrix equation is

$$\sum_j \left[\frac{c_j(\underset{\sim}{k}) - \mathcal{E}(\underset{\sim}{k})}{2} (\underset{\sim}{k} + \underset{\sim}{K}_j)^2 \delta_{jm} + \frac{c_j(\underset{\sim}{k})}{\Omega_0} V_\ell (\underset{\sim}{K}_j - \underset{\sim}{K}_m) \right] = 0. \qquad (28)$$

Use of this expression facilitates the calculation since the potential interaction is no longer $\underset{\sim}{k}$-dependent and we have found this form convenient for calculating the symmetry points over a wide range of lattice constants. This form is also convenient for another extension which we will now describe.

Expressions (22) and (28) treat the conduction electrons as being distributed throughout the lattice in such a way that if an electron is in the vicinity of a given a site, it is unlikely that another a site electron will be in the vicinity of that cell, that is, it is screened from other a sites. However, as yet we have not included any interaction with b site electrons. Since the GI sc

primitive cell contains on the average two electrons (due to the presence of these b sites at its corners) we must modify our expression to treat the interaction with these b sites. In fact we wish to include the interaction with all other b sites throughout the lattice. The question arises now of what potential interaction is appropriate. GI calculations on the Li^- ion lead to a stable Li^-_{2s} singlet,[20a] but the 2p-state is not stable. However, the 2s stability is primarily due to the strong two-electron exchange energy.[20b] In the metal the situation is significantly different from the atomic case since there is no longer the pair-wise coupling characteristic of Li^- ion[20a]. In fact for an N-electron system this exchange interaction is diminished by a factor of 1/N which goes to zero as $N \to \infty$ and all that remains is the Li^- Coulomb interaction. The effective potential for this interaction is readily obtained by evaluating the self-Coulomb term due to the atomic valence orbital and combining it with the appropriate V_ℓ^{eff} for the case potential to obtain the corresponding V_ℓ^- effective potential. That is

$$V_\ell^-(\underset{\sim}{r}) = \langle \phi_{2s}^{atom} | \frac{1}{r_{12}} | \phi_{2s}^{atom} \rangle + V_\ell^{eff}(\underset{\sim}{r}) \ . \qquad (29)$$

We can now evaluate the Fourier coefficients in a Fourier expansion of (29) and include these with appropriate phase factors in (28). (For a more complete discussion of this point see Appendix 2.) However, these phase factors alter the symmetry of the transformation properties of the orbital at the b sites relative to that appropriate for a given symmetry state at the a site. That is, an orbital which transforms according to some irreducible representation at an a site in a simple cubic lattice when translated by a

vector other than a lattice translation vector can have a different symmetry with respect to that site. Thus incorporating the required phase factors equation (28) becomes

$$\sum_j \left\{ \left[-\frac{[c_j(\underset{\sim}{k}) - \epsilon(\underset{\sim}{k})]}{2} (\underset{\sim}{k} + \underset{\sim}{K}_j)^2 \delta_{jm} \right. \right.$$

$$+ \frac{c_j(\underset{\sim}{k})}{\Omega_o} \left[V_\ell(\underset{\sim}{K}_j - \underset{\sim}{K}_m) \right.$$

$$\left. \left. + e^{i(\underset{\sim}{K}_j - \underset{\sim}{K}_m)\cdot \underset{\sim}{R}_i} V_{\ell'-}(\underset{\sim}{K}_j - \underset{\sim}{K}_m) \right] \right\} = 0 \qquad (30)$$

where ℓ' is determined by the symmetry at $\underline{a}$ and the phase factors $e^{i(\underset{\sim}{K}_j - \underset{\sim}{K}_m)\cdot \underset{\sim}{R}_i}$, $\underset{\sim}{R}_i$ is a translation vector between an $\underline{a}$ and a $\underline{b}$ site, e.g., $(\frac{a}{2}, \frac{a}{2}, \frac{a}{2})$ and $V_{\ell'-}(\underset{\sim}{K})$ which will be defined below is the Fourier transform of the potential. At this point we want to reconsider the effective field at the $\underline{b}$ sites. Thus far we have found the correct bare potential to represent such an effective interaction and we say that all $\underline{b}$ sites are included in this term, since we will integrate over all space and thus effectively treat these potentials as overlapping and having an infinite extent. In fact the potential goes to zero before 9 a_o so that the furthest sites which could contribute are one unit cell removed from the nearest $\underline{b}$ neighbors. Now we know that these electrons are also screened by the conduction electrons. We show in Appendix 2 that the Wigner Seitz approximation is inappropriate here and that a reasonable screening

correction is the Bardeen screening factor. In the form of equation (30) which is applicable to high symmetry states such an expression is readily incorporated. Thus, we define

$$V_{\ell'-}(\underset{\sim}{K}) = \int_{\substack{\text{all}\\ \text{space}}} \bar{V}_{\ell'}(r)\, e^{i\underset{\sim}{K}\cdot\underset{\sim}{r}}\, d\underset{\sim}{r}/\epsilon(|\underset{\sim}{K}|) \tag{31}$$

which is a special case of the more general expression derived in Appendix 2. Here,

$$\epsilon(|K|) = 1 + \left(\frac{1-\eta^2}{2\eta}\ln\left|\frac{1+\eta}{1-\eta}\right| + 1\right)/2\pi k_f \eta^2, \tag{32}$$

$$\eta = \frac{|\underset{\sim}{K}|}{2k_f} \text{ and } k_f = \left(\tfrac{3}{4}\pi\right)^{\frac{1}{3}}\left(\frac{2\pi}{a}\right),\ a = \text{lattice const.}$$

Inserting this definition for $V_{\ell'-}(\underset{\sim}{K})$ into (30) then provides us with an expression for calculating the band structure of the alkalis within the GI framework.

F. RESULTS AND DISCUSSION

1. BAND STRUCTURE OF LITHIUM METAL

The formalism described in the last section has been applied to bcc lithium metal. All calculations were carried out for an equilibrium lattice constant of 6.575 a_0.[21a] The Li_{2s} and Li_{2p} pseudopotentials in Fig. 1 were used for the a site interaction. In

Appendix 1 we discuss the method used for evaluating the Fourier components of these effective potentials out to the correct cell boundary. The resulting Fourier coefficients of these potentials for all simple cubic (sc) lattice vectors up to a (4, 1, 1) are reported in Table 1. Fig. 3 shows the band structure resulting from using these potentials only as per (22) thus neglecting electron interactions with $\underline{b}$ sites. For this case a set of 57 reciprocal lattice vectors up to $|\underset{\sim}{K}| = 2\pi/a(2, 0, 0)$ was used in the wavefunction expansion (18) and points throughout the zone in increments of $\Delta k = 0.1\ (2\pi/a)$ were calculated. In this figure are shown the energies along the principal symmetry directions where the high symmetry points for a sc lattice are $\Gamma, X, M,$ and R.[21b] For reference, Table 2 gives the transformation properties of states at these points in terms of spherical harmonics.

Then the curves in Fig. 3 are based on energies at the high symmetry points and four intermediate equidistant points along each axis. The lines shown have been interpolated through this energy grid. The distance between the vertical lines representing high symmetry points are proportional to the k-space separations of these points. The energies for the symmetry points corresponding to those in Fig. 3 are reported in Column 2 of Table 3.

For comparison, the calculated HF band structure[15, 22] is given in Fig. 4. Here the same pseudopotential expression as above was used but the respective Fourier components[15] differ because in HF the cell over which it extends is the bcc cell of half the volume appropriate to the GI case. Also only high

symmetry points were evaluated here and the lines connecting these points are only approximate. The plane wave expansion for this HF structure contained bcc reciprocal lattice vectors up to $|\underset{\sim}{K}| = 2\pi/a(2,1,1)$ (a set of 43 vectors).

The most striking difference between these two structures is that, whereas in HF the Fermi surface is well inside the first BZ, in the GI band structure the Fermi surface goes beyond the point X on the zone boundary. This point X splits into two states X_1 and X_4' separated by a small gap, 0.016 a.u. (0.435 eV). Along the symmetry direction from X to M this splitting decreases to zero, so that the separation of the bands at the Fermi surface is $\sim \frac{1}{4}$ of that at the X point. Similar behavior is observed along the X to R direction and the band gap at the Fermi surface in this direction is about the same.

Another interesting distinction between the HF and GI band structures is that at the N point in HF (corresponding in the sc structure to the M point) the lowest energy state is N_1' which is singly degenerate. In the GI band scheme, this state becomes M_5' which is doubly degenerate and the band is continuous.

In fact we have three states M resulting from a four-fold degenerate point in the sc free electron band scheme, whereas in HF there are only two singly degenerate N states. This comes about because in this sc structure the $H[2\pi/a(0,0,1)]$ point is mapped back into the Γ point to yield three states Γ_1, Γ_{15}, and Γ_{12} (corresponding to H_1, H_{15}, and H_{12}). The point about which it is reflected $[2\pi/a(0,0,\frac{1}{2})]$ generates the two X states. Hence the symmetry

lines which connected H to N here become Γ to M with the new states being similarly connected. One further interesting observation is that the M state (here M_3) which would in HF have connected to the first excited Γ state, in the GI scheme crosses the band which would have connected the H point to a high lying N state. Here this crossing is forbidden (since both Γ_{12} and M_3 have Σ_1 symmetry along the axis) and M_3 in fact connects with Γ_{12}. Similar behavior is noted along the R to Γaxis where the same considerations apply. Hence the strange turning over of some of the bands results from a crossing of bands which in HF could never have intersected. Thus, this additional X-symmetry point leads to a much more complex band structure than that encountered in HF.

Using the data available for the energies at a grid of points throughout the BZ, an approximate interpolation scheme was used to determine the Fermi level and the anisotropy of the Fermi surface. In fact it is found to be quite spherical ($\sim 5\%$ distortion) and the Fermi energy is determined to be at about 0.153 hartrees (~ 4.16 eV) above Γ_1. This calculation also indicates that the surface bulges out slightly in the M direction and is pulled inward along the [100] and [111] axes. The amount of distortion in the vicinity of the BZ intersection appears to be minimal, and the gap is found to be nearly isotropic.

Now we will consider how the inclusion of the b site potentials in the energy expression modifies this structure. The unscreened Li^- 2s and 2p Fourier coefficients are given in Table 1. These were derived from the coulombic Li^- potentials described in

Section E. Then using expression (30), energies for the high symmetry points were evaluated to yield the structure in Fig. 5. For these energies our basis set included all reciprocal lattice vectors up to $|\underset{\sim}{K}| = 2\pi/a(2,1,1)$, a set of 81 vectors. These energy values are tabulated in Column 1 of Table 3.

Comparison of Figs. 3 and 5, i. e., the band structures without and with the b site included, leads to a surprising observation. Generally the structure is little affected by including the b potentials except for minor shifts in some high lying states. This result facilitated inserting the lines connecting the states in Fig. 5 by reference to Fig. 3. However, the one major change which has occurred is that the X_4' state has been reflected above the X_1 state resulting in a gap which is nearly identical with that previously obtained with only a sites. Now the X_4' state lies nearest the Fermi level. This should result in a slightly more distorted Fermi surface than that discussed above, but in fact it still appears to be nearly isotropic although it has shifted down to $\sim$.15 hartrees (4.1 ev) above Γ_1. The energy gap at the Fermi surface should be little affected by this shift since the X point separation is essentially unchanged and the M_5' state to which they are connected has also undergone an insignificant shift. Based on the calculation throughout the zone as shown in Fig. 3, the band gap is estimated to be .005 hartree (.13 eV).

One further point about the Fermi surface determination should be made here. For the HF band scheme, the Fermi surface does not intersect the zone boundary so that the major distortions which occur should be along the principal symmetry directions, and it is only

necessary to calculate the energies at points along these axes to characterize the shape of the Fermi surface. Using the GI method, the first BZ occupies the same volume as the Fermi surface, and thus the Fermi surface extends well into the second zone. It is gratifying that the surface still appears to be nearly isotropic, but a calculation of the density of states is by no means as simple as in HF. Energy bands in the vicinity of the BZ intersection must approach normal to the boundary and even if this distortion of the bands occurs over only a small region in $\underset{\sim}{k}$-space, this behavior introduces singularities into the density expression, enormously complicating the calculation. In addition this means that the energy over a fine grid of points throughout the whole BZ must be evaluated, rendering the venture quite costly in terms of computer time. Estimates which have been made for the Fermi surface parameters were based on a hand interpolation of $E(\underset{\sim}{k})$ values in the vicinity of points of interest, since no density of states results are as yet available. Based on the calculated states nearest the botton of the band, we estimate an effective mass of 1.21 at $\underset{\sim}{k} = 0$.

We will now consider some of the physical properties of the alkalis and see what modifications in their interpretation result from this new band structure description.

2. OPTICAL ABSORPTION

In the HF description of the band structure of the alkalis, the

smallest interband transition which can occur is along the axis to the high symmetry BZ point N which is split into two states, N_1 and N_1'. Since the Fermi surface lies below this point, the gap from the surface to the vertical excited state along this direction is larger than the N_1-N_1' splitting, and is on the order of 1.2 ev for K, 2.0 for Na, and 3.6 for Li.[23] We saw that in the GI band scheme, a high symmetry point X occurs inside the Fermi surface and half way to the HF symmetry point H. In the GI band structure, the point H is reflected back into the Γ point. This X point splits into two states separated by a small gap which decreases to zero along the X to M and X to R directions on the BZ. Thus direct transitions down to very small energies can now occur where none were previously permitted, as illustrated in Fig. 6.

The optical absorption spectra of the alkalis have recently been the subject of some controversy. In 1963, Mayer and El Naby[24] reported a strong peak in the optical absorption of K centered at about 0.6 ev, well below the expected threshold of 1.2 ev, and in 1965 Mayer and Hietel[25] showed that a strong absorption peak occurred in Na at 1.6 ev, prior to the 2.1-2.5 ev threshold. This led to numerous speculations that the existence of such peaks indicated the presence of a collective resonance state,[26] spin density waves,[27] strong phonon interactions,[28] and exciton states.[29] More recently Smith[30] has reported optical spectra for Na and K in which he finds no structure below the normal interband transition threshold. However he does find the absorption in the upper Drude region to be much larger than expected (starting at 0.5 eV for K). He suggests that this may be

due to relaxation time anisotropy.

As a result of the direct transitions now allowed in the GI framework, (corresponding to indirect transitions in the HF band scheme since half of the HF BZ must be mapped back into the GI BZ), we would expect that these would lead to increased absorption in the region prior to the absorption edge over that normally predicted in the Drude region. Although the matrix elements for these transitions should be nonzero, they may still be quite small (they are zero for the HF band scheme). There seems to be no reason to assume that these new transitions would peak at some energy. Hence we would expect a small increase in absorption intensity below the expected threshold, in qualitative agreement with the experimental results. However to establish agreement it is necessary to calculate the expected absorption intensity, preferably for Na or K on which reliable experimental results are available.

3. SOFT X-RAY EMISSION SPECTRA

Emission spectroscopy is a direct experimental method for obtaining information about the density of occupied states in the conduction band of a metal. The spectra are generally in good qualitative agreement with what would normally be expected based on the standard nfe theory. However in this respect, the spectra of the alkalis have been viewed as anomalous.[31] The results for Li have been interpreted as implying that the Fermi surface (FS) must intersect the BZ,[31] but band structure calculations within the HF framework lead to nowhere near the amount of distortion of the FS to account for this.[23] In addition, the amount of distortion required for the FS to intersect the HF BZ would lead to long necks on the surface which would be readily detectable in deHaas van Alphen,[32, 33] radio frequency size effects[34] and other experiments

which on the contrary indicate a very spherical surface.

Now we will consider what might be expected in the GI band scheme. In the experiment, a metal is bombarded with high energy electrons which ionize the core electrons (i. e., the K and L levels) thus inducing transitions from the occupied states in the conduction band. Since the core levels are quite sharp in energy, the observed emission band scans the breadth of the Fermi distribution. A sharp high energy drop in intensity called the emission edge corresponds to the Fermi energy above which the states are unoccupied. Angular momentum separation is achieved due to the selection rules imposed by the vacated core state. Thus in lithium, the only level which can be ionized is the K level leading to a spectrum which samples the p-like states in the conduction band. On the other hand in sodium, the L level is vacated thus yielding information on the s- and d-like density of states. The intensity of emission as a function of energy is directly proportional to the transition probability multiplied by the density of states of conduction electrons at that energy, $I(E) \propto P(E)N(E)$. Hence in lithium if the Fermi surface does not intersect the BZ, we would expect, going from the bottom of the band, an increase in intensity, since the density of p-like states is increasing and of course at the Fermi level a sharp emission edge is expected.

The actual experimental spectrum is shown in Figure 7. This spectrum was reported by Skinner[31] in 1940 and has the same features as more recently published spectra.[35, 36, 37] As seen the spectrum is generally as anticipated except for the sharp peak prior to the high energy edge. This behavior is perhaps best illustrated by considering

the expected behavior based on a HF OPW calculation reported by Parmenter[38] also shown in Fig. 7. This prepeaking has been interpreted as indicating that the Fermi surface intersects the first BZ, in which case the energy at which this peak occurs should correspond to a point of pure p-like symmetry. This can only occur at a high symmetry point on the zone boundary. We saw that in the GI band scheme, the first BZ occupies half the volume of the corresponding HF BZ and that the Fermi surface does intersect this BZ. On this zone boundary, the high symmetry X point produced a splitting into two states, X_1 and X_4', separated by a small gap, with both states lying within the Fermi surface. Therefore we would interpret the energy at which the peak occurred (relative to the bottom of the band) as corresponding to that of the pure p state X_4'. To the high energy side of this peak, a fall-off in intensity of p-like character should occur since s-like symmetries are again mixing into the states, and clearly a sharp edge is expected. Approximate calculations of the Fermi level discussed earlier indicate that X_4' state is about 0.8 ev below the Fermi level. The emission spectrum shows the peak as occurring about 0.9 ev short of the Fermi edge. This is in good agreement with our estimation of its position at 0.8 ev below the edge. Several theoretical approaches have been used to attempt to account for the spectrum by incorporating electron-1s hole scattering[39] and many body effects.[40, 41] The former of these can possibly explain the Li spectrum but cannot account for the Na spectrum (discussed below). However, we see that within the GI framework at least qualitative agreement is achieved with no recourse to electron-electron or electron-phonon interactions. Of course a calculation of

the transition matrix elements would be required to establish the actual degree of quantitative agreement.

Similar features are also observed in the sodium emission spectra[31] shown in Fig. 8, although in this case the experiment samples the s- and d-like density of occupied states since it is the L_2 and L_3 core levels which are vacated. Here a distinct kink occurs short of the emission edge. Preliminary calculations on sodium at the high symmetry points of the BZ lead to a band structure quite similar to lithium in the occupied energy region, and likewise the band gap at the Fermi surface is found to be small. Then in this framework, since the s-like character of states is decreasing going from the bottom of the band while the electron density is increasing, the intensity should initially rise, then come to a maximum and start to fall off. But the onset of the X_1 state should cause a surge in the intensity curve followed by a sharp Fermi edge. As can be seen, this is again in good qualitative agreement with the observed spectrum.

Hence it would seem that the GI description of the energy bands in the alkali metals resolves the dilemma introduced by the experimental soft X-ray emission spectra.

4. MAGNETORESISTANCE AND THE HALL COEFFICIENT

The galvanomagnetic properties of the alkalis, in particular the transverse magnetoresistance, have been the subject of the continuing experimental interest for a number of years. Theoretically only two types of behavior are predicted in the limit of high magnetic fields, namely saturation resulting from closed orbits and a quadratic dependence

in the presence of open orbits. To the contrary extensive experiments on K[42] and also on Na[43] have demonstrated an anomalous linearity up to very high fields. In addition the slopes were found to be orientation dependent in single crystals of K. These observations are at clear variance with the saturation expected for closed nearly spherical Fermi surfaces.

The GI band structure on the other hand leads to a two band description with small gaps occurring at the intersections. In this model, high fields can lead to magnetic breakdown (or interband transitions) yielding extended random orbits in intermediate fields, but in extremely high fields where total breakdown has occurred, the resulting closed Fermi surface should lead to eventual saturation. We have carried out calculations on the magnetoresistance incorporating magnetic breakdown[44] and for two field orientations find broad ranges of essentially linear behavior. For the [100] direction the maximal orbit has closed electron and closed hole orbits, but the [110] direction possesses an open orbit in the first zone and closed electron orbits in the second. This open orbit results in one transverse component which has an initial quadratic dependence but eventually saturates. These calculations are considered more thoroughly in Part II, but it suffices to say that this description leads to the same type of behavior as is observed experimentally.

The field dependence of the Hall coefficient is also determined in these calculations. Since the effective number of electrons in low fields is smaller than that under total breakdown conditions, the Hall coefficient is found to decrease with increasing field until free electron

value is attained after which it remains constant. A similar sloping off with increasing fields has been observed in K by several workers[45] in agreement with these predictions. It is hoped that more thorough experimental investigation of this property with single crystals will permit a more quantitative comparison.

5. de HAAS-van ALPHEN EFFECT

The question now arises of how the GI band structure compares with information gleaned on features of the Fermi surface through studies of the de Haas-van Alphen effect which appear to be in accord with the HF band structure, and for which no discrepancies are apparent. Lee[32] has reported de Haas-van Alphen studies on Na, and Shoenberg and Stiles[33] have carried out similar investigations on K and Rb. The field at which these experiments were conducted was 50 kG, which, for the size gap found in our calculations, would probably be in the total magnetic breakdown region, so that the GI band structure would reduce from the two band Fermi surface description to one effective band with orbits similar to those expected from the nearly free electron (nfe) model. Nevertheless the distortions of the Fermi surface should be directly relatable to the geometry of the first (simple cubic) BZ. The second GI BZ is bounded by just the familiar dodecahedral HF BZ.

Experimentally very small distortions of the Fermi surface were found (on the order of 0.1% for Na[32] and K,[33] and 1% for Rb[32]). This is not unexpected since in lithium we found little distortion from sphericity (about 5%) and in Na and K the distortion should be even

smaller due to the effect of the existence of high lying core p (and d) levels which cause smaller Fourier component contributions from the resulting weaker p (and d) pseudopotentials. The measurement consists of observing phase changes (with crystal orientation) in magnetic susceptibility oscillations induced by quantization of electron orbits in a magnetic field. The phase of the oscillations is directly proportional to the extremal area of the orbits. The experimental extremal area changes for K are shown in Fig. 9. This indicates a maximum in the (110) plane and minima in the (100) and (111) planes. It is of interest to compare these results with those obtained for Na. With the field oriented in the indicated directions, the angles of planes for extrema for K and Na are given in Table 4. This shows that the Fermi surface anisotropies for these two alkalis are somewhat different. If we now consider the GI band scheme, and assume that the field is such as to result in total breakdown, we are led to conclude that extrema are likely for a number of planes which seem to be unimportant directions in the HF band. Such planes are given in Table 4, and Fig. 10 shows the type of planar configurations which might be important here when consideration is made of the Fermi surface intersection with the BZ boundary planes. Whether such points would be a maximum, minimum, or extrema at all would depend upon the individual band structure of the system, the lattice constant, the size of the energy gap, the Fourier coefficients resulting from s, p, d, etc. core electron interactions, and so on. However for lithium we have found that the (110) plane to be a maximum and the (111) and (001) plane to be minima. This as seen in Fig. 9 is the case for potassium. Hence it seems that

the GI band scheme would not lead to any drastic changes in the interpretation of de Haas van Alphen results, but may shed some light on some of the minor structure observed.

6. POSITRON ANNIHILATION

Evidence on the amount of distortion of the Fermi surface of Li from sphericity is afforded by positron annihilation studies reported by Donaghy and Stewart.[46] These experiments were conducted at temperatures above that at which the martenistic phase transformation is known to occur in Li so that only the bcc phase was present. Their analysis of the differences in the momentum distribution of electrons with crystal orientation yielded probable values for the relative k vectors at the surface for high symmetry directions as given in Table 6. With these values we report estimates of the relative vector lengths using our band structure data throughout the zone. For comparison, results of Ham's[23] HF band structure calculation on Li are included. The proximity of our results to experimental is probably fortuitous since our estimates are only reliable to ~1%, but this comparison indicates that the GI band structure for lithium predicts a distortion from sphericity comparable with HF band calculations.

7. CYCLOTRON RESONANCE

Azbel-Kaner Cyclotron Resonance measurements (of surface impedance in a magnetic field in the anomalous skin effect region) have been reported on K and Na by Grimes and Kip.[47] but as yet no data is

available on Li. These experiments made use of field ranges from 1 to 20 kG. Despite the relatively low fields used here as opposed to those required in magnetoresistance and de Haas van Alphen studies, the relevant quantity is $\omega_c\tau$ which here is $\gg 1$, thus being in the breakdown region, at least for K. Assuming that such is the case, the GI two band description coalesces into one double band and essentially free electron-like behavior is expected. If complete breakdown is not effective, then random orbits would lead to few resonances and a very weak signal would be observed. Assuming no breakdown, since the surface is very spherical, $dA/d\epsilon$ would have the free electron value for closed orbits and the cyclotron mass for most directions would be isotropic. However the (110) plane possesses an open orbit and for such orbits, no resonance would be expected. For this condition, quite accurate field alignment would be required.

The studies on K led to free electron-like isotropic resonance signals, but a slight tilting of the crystal plane relative to the field led to a splitting in the peaks which with large enough tilt became inverted. This could imply similar cyclotron masses which change somewhat with tipping, but the isotropy of the resonances tends to invalidate this conclusion and Grimes and Kip postulate a refocusing mechanism to explain this behavior. The results for NA are less clear. The experiment is complicated by the martenistic phase transformation which it undergoes at low temperatures. For crystals with (111) planes and for polycrystalline samples, weaker signals than in K were obtained.

These all possessed split peaks and all orientations gave similar results. However their crystals with (110) planes yielded no resonances at all. Of course some interference may have been due to hexagonal close packed crystals formed in the samples and so an interpretation based on assuming a bcc structure might be premature. It is tempting to interpret these split peak resonances as due to a combination of resonances resulting from several breakdown orbits. Such an analysis could only be corroborated by a careful theoretical treatment incorporating magnetic breakdown so that no more conclusive statements can as yet be made.

8. THERMOELECTRIC POWER

One readily measurable transport property reflecting direct information about the geometry of the Fermi surface is the thermoelectric power, Q, in that it is proportional to the logarithmic derivative of the conductivity $\sigma(\epsilon)$ with respect to the electron energy, specifically

$$Q = \frac{\pi^2}{3} \frac{k^2 T}{e} \left[\frac{\partial \ell n\, \sigma(\epsilon)}{\partial \epsilon}\right]_{\epsilon=\epsilon_f} . \tag{33}$$

This expression is valid for high temperatures and not limited to any particular Fermi surface shape. Here the familiar form for the conductivity applies

$$\sigma = \frac{1}{4\pi^3} \frac{e^2}{\hbar} \frac{\tau}{3} \int v\, dS_f , \tag{34}$$

where the integral is over the Fermi surface S_f, so that

$$\frac{\partial \ell n\, \sigma(\epsilon)}{\partial \epsilon}\Big]_{\epsilon=\epsilon_f} = \Big[\frac{\partial \ell n\, \Lambda}{\partial \epsilon} + \frac{\partial \ell n\, S_f}{\partial \epsilon}\Big]_{\epsilon=\epsilon_f}, \quad \Lambda = \tau v, \tag{35}$$

τ being the relaxation time and Λ the mean free path. Thus for a spherical free electron Fermi surface, the thermopower is given by

$$Q = \frac{\pi^2}{3}\frac{k^2 T}{e}\frac{1}{\epsilon_f} = -\frac{2.45 \times 10^{-2} T}{\epsilon_f(ev)} \text{ microvolts/degree} \tag{36}$$

assuming an isotropic mean free path, Λ, so that Q is expected to be negative. In terms of these straightforward considerations the baffling positive thermopower observed in Li and the wide range of negative values assumed by the other alkalies seem inexplicable.

This simple argument however is in flagrant disregard of the contribution of electron diffusion to the thermopower, resulting from electron-phonon interactions via mean free path anisotropy Λ (k) and this factor has been shown to contribute quite substantially to Q. Bortolani and Calandra[48] using the Heine-Abarenkov pseudopotential[49] (including the nonlocality and energy dependence explicitly) and accurate phonon structure factors obtained thermopower coefficients for the alkalis which agreed in sign and in trend with experimental values although there is some apparent discrepancy in Rb and Cs. While the sign in Li was correct the magnitude was off ~29-40%[50] (depending on which experimental value was accepted). While these results are very encouraging, a closed sphere surface was assumed.

Using the band scheme proposed in this paper, considerable overlap of the Fermi surface into the second zone results, but the

surface remains quite spherical. Within the spherical approximation, a simple calculation can illustrate the type of effect such a BZ intersection might have on Q. The pertinent term to consider is $(\partial\ \ell n S_f/\partial\epsilon)_{\epsilon_f}$ in which that part of the surface enclosed within the first zone will have hole-like character and hence diminish the $1/\epsilon_f$ dependence classically expected. Elementary geometry leads to

$$S_{hole} = 4\pi\ k_f^2 - S_{elec}\ , \qquad S_{elec} = 12\pi\ k_f(k_f - \frac{\pi}{a})$$

$$S_{elec}(\epsilon_f) = 24\pi\ \epsilon_f - \frac{12\pi^2}{a}\ (2\epsilon_f)^{\frac{1}{2}}\ ;$$

$$S_{hole}(\epsilon_f) = \frac{12\pi^2}{a}\ (2\epsilon_f)^{\frac{1}{2}}\ - 16\pi\ \epsilon_f\ .$$

Therefore

$$\left.\frac{\partial\ \ell n\ S_f}{\partial\epsilon}\right)_{\epsilon=\epsilon_f} = \frac{1 - \frac{3\pi}{ak_f}}{\epsilon_f(1 - \frac{6\pi}{ak_f})} \sim \frac{1 - 1.42}{1 - 4.84}\ \frac{1}{\epsilon_f}\ \sim \frac{0.37}{\epsilon_f} \qquad (37)$$

This would diminish the factor of 1 in the assumed diffusion thermopower coefficient

$$\xi_{av} = \frac{\sum_{\hat{k}} \Lambda(\hat{k})\ (1. + \partial\ \ell n\ \Lambda(\hat{k})/\partial\ \ell n\ \epsilon(k)]_{\epsilon=\epsilon_f})}{\sum_{\hat{k}} \Lambda(\hat{k})} \qquad (38)$$

by -1 + .37, changing the Li coefficient calculated by Bortolani et al.,[48] ξ_{av} = -4.5 to -5.13, in reasonable agreement with the experimental values of -6.7 and -5.2. However such a correction would also alter the values for Na and K in the same direction thus rendering them in

even poorer agreement with experiment. Although the estimate is admittedly crude, the trend should be reliable, with the following reservations.

It is also imperative here to consider the possibility that the size of the band gap could be quite important. If the gap in Na and K is significantly smaller than that found in Li, thermal breakdown across the gaps at room temperature and above could lead to significant changes in the number of effective carriers. If the gaps are small enough, no correction such as described above would be appropriate because the double zone would be in effect. Certainly serious consideration should be given these possibilities to establish the type of quantitative behavior which would result from this band scheme.

9. MOTT PARADOX

We have said that the GI description for molecules is valid at all internuclear distances. For the solid, the system at equilibrium has orbitals which are localized at alternate sites throughout the lattice. Now as the lattice is pulled apart, this localization can increase until the orbitals resemble atomic states in the vicinity of any lattice site.

Within the HF framework, since the orbitals are doubly occupied, there are N/2 occupied states for a system with N electrons, and this remains true for all internuclear distances. However when the nuclei are at infinite separation the stable configuration is a lattice of infinitly separated neutral atoms, requiring N singly occupied states. Thus the HF approach leads to improper dissociation, and since the BZ is always 1/2 full, the system must be a conductor at all distances. This

problem with dissociation is known as the Mott Paradox.[51, 51] Mott[52] has suggested that as one brings a set of atoms in from infinity, there is a critical distance at which an electron, interacting with neighboring electrons can suddenly delocalize and contribute to shielding the other electrons from their nuclei, thus forming a conductor. This description may well apply to known metal-oxide conductor to insulator transitions.[52] Of course such considerations are of little consequence in the alkalis since such a transition would occur at an internuclear separation much too large to be experimentally accessible. Nevertheless the same type of theoretical considerations could very well be applicable to both systems.

Actually although Mott's description of what physically occurs may very well be valid, the problem with the theoretical description of the dissociation of the alkalis lies in the limitations inherent in the HF method, and is similar to the problems encountered in the description of the dissociation of even such simple molecules as H_2. We have said that the GI method leads to a description for molecules which is valid at all internuclear distances. For the solid, the system at equilibrium has N singly occupied orbitals which are localized at alternate sites throughout the lattice. Now as the lattice is pulled apart, this localization can increase until at infinite separation the orbitals resemble atomic states in the vicinity of any lattice site and the system is correctly an insulator. Calculations have been carried out on Li metal at a number of different lattice constants, and indeed the system is found to change continuously from a conductor at equilibrium ($a = 6.575\ a_0$) to an insulator at about $10\ a_0$ and finally to look like a system of

isolated ground state Li atoms at 18 a_0. The details of these calculations and a more complete discussion of this phenomena are given in Part III. It suffices to state here that although Mott's physical description[54] of what takes place may be qualitatively correct, a valid theoretical description of the transition from a conductor to an insulator is afforded by the GI method without invoking any discontinuous changes in the basic framework for carrying out calculations.

G. SUMMARY AND CONCLUSIONS

The alkali metals have often been thought to have the simplest electronic structure and to be describable in terms of the nearly free electron (nfe) model. However, it has been quite difficult to explain many properties of these systems. For example, it has been necessary to assume (1) highly anisotropic relaxation times to explain the behavior of the Hall coefficient with pressure, the sign and magnitude of the thermopower, and low energy optical absorption; (2) extremely large Umklapp electron-phonon scattering to explain the variation of magnetoresistance and Hall coefficient with magnetic field and (3) deviations from the Koopmans theorem approximations to explain the soft X-ray emission. If all these deviations from the nfe model are so important for the alkalis, then similar complications might be expected for all metals.

We have found that by relaxing the double occupation restriction in Hartree-Fock and by properly taking the spin symmetry into account one arrives at a band structure which is nfe-like, however, with a

smaller Brillouin zone (BZ) so that energy gaps occur within what is the usual BZ. For the alkali metals this slight modification in the electronic structure is sufficient to explain these puzzling properties without any strong deviations from the nfe model. Thus the removal of the double occupation restriction would seem to be important and it may be that the GI description of the electronic structure of the solids can provide a useful framework for discussing the electronic properties of these systems.

APPENDIX 1

It has been commonly assumed in the past that the Fourier components for say a bcc structure could be accurately approximated by replacing the cell by a sphere having the same volume. This greatly simplifies the computation, but it appears that little investigation has gone into establishing the validity of this assumption.

At the onset of this research we carried out a HF type calculation but replaced the usual HF type potentials by the weak GI pseudopotentials obtained from ab initio calculations on Li atom and used plane wave expansions. However instead of using the spherical approximation to the Fourier transforms we correctly evaluated these integrals over the truncated octahedron. The techniques used in this evaluation will be discussed shortly. We then compared these resulting values with those evaluated using a sphere of the same volume, and also using an inscribed sphere. It was found that any spherical integration led to Fourier components which when plotted as a function of $\hat{k}$ had oscillations superimposed about the correct curve. The strongest deviations occurred for the smaller $\hat{k}$-vectors and died off rapidly as $\hat{k}$ increased. The type of behavior observed is shown in Fig. 11 for the Fourier coefficients over the cubic cell. (A similar type of oscillatory behavior is apparent in the Heine Abarenkov[49] and Ashcroft[53] form factors for Li and the other alkalis, but here they are at least in part dependent on the choice of the ion core radius.) These errors in the HF matrix elements and the resulting differences in the eigenspectrum are reported in Ref.

15. It is thus concluded that significant errors could be introduced into a band calculation by using a spherical approximation to the cell boundary.

Several techniques for evaluating these transforms were investigated to determine a method which gives rapid convergence. Typically the integral to the inscribed sphere was evaluated using a Simpson integration. From the inscribed sphere to the cellular surface, either a truncated octahedron (bcc) or a cube (sc), three different method have been tried. Initially solid angle subdivisions were made and a Simpson type integration was carried out. This approach was found to result in poor convergence. Next a Conroy type[54] integration technique was used in which multidimensional numerical integrations are evaluated using a systematic distribution of points generated for traversal over the (θ, ϕ) variables. Again consistent accuracy was not achieved. Finally a technique was developed which yielded good convergence. A grid of points was generated on the surface, forming the centers of squares for the cubic faces and triangles for the hexagonal faces. Using the point group for a system with cubic symmetry, only a half-octant of the bcc cell and 1/48 of the simple cube need be used. Thus a set of radial pyramids were formed which were truncated by the inscribed sphere. A Simpson type integration was then carried out over the radial elements, associating the appropriate volume element with each point, and an adjusted internal radius for each pyramid at the inscribed sphere was used to give the correct volume. A Riemann integration was then made over all the truncated pyramids. An analytic expression for the Fourier transform of -1/r from the inscribed

sphere to the cube was obtained and the convergence features of this method of evaluation were studied. The results are shown in Table 6 along with some Fourier transforms for the atomic pseudo-potentials (values linearly interpolated from an increment in r of 0.01 a_0). The set using 19 divisions from the center to the edge of the cube was used in all calculations. It is seen that for this set, convergence to 0.013% is achieved. This accuracy is quite sufficient for our purposes and this size set was used throughout the calculations reported here.

Appendix 2

One of the crucial features of any band structure calculation is the manner chosen to treat the interactions of the conduction electrons with each other and with the ion cores. We will describe here the approach we have taken in solving for the conduction orbitals in lithium metal. We write our one-electron hamiltonian for the a-site electrons as

$$h^a \varphi_k = (-\tfrac{1}{2}\nabla^2 + V^a)\,\varphi_k = \epsilon_k \varphi_k \tag{1b}$$

where V^a represents the potential due to the cores and all of the other conduction electrons in the crystal. Since the effective potentials due to the ion cores are weak, we can expand φ_k in plane waves

$$\varphi_k(r) = \sum_K a_K(k) e^{i(\underset{\sim}{k} + \underset{\sim}{K})\cdot \underset{\sim}{r}} \tag{2b}$$

where the expansion is over the sc reciprocal lattice vectors $\underset{\sim}{K}$ appropriate to the a sublattice. Multiplying (1b) through by $e^{-i(\underset{\sim}{k} + \underset{\sim}{K}_l)\cdot \underset{\sim}{r}}$ and integrating over all space, we obtain

$$N\Omega_0 \frac{|\underset{\sim}{k} + \underset{\sim}{K}_l|^2}{2} a_{K_l}(k) + \sum_j \langle \underset{\sim}{k} + \underset{\sim}{K}_l | V^a | \underset{\sim}{k} + \underset{\sim}{K}_j \rangle\, a_{K_j}(k)$$

$$= N\Omega_0 \epsilon_k a_{K_l}(k) \tag{3b}$$

where Ω_0 is the volume of the sc unit cell, N is the number of unit cells in the crystal, and the matrix element $\langle \underset{\sim}{k} + \underset{\sim}{K}_l \,|V^a|\, \underset{\sim}{k} + \underset{\sim}{K}_j \rangle$ is evaluated over all space.

We now consider more explicitly the form to be used for V^a. Since the a-orbitals are more localized near the a-sites, and the b-orbitals are more localized near the b-sites, it is appropriate to write V^a in terms of potentials centered at these respective sites, that is,

$$V^a = \sum_{\underset{\sim}{R}_j} [V_a^{\,eff}(\underset{\sim}{r} - \underset{\sim}{R}_j) + V_b^{\,eff}(\underset{\sim}{r} - \underset{\sim}{R}_j - \underset{\sim}{R}_{ab})] \tag{4b}$$

where $\underset{\sim}{R}_j$ is the vector to the j^{th} a-site (centered in the j^{th} sc unit cell), $\underset{\sim}{R}_{ab}$ is a vector from the center to a corner of the sc unit cell, and the sum extends over all a-sites. Since there is a one-to-one correspondence between a- and b-sites, all b-sites are also covered in this sum.

If there are N = 2m conduction electrons in the crystal, then V^a includes field terms due to m a-orbitals and m b-orbitals. But the orbital $\varphi_k{}^a$ should see a field due to (m - 1) a-orbitals and m b-orbitals. Thus there is a self term present in V^a which has no physical significance and should be subtracted out.

In addition there are two other effects which facilitate determining a form for V^a. One of these is the electrostatic repulsion which acts to keep the electrons apart and thus introduces correlation into the electronic motion. The other is the exchange term which arises from the interaction of electrons with parallel spins and which generates an exchange hole around each electron. Therefore if an a-site electron is in the neighborhood of some ion core, then it is surrounded by an exchange hole which tends to exclude other a-electrons. It should then see a field due to neutral lithium atoms at all the other a-sites, thus correctly including (m - 1) a-valence orbitals, plus the field due to the lithium core in its immediate vicinity, and finally a field due to neutral lithium atoms centered on all of the b-sites (m of these) throughout the lattice.

Now if we say that there is an exchange hole associated with our a-site orbital tending to exclude orbitals with which it is triplet coupled, then recalling that the spin coupling between a-orbitals corresponds to triplet coupling, we expect that the interaction between these orbitals

will be quite small. We know that the potential due to a neutral atom is very weak and goes to zero by $\sim 9a_0$ (as compared to the ion core potential it behaves asymptotically like $1/r$). If in addition consideration is made of the screening of these a-site potentials by the nearest neighbor b-site orbitals, it is a reasonable assumption to take these other a-site potentials to be zero. We thus make the Wigner-Seitz approximation, but here applied only to the a-sites, and say that the ion core potential extends to the boundary of the immediate sc unit cell and is zero past this surface. (Note that this correctly accounts for the self-term and also includes corrections for exchange and correlation.)

Thus we take $\sum_{R_j} V_a^{eff}(\underset{\sim}{r} - \underset{\sim}{R}_j) \equiv V_a^{ion}(\underset{\sim}{r} - \overline{\underset{\sim}{R}}_j)$ where $\overline{R}_j$ is the vector to the j^{th} nearest a-site. Hence we have that

$$\langle \underset{\sim}{k} + \underset{\sim}{K}_l | V_a^{ion}(\underset{\sim}{r} - \overline{\underset{\sim}{R}}_j) | \underset{\sim}{k} + \underset{\sim}{K}_i \rangle$$

$$= \sum_{R_j} \langle \underset{\sim}{k} + \underset{\sim}{K}_l | V_a^{ion}(\underset{\sim}{r} - \underset{\sim}{R}_j) | \underset{\sim}{k} + \underset{\sim}{K}_i \rangle_{\text{cell } j}$$

where cell j indicates that the integration is over the j^{th} cell. But this integral is independent of j, so that we can write

$$\sum_{R_j} \langle \underset{\sim}{k} + \underset{\sim}{K}_l | V_a^{ion}(\underset{\sim}{r} - \underset{\sim}{R}_j) | \underset{\sim}{k} + \underset{\sim}{K}_i \rangle_{\text{cell } j}$$

$$= N \langle \underset{\sim}{k} + \underset{\sim}{K}_l | V_a^{ion}(\underset{\sim}{r}) | \underset{\sim}{k} + \underset{\sim}{K}_i \rangle_{\Omega_0} \quad . \tag{5b}$$

We now consider the b-site orbitals. We have stated that these also contribute to the field seen by an a-orbital in the form of a neutral

atom potential. Thus we have that

$$\langle \underset{\sim}{k} + \underset{\sim}{K}_l \left| \sum_{R_j} V_b^{\,eff}(\underset{\sim}{r} - \underset{\sim}{R}_j - \underset{\sim}{R}_{ab}) \right| \underset{\sim}{k} + \underset{\sim}{K}_i \rangle$$

$$= N \langle \underset{\sim}{k} + \underset{\sim}{K}_l \left| V_b^{\,eff}(\underset{\sim}{r} - \underset{\sim}{R}_j - \underset{\sim}{R}_{ab}) \right| \underset{\sim}{k} + \underset{\sim}{K}_i \rangle$$

where these matrix elements extend over the entire crystal. As discussed in section E, $V_b^{\,eff}$ is just the sum of V^{ion} and the coulomb potential due to the valence electron at the $\underline{b}$ site (taken to be the atomic valence orbital). However, these potentials are unshielded and we know that the conduction electrons will act to screen them. We therefore consider the form that the screening will take due to the presence of the other electrons in the crystal. We can use the conventional first-order perturbation approach to obtain an expression for this shielded potential. Since we are concerned only with the screening correction for the $\underline{b}$-site potentials we take our zero-order wavefunction to be a plane wave, $\varphi_0 = e^{i\underset{\sim}{k}\cdot\underset{\sim}{r}}$, and assume that these $\underline{b}$-potentials perturb the system leading to a wavefunction

$$\varphi_k = \varphi_k^0 + \sum_K{}' \, a_K e^{i(\underset{\sim}{k} + \underset{\sim}{K})\cdot\underset{\sim}{r}} = \varphi_k^0 + \varphi_k' \qquad (6b)$$

where the prime on the sum indicates all K, $K \neq 0$. The to first order we have

$$-\tfrac{1}{2}\nabla^2 \varphi_k' + V_b^{\,eff}(|\underset{\sim}{r} - \underset{\sim}{R}_{ab}|)\varphi_k^0 = \mathcal{E}_k^0 \varphi_k' + \mathcal{E}_k' \varphi_k^0 \ ,$$

therefore

$$\sum_K{}' \frac{a_{K(k)}}{2} \left|(\underset{\sim}{k} + \underset{\sim}{K})\right|^2 e^{i(\underset{\sim}{k} + \underset{\sim}{K})\cdot\underset{\sim}{r}} + V_b^{\,eff}(|\underset{\sim}{r} - \underset{\sim}{R}_{ab}|)e^{i\underset{\sim}{k}\cdot\underset{\sim}{r}} =$$

$$= \sum_{K}{}' \frac{k^2}{2} a_K(k) e^{i(\underset{\sim}{k} + \underset{\sim}{K}) \cdot \underset{\sim}{r}} + \varepsilon_k' e^{i\underset{\sim}{k} \cdot \underset{\sim}{r}} \quad . \tag{7b}$$

Multiplying through with $e^{-i(\underset{\sim}{k} + \underset{\sim}{K}) \cdot r}$ and integrating we obtain

$$\frac{|\underset{\sim}{k} + \underset{\sim}{K}|^2}{2} a_K(k) + e^{-i\underset{\sim}{K} \cdot \underset{\sim}{R}ab} \langle \underset{\sim}{k} + \underset{\sim}{K} | V_b{}^{eff}(r) | \underset{\sim}{k} \rangle = a_K(k) \frac{k^2}{2} \tag{8b}$$

Solving for $a_K(k)$,

$$a_K(k) = \frac{e^{-i\underset{\sim}{K} \cdot \underset{\sim}{R}ab} \langle \underset{\sim}{k} + \underset{\sim}{K} | V_b{}^{eff} | \underset{\sim}{k} \rangle}{\frac{1}{2}[k^2 - |\underset{\sim}{k} + \underset{\sim}{K}|^2]} = \frac{\langle \underset{\sim}{k} + \underset{\sim}{K} | V_b{}^{eff}(\underset{\sim}{r} - \underset{\sim}{R}_{ab}) | \underset{\sim}{k} \rangle}{\frac{1}{2}[k^2 - |\underset{\sim}{k} + \underset{\sim}{K}|^2]} \tag{9b}$$

The total electron density due to the b-orbitals is

$$\rho(r) = \sum_{k} \frac{1}{N\Omega_0} (-\varphi_k{}^* \varphi_k)$$

(where we have taken φ_k to be normalized to one electron per unit volume). Using (6b) this becomes (to first order)

$$\rho(r) = -\frac{1}{N\Omega_0} \sum_{k} \varphi_k^{0*} \varphi_k^0 - \frac{1}{N\Omega_0} \sum_{k} (\varphi_k^{0*} \varphi_k' + \varphi_k'^* \varphi_k^0)$$

Thus the zero order change density is uniform, $\rho^0 = -\frac{1}{\Omega_0}$, and the first order charge density is

$$\rho' = -\frac{1}{N\Omega_0} \sum_{k} (\varphi_k^{0*} \varphi_k' + \varphi_k'^* \varphi_k{}^0)$$

which becomes

$$\rho'(r) = -\frac{1}{N\Omega_0} \sum_{k} \sum_{K}{}' [a_K(k) e^{i\underset{\sim}{K} \cdot \underset{\sim}{r}} + a_K{}^*(k) e^{-i\underset{\sim}{K} \cdot \underset{\sim}{r}}] =$$

$$= -\frac{2}{(2\pi)^3} \sum_{K}' \int_{\Omega_f} d\underset{\sim}{k} \left[a_K(k) e^{i\underset{\sim}{K}\cdot\underset{\sim}{r}} + a_K^*(k) e^{-i\underset{\sim}{K}\cdot\underset{\sim}{r}} \right] . \qquad (10b)$$

Here Ω_f indicates integration over the fermi volume. This expression can be rewritten as

$$\rho'(r) = -\frac{2}{(2\pi)^3} \sum_{K}' e^{i\underset{\sim}{K}\cdot\underset{\sim}{r}} \int_{\Omega_f} d\underset{\sim}{k} \left[a_K(k) + a_{-K}^*(k) \right]$$

$$= -\sum_{K}' \rho_K e^{i\underset{\sim}{K}\cdot\underset{\sim}{r}} . \qquad (11b)$$

Now we can use Poisson's equation to determine the local screening potential δV_{sc} resulting from this oscillating charge density,

$$\nabla^2 \delta V_{sc}(r) = 4\pi \rho(r) . \qquad (12b)$$

Taking a Fourier transform on this equation we obtain

$$K^2 \delta V_{sc}(K) = 4\pi \rho_K . \qquad (13b)$$

To be self-consistent our original potential should have included this δV_{sc}, giving a total potential of

$$V_b^{tot}(r) = \delta V_{sc}(r) + V_b^{eff}(|\underset{\sim}{r} - \underset{\sim}{R}_{ab}|) . \qquad (14b)$$

Thus replacing $V_b^{eff}(|\underset{\sim}{r} - \underset{\sim}{R}_{ab}|)$ in (9b) with $V_b^{tot}(r)$, and using (11b) and (13b) we obtain

$$\delta V_{sc}(K) = \frac{4\pi}{K^2} \left(\frac{2}{(2\pi)^3} \right) \int_{\Omega_f} \left\{ \frac{\langle \underset{\sim}{k} + \underset{\sim}{K} | V_b^{tot} | k \rangle}{\frac{1}{2}[k^2 - |\underset{\sim}{k} + \underset{\sim}{K}|^2]} + \frac{\langle \underset{\sim}{k} - \underset{\sim}{K} | V_b^{tot} | \underset{\sim}{k} \rangle^*}{\frac{1}{2}[k^2 - |\underset{\sim}{k} - \underset{\sim}{K}|^2]} \right\} d\underset{\sim}{k} . \qquad (15b)$$

Now $\delta V_{sc}(r)$ is local so that

$$\langle \underset{\sim}{k} + \underset{\sim}{K} | V_b^{tot} | \underset{\sim}{k} \rangle = \delta V_{sc}(K) + e^{-i\underset{\sim}{K}\cdot\underset{\sim}{R}ab} \langle \underset{\sim}{k} + \underset{\sim}{K} | V_b^{eff} | \underset{\sim}{k} \rangle$$

If $V_b^{eff}(r)$ can also be taken as local we are then left with the expression

$$\delta V_{sc}(K) = \frac{4\pi}{K^2} \left(\frac{4}{(2\pi)^3}\right) Re[V_b^{eff}(K) e^{-i\underset{\sim}{K}\cdot\underset{\sim}{R}ab} + \delta V_{sc}(K)] \times \int_{\Omega_f} \frac{d\underset{\sim}{k}}{\frac{1}{2}[k^2 - |\underset{\sim}{k} + \underset{\sim}{K}|^2]} \qquad (16b)$$

The integral in this expression can then be readily evaluated,

$$\frac{4\pi}{K^2} \left(\frac{4}{(2\pi)^3}\right) \int_{\Omega_f} \frac{d\underset{\sim}{k}}{\frac{1}{2}[k^2 - |\underset{\sim}{k} + \underset{\sim}{K}|^2]} \equiv 1 - \epsilon(K) = -\frac{1}{2\pi\eta^2 k_f} \left[\frac{(1-\eta^2)}{2\eta} \ln\left|\frac{\eta+1}{\eta-1}\right| + 1\right] \qquad (17b)$$

where $\eta = K/2k_f$ and $\epsilon(K)$ is the usual Bardeen screening factor.[56]

Thus (16b) reduces to

$$\delta V_{sc}(K) = [1 - \epsilon(K)] Re[\delta V_{sc}(K) + e^{-i\underset{\sim}{K}\cdot\underset{\sim}{R}ab} V_b^{eff}(K)],$$

and

$$\delta V_{sc}(K) = \frac{[1 - \epsilon(K)]}{\epsilon(K)} Re[e^{-i\underset{\sim}{K}\cdot\underset{\sim}{R}ab} V_b^{eff}(K)]$$

so that

$$V_b^{tot}(K) = Re\left\{\frac{e^{-i\underset{\sim}{K}\cdot\underset{\sim}{R}ab}}{\epsilon(K)} V_b^{eff}(K)\right\} \qquad (18b)$$

(Note that in a centrosymmetric system such as we have, this expres-

sion is real.) This form is appropriate at the high symmetry points in the lattice where predominately one of the angular momentum dependent potentials contributes, and the matrix elements of V_b^{eff} can then be taken to be local. However, for general points in the zone, (16b) is invalid[55, 56] and we must return to (15b). $\delta V_{sc}(K)$ can still be removed from the integral, and we are then led to

$$\delta V_{sc}(K) = \frac{4\pi}{K^2\epsilon(K)} \frac{2e^{-i\underset{\sim}{K}\cdot\underset{\sim}{R}ab}}{(2\pi)^3} \int_{\Omega_f} \left\{ \frac{\langle \underset{\sim}{k}+\underset{\sim}{K}|V_b^{eff}|\underset{\sim}{k}\rangle}{\frac{1}{2}[k^2 - |\underset{\sim}{k}+\underset{\sim}{K}|^2]} + \frac{\langle \underset{\sim}{k}|V_b^{eff}|\underset{\sim}{k}-\underset{\sim}{K}\rangle}{\frac{1}{2}[k^2 - |\underset{\sim}{k}-\underset{\sim}{K}|^2]} \right\} d\underset{\sim}{k} \tag{19b}$$

Going one step further, in lithium metal the general expression for V_b^{eff} (see section E) is

$$V_b^{eff}(r) = \sum_l V_l^b - (r)|l\rangle\langle l| = V_{p^-}^b (r) + [V_s^b(r) - V_{p^-}^b(r)][1 - |s\rangle\langle s|]$$

leading to

$$\delta V_{sc}(K) = [\frac{1}{\epsilon(K)} - 1]\, e^{-i\underset{\sim}{K}\cdot\underset{\sim}{R}ab}\, V_{p^-}(K) +$$

$$\frac{4\pi e^{-i\underset{\sim}{K}\cdot\underset{\sim}{R}ab}}{K^2\epsilon(K)} \frac{2}{(2\pi)^3} \int_{\Omega_f} \left\{ \frac{\langle \underset{\sim}{k}+\underset{\sim}{K}|V_{s^-}-V_{p^-}|s\rangle\langle s|\underset{\sim}{k}\rangle}{\frac{1}{2}[k^2 - |\underset{\sim}{k}+\underset{\sim}{K}|^2]} + \right.$$

$$\left. + \frac{\langle \underset{\sim}{k}|V_{s^-}-V_{p^-}|s\rangle\langle s|\underset{\sim}{k}-\underset{\sim}{K}\rangle}{\frac{1}{2}[k^2 - |\underset{\sim}{k}-\underset{\sim}{K}|^2]} \right\} d\underset{\sim}{k} \tag{20b}$$

(Note that the principal value should be taken at critical points.) This is then the requisite screening factor appropriate for general points in the zone.

REFERENCES

1. J. C. Slater, Quantum Theory of Molecules and Solids (McGraw-Hill Book Company, Inc., New York, 1965), Vol. II.
2. W. A. Goddard III, Phys. Rev. 157, 81 (1967).
3. W. A. Goddard III, J. Chem. Phys., 48, 450 (1968); ibid. 48, 5337 (1968).
4. Hartree atomic units are used, $e = \hbar = m_e = 1$; thus the unit of energy is 1 Hartree = 27.211 ev and the unit of length is 1 Bohr (a_o) = 0.52917 Å.
5. D. E. Rutherford, Substitutional Analysis (Edinburg University Press, London, 1948).
6. See Part III for a more complete discussion.
7. W. A. Goddard III, Phys. Rev. 169, 120 (1968).
8. J. C. Phillips and L. Kleinmann, Phys. Rev. 116, 287 (1959).
9. a) B. J. Austin, V. Heine, and L. J. Sham, Phys. Rev., 127, 276 (1962). b) See, for example, V. Heine and I. V. Abarenkov, Phil. Mag. 9, 451 (1964).
10. W. A. Goddard III, Phys. Rev. 174, 659 (1968).
11. L. R. Kahn and W. A. Goddard III, Chem. Phys. Letters 2, 667 (1968).
12. L. R. Kahn and W. A. Goddard III, to be published.
13. C. F. Melius, W. A Goddard III, and L. R. Kahn, to be published.
14. W. J. Hunt, W. A. Goddard III, T. H. Dunning, Jr., L. R. Kahn, and P. K. Pearson, to be published.
15. P. M. O'Keefe and W. A. Goddard III, Phys. Rev. 180, 747 (1969).
16. R. C. Ladner and W. A. Goddard III, J. Chem. Phys., 51, 1073 (1969).

17. A Bloch function is a function satisfying the condition

$$\varphi(\underset{\sim}{r} + \underset{\sim}{R}) = e^{i\underset{\sim}{k} \cdot \underset{\sim}{R}} \varphi(\underset{\sim}{r})$$

where $\underset{\sim}{R}$ are the set of lattice translation vectors.

18. J. M. Ziman, Electrons and Phonons (Oxford University Press, Great Britian, 1960), p. 20.

19. V. Heine, Group Theory in Quantum Mechanics (Macmillan Co., New York, 1964), p. 414.

20. a) W. A. Goddard III and W. E. Palke, unpublished GI calculations.
b) W. A. Goddard III, Phys. Rev., 172, 7 (1968).

21. a) We use a lattice constant of a = 6.575 a_0 (3.479_3 Å) appropriate at 4°K corresponding to an atomic volume ($a^3/2$) of $142.12068 a_0^3$ [from W. Pearson, Can. J. Phys., 32, 708 (1954), using conversion constants from E. R. Cohen and J. M. W. Dumond, Rev. Mod. Phys. , 37, 537 (1965)].
b) The symmetry point notation is Γ for $\underset{\sim}{k}$ = (0, 0, 0) at the center of the BZ, and X for $\underset{\sim}{k}$ = $(2\pi/a)$ $(\frac{1}{2}, 0, 0)$, M for $\underset{\sim}{k}$ = $2\pi/a$ $(\frac{1}{2}, \frac{1}{2}, 0)$, and R for $\underset{\sim}{k}$ = $(2\pi/a)$ $(\frac{1}{2}, \frac{1}{2}, \frac{1}{2})$ at the face center, edge center and corner of the BZ boundary, respectively. Here a is the lattice constant (see Ref. 20).

22. For the HF bcc description the symmetry points are Γ for $\underset{\sim}{k}$ = $2\pi/a$ (0, 0, 0), H for $\underset{\sim}{k}$ = $2\pi/a$ (1, 0, 0), N for $\underset{\sim}{k}$ = $2\pi/a$ $(\frac{1}{2}, \frac{1}{2}, 0)$ and P for $\underset{\sim}{k}$ = $2\pi/a$ $(\frac{1}{2}, \frac{1}{2}, \frac{1}{2})$.

23. F. S. Ham, Phys. Rev. 128, 2524 (1962); Ibid., Phys. Rev. 128, 82 (1962).

24. H. Mayer and M. H. El Naby, Z. Physik 280, 289 (1963).

25. H. Mayer and B. Hietel, in Optical Properties and Electronic... (Ref 29, p. 47

26. M. H. Cohen and J. C. Phillips, Phys. Rev. Let. 12, 662 (1964).

27. A. W. Overhauser, Phys. Rev. Let. 13, 190 (1964).

28. J. J. Hopfield, Phys. Rev. 139, A419 (1965).

29. M. H. Cohen, Optical Properties and Electronic Structure of Metals and Alloys, F. Abeles, Ed., (John Wiley and Sons, Inc., New York, 1966), p. 66.

30. N. V. Smith. Phys. Rev. 183, 634 (1969).

31. H. W. B. Skinner, Phil. Trans. Roy. Soc. 239, 95 (1940).

32. M. J. G. Lee, Proc. Roy. Soc. A295, 440 (1966).

33. D. Shoenberg and P. J. Stiles, Proc. Roy. Soc. A281, 62 (1964).

34. P. S. Peercy, W. M. Walsh, L. W. Rupp, and P. H. Schmidt, Phys. Rev. 171, 713 (1968).

35. D. E. Bedo and D. H. Tomboulian, Phys. Rev. 109, 35 (1958).

36. R. S. Crisp and S. E. Williams, Phil. Mag. 5, 525 (1960).

37. R. S. Crisp and S. E. Williams, Phil. Mag. 6, 365 (1960).

38. R. H. Parmenter, Phys. Rev. 86, 552 (1952).

39. F. K. Allotey, Phys. Rev. 157, 467 (1967).

40. P. Nozieres and C. T. de Dominicis, Phys. Rev. 178, 1097 (1969).

41. G. A. Ausman, Jr., and A. J. Glick, Phys. Rev. 183, 687 (1969).

42. P. A. Penz and R. Bowers, Phys. Rev. 172, 991 (1968).

43. D. K. C. MacDonald, Phil. Mag. 2, 97 (1957); F. E. Rose, Ph. D. Thesis, Cornell University (1965).

44. L. M. Falicov and P. R. Sievert, Phys. Rev. 138, A88 (1965).

45. R. C. Chambers and B. K. Jones, Proc. Roy. Soc. (London) A270, 417 (1962); P. A. Penz, Phys. Rev. Let., 20, 725 (1968).

46. J. J. Donaghy and A. T. Stewart, Phys. Rev. 164, 391 (1967).

47. C. C. Grimes and A. F. Kip, Phys. Rev. 132, 1991 (1963).

48. V. Bortolani and C. Calandra, Il Nuovo Cimento 58, 393 (1968).

49. V. Heine and A. Abarenkov, Phyl. Mag. 9, 451 (1964).

50. These values are based on the note added in proof in Ref. (50) where measured phonon frequencies for Li were incorporated in the calculation, and improved their value by 20%.

51. J. M. Ziman, Principles of the Theory of Solids, (Cambridge University Press, New York 1965), p. 144.

52. N. F. Mott, Can. J. Phys. 34, 1356 (1956); Phil Mag. 6, 287 (1961).

53. N. W. Ashcroft, J. Phys. C. (Proc. Phys. Soc.) 1, 232 (1968).

54. H. Conroy, J. Chem. Phys. 47, 5307 (1967).

55. W. A. Harrison, Phys. Rev., 129, 2503 (1963).

56. W. A. Harrison, Pseudopotentials in the Theory of Metals, [W. A. Benjamin, Inc., New York (1966)] pp. 49, 280.

Table 1. Fourier Transforms[a] of Li GI pseudopotentials. The 2s and 2p potential transforms are evaluated over the cubic primitive cell with a = 6.575 a_0. The $2s^-$ and $2p^-$ coulombic potential transforms are calculated to a radius where the potentials go to zero.

K ($\frac{a}{2\pi}$)	V_{2s}^{FT}	V_{2p}^{FT}	$V_{2s^-}^{FT}$	$V_{2p^-}^{FT}$
000	-0.29097	-0.37563	-0.05767	-0.13947
100	-0.00745	-0.07070	0.00628	-0.05676
110	0.01227	-0.03754	0.01446	-0.03517
111	0.01363	-0.02685	0.01419	-0.02626
200	0.01610	-0.01724	0.01204	-0.02144
210	0.01074	-0.01753	0.01005	-0.01826
211	0.00842	-0.01579	0.00827	-0.01598
220	0.00541	-0.01294	0.00544	-0.01289
221	0.00439	-0.01181	0.00439	-0.01181
300	0.00265	-0.01364	0.00439	-0.01181
310	0.00323	-0.01119	0.00350	-0.01092
311	0.00266	-0.01021	0.00272	-0.01016
222	0.00206	-0.00949	0.00206	-0.00949
320	0.00153	-0.00890	0.00150	-0.00891
321	0.00102	-0.00841	0.00102	-0.00840
400	0.00125	-0.00649	0.00024	-0.00755
410	0.00005	-0.00705	-0.00008	-0.00719
322	-0.00008	-0.00719	-0.00008	-0.00719
411	-0.00033	-0.00683	-0.00037	-0.00686

[a] Units are in Hartree atomic units. See Ref. 4.

Table 2. Transformation properties of the lower states for simple cubic (sc) and body centered cubic (bcc) structures and their lowest spherical harmonic types.

States

bcc and sc	bcc	sc	Symmetry	Type
Γ_1	H_1	R_1	1	s
Γ_{15}	H_{15}	R_{15}	x, y, z	p
Γ_{12}	H_{12}	R_{12}	$x^2 - y^2$, $z^2 - \frac{1}{2}(x^2 + y^2)$	d
Γ_{25}'	H_{25}'	R_{25}'	xy, yz, zx	d
Γ_{25}	H_{25}	R_{25}	$z(x^2 - y^2)$, $x(y^2 - z^2)$, $y(z^2 - x^2)$	f
Γ_2'	H_2'	R_2'	xyz	f

States-bcc	Symmetry	Type
N_1	1	s
N_1'	x + y	p
N_3'	z	p
N_4'	x - y	p
N_2	z(x - y)	d
N_4	$x^2 - y^2$	d
N_3	z(x + y)	d
N_2'	$z(x^2 - y^2)$	f

States-sc		Symmetry	Type
X_1	M_1	1	s
X_4'	M_4'	z	p
X_5'	M_5'	x, y	p
X_2	M_2	$x^2 - y^2$	d
X_5	M_5	yz, zx	d
X_3	M_3	$z(x^2 - y^2)$	d
X_3'	M_3'	xy	f
X_2'	M_2'	xyz	f

States-bcc	Symmetry	Type
P_1	1	s
P_4	x, y, z	p
P_3	$x^2 - y^2$, $z^2 - \frac{1}{2}(x^2 + y^2)$	d
P_5	$z(x^2 - y^2)$, $x(y^2 - z^2)$, $y(z^2 - x^2)$	f

Table 3. Energies[a] calculated for high symmetry states in bcc lithium.

State	a and b sites[b]	a sites[c]	a sites (local)[b]
Γ_1 1st	-0.2992	-0.2978	-0.2969
2nd	0.2013	0.2138	0.2152
Γ_{15}	0.0630	0.0553	0.0553
Γ_{12}	0.1534	0.1303	0.1306
X_1	-0.1942	-0.1941	-0.1920
X_4'	-0.1783	-0.2107	-0.2110
X_5'	0.1450	0.1141	0.1141
M_5'	-0.1339	-0.1332	-0.1333
M_1	-0.0743	-0.0818	-0.0791
M_3	-0.0491	-0.0492	-0.0493
M_4'	0.1790	0.1652	0.1606
R_{15}	-0.0412	-0.0600	-0.0641
R_{25}'	0.0030	0.0411	0.0427
R_1	0.0337	0.0543	0.0533
R_2'	0.1163	0.0913	0.0906

[a] All energies are in hartree atomic units and are calculated using a set of 81 plane waves up to $\underset{\sim}{K} = 2\pi/a(2,1,1)$.

[b] Calculated assuming pure spherical harmonic type with appropriate local potential. (a and b sites include shielded b-site potential.)

[c] Calculated using general projected potential.

Table 4. Relative extrema observed in de Haas van Alphen experiments associated with orientations which could be important in the GI band scheme for the alkalis. Extrema in parenthesis indicate peaks or directions not clearly defined in the spectra.

(100) Plane

	[100]	[310]	[210]	[110]
Na	min	(max)		min
K	min		0	max
Rb	min		max	min

(110) Plane

	[100]	[311]	[211]	[111]	[011]
Na	(min)	max	0	min	max
K	min		max	min	max
Rb	min	max		min	max

(211) Plane

	[110]	[311]	[312]	[201]	[1-11]
K	max		min		min

(111) Plane

	[110]	[211]	[101]
Rb	max	min	max

Table 5. The GI wave vector lengths along symmetry axes relative to the isotropic Fermi wave vector compared with experimental and calculated HF values.

	EXPERIMENTAL	CALCULATED	
	Positron Annihilation[a]	GI[b]	HF[c]
$\frac{k_{110}}{k_f}$	1.04	1.046	1.023
$\frac{k_{100}}{k_f}$	0.99	0.994	0.973
$\frac{k_{111}}{k_f}$	0.99	0.996	0.983

[a] Donaghy, J. J. and A. T. Stewart, (1967).

[b] a = 6.575 a.u.

[c] Ham, F. S. (1962); a = 6.651 a.u.

TABLE 6. Convergence properties of method used to evaluate the Fourier Transforms from the inscribed sphere (radius 3.2875 a_0) to the cubic cell boundary.

	9[a] - 45[b]	15 - 120	19 - 190	Exact[c]
$-1/r$[d, e]	-.123160	-.123112	-.123102	-.123085
$V_{FT_s}(0)$	-.121719	-.121675	-.121665	
$V_{FT_p}(0)$	-.123433	-.123384	-.123374	

[a]Number of pts. from center of face to cube edge.

[b]Total number of points required on the section of the cubic surface.

[c]Evaluated from analytic expression.

[d]Definition includes division by volume of cubic cell. (Equal to 284.24126 a_0)

[e]All values are in Hartree atomic units. (See Ref. 4)

Fig. 1 The GI effective potentials for lithium.

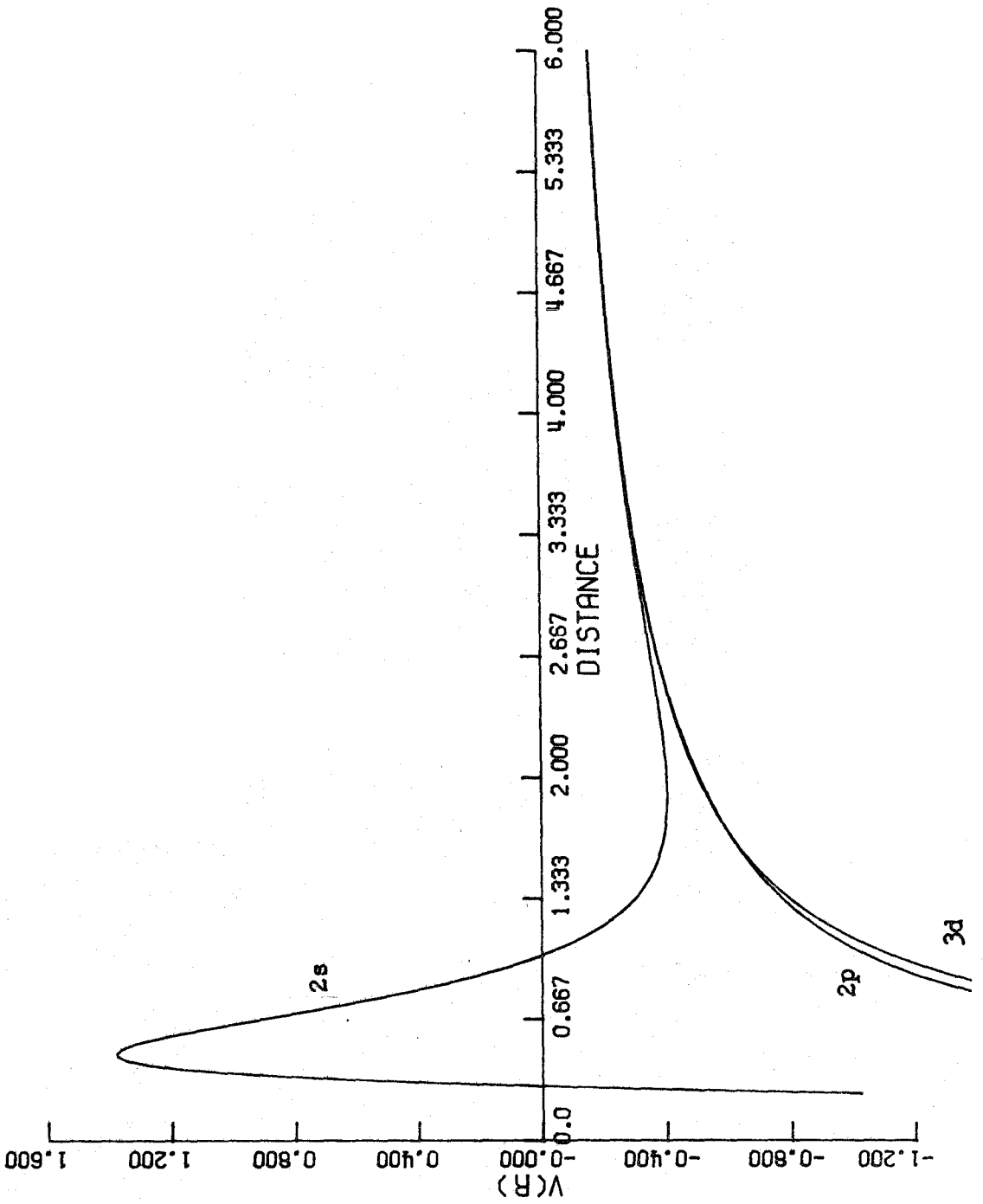
V(R)
-1.200
-0.800
-0.400
-0.000
0.400
0.800
1.200
1.600
0.0
0.667
1.333
2.000
2.667
3.333
4.000
4.667
5.333
6.000
DISTANCE
2s
2p
3d

Fig. 2 The tableau appropriate for the alkali metals.

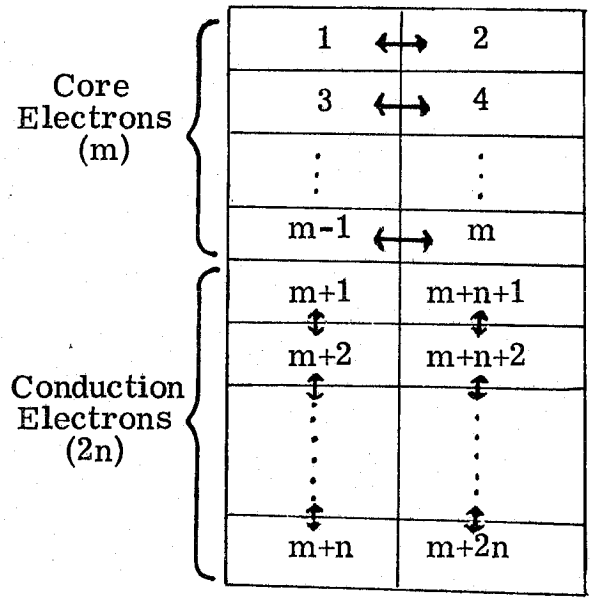
Core
Electrons
(m)
Conduction
Electrons
(2n)
1
2
3
4
m-1
m
m+1
m+n+1
m+2
m+n+2
m+n
m+2n

Fig. 3 The GI energy band structure for Li, using a-site potential only.

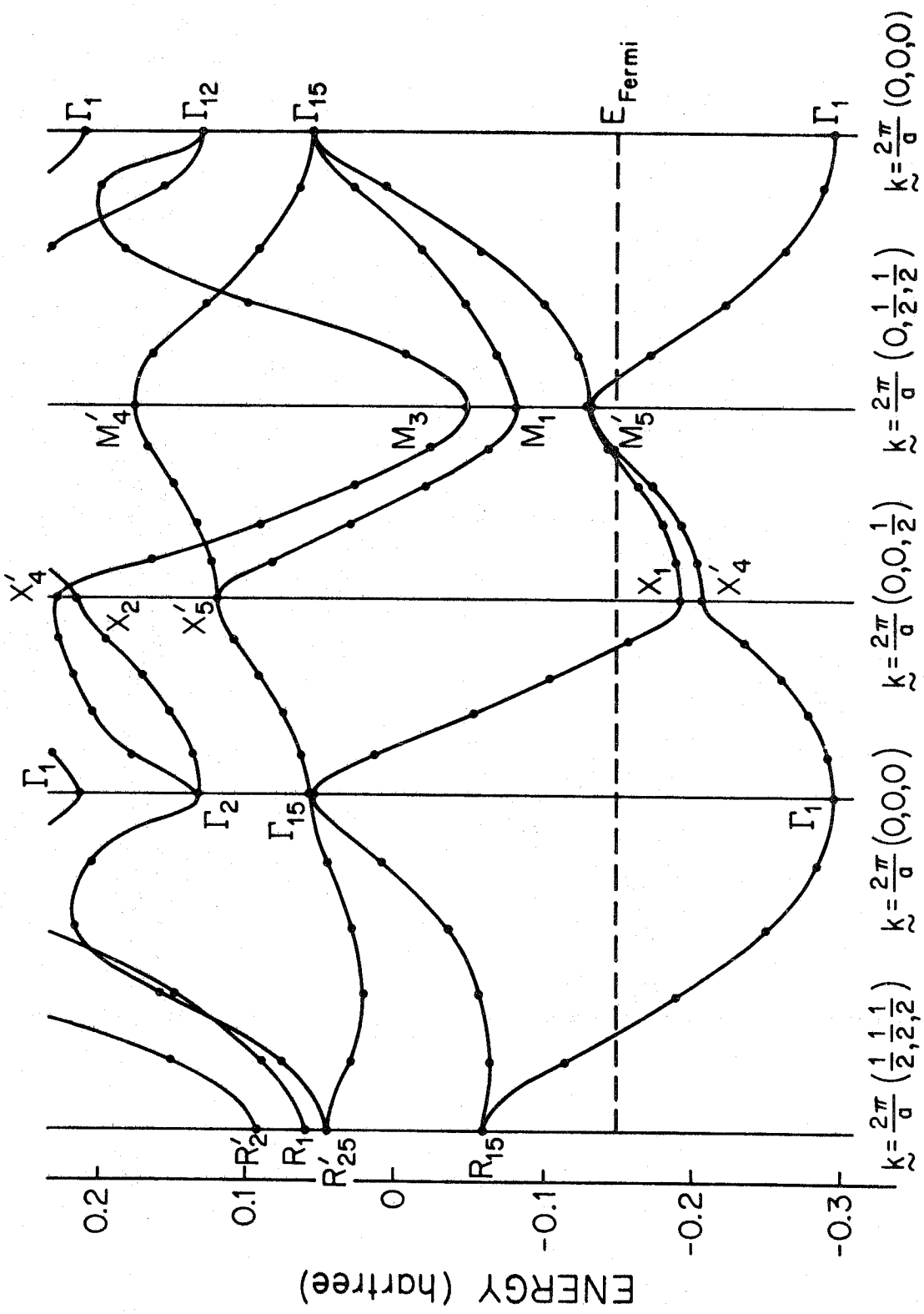
ENERGY (hartree)
0.2
0.1
0
-0.1
-0.2
-0.3
E_{Fermi}
Γ_1
Γ_{12}
Γ_{15}
Γ_2
X'_4
X_2
X'_5
M'_4
M_3
M_1
M'_5
X_1
X'_4
R'_2
R_1
R'_{25}
R_{15}
$k=\frac{2\pi}{a}(\frac{1}{2},\frac{1}{2},\frac{1}{2})$
$k=\frac{2\pi}{a}(0,0,0)$
$k=\frac{2\pi}{a}(0,0,\frac{1}{2})$
$k=\frac{2\pi}{a}(0,\frac{1}{2},\frac{1}{2})$
$k=\frac{2\pi}{a}(0,0,0)$

Fig. 4 The HF energy band structure using GI effective potentials. Lines between symmetry points are only approximate. Solid lines indicate HF bands. Dashed lines indicate how these HF bands map into the smaller GI zone.

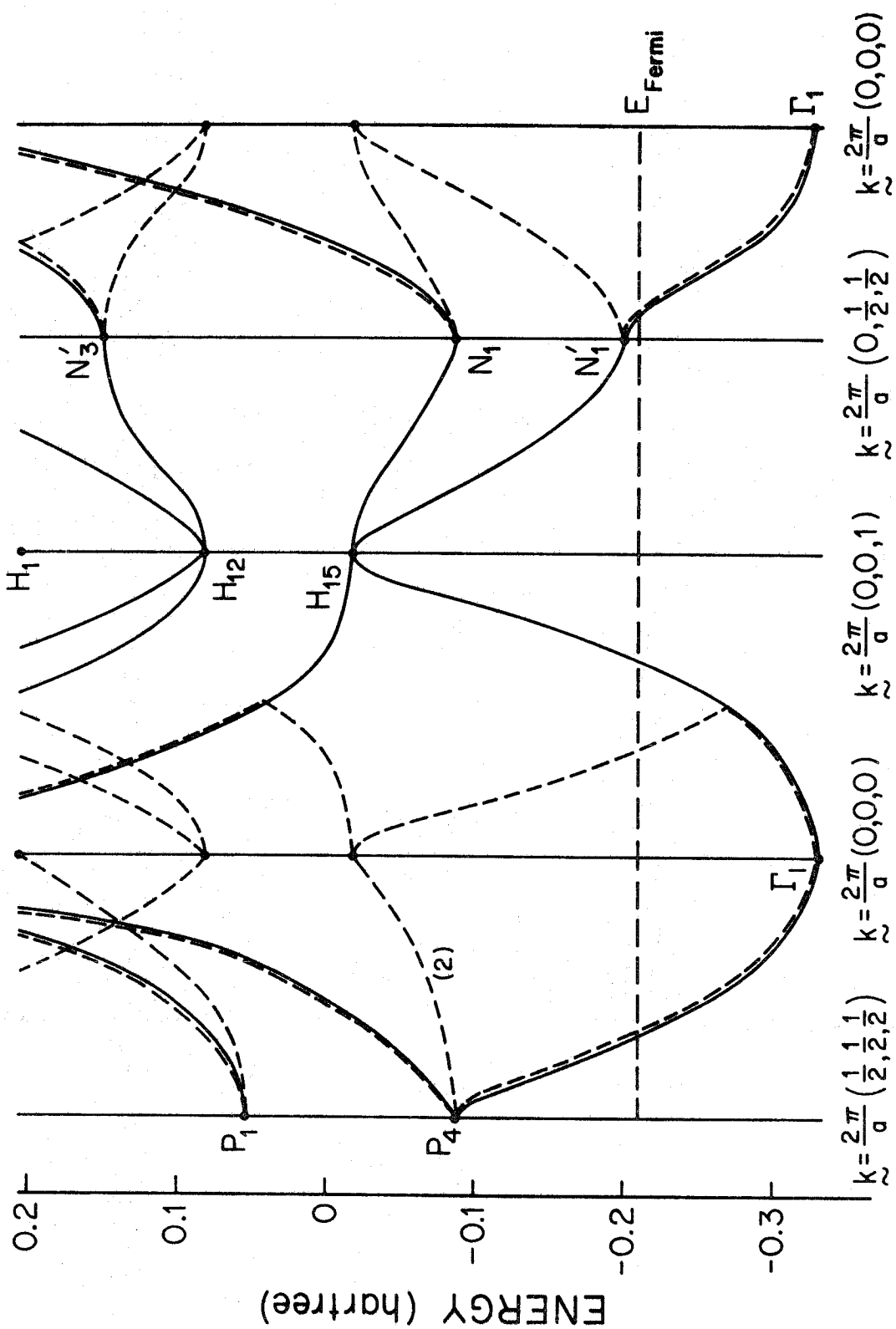
ENERGY (hartree)
0.2
0.1
0
-0.1
-0.2
-0.3
E_{Fermi}
$k=\frac{2\pi}{a}(\frac{1}{2},\frac{1}{2},\frac{1}{2})$
$k=\frac{2\pi}{a}(0,0,0)$
$k=\frac{2\pi}{a}(0,0,1)$
$k=\frac{2\pi}{a}(0,\frac{1}{2},\frac{1}{2})$
$k=\frac{2\pi}{a}(0,0,0)$
P_1
P_4
H_1
H_{12}
H_{15}
N'_3
N_1
N'_1
Γ_1
Γ_1
(2)

Fig. 5 The GI energy band structure for Li in which the b-site interaction is included.

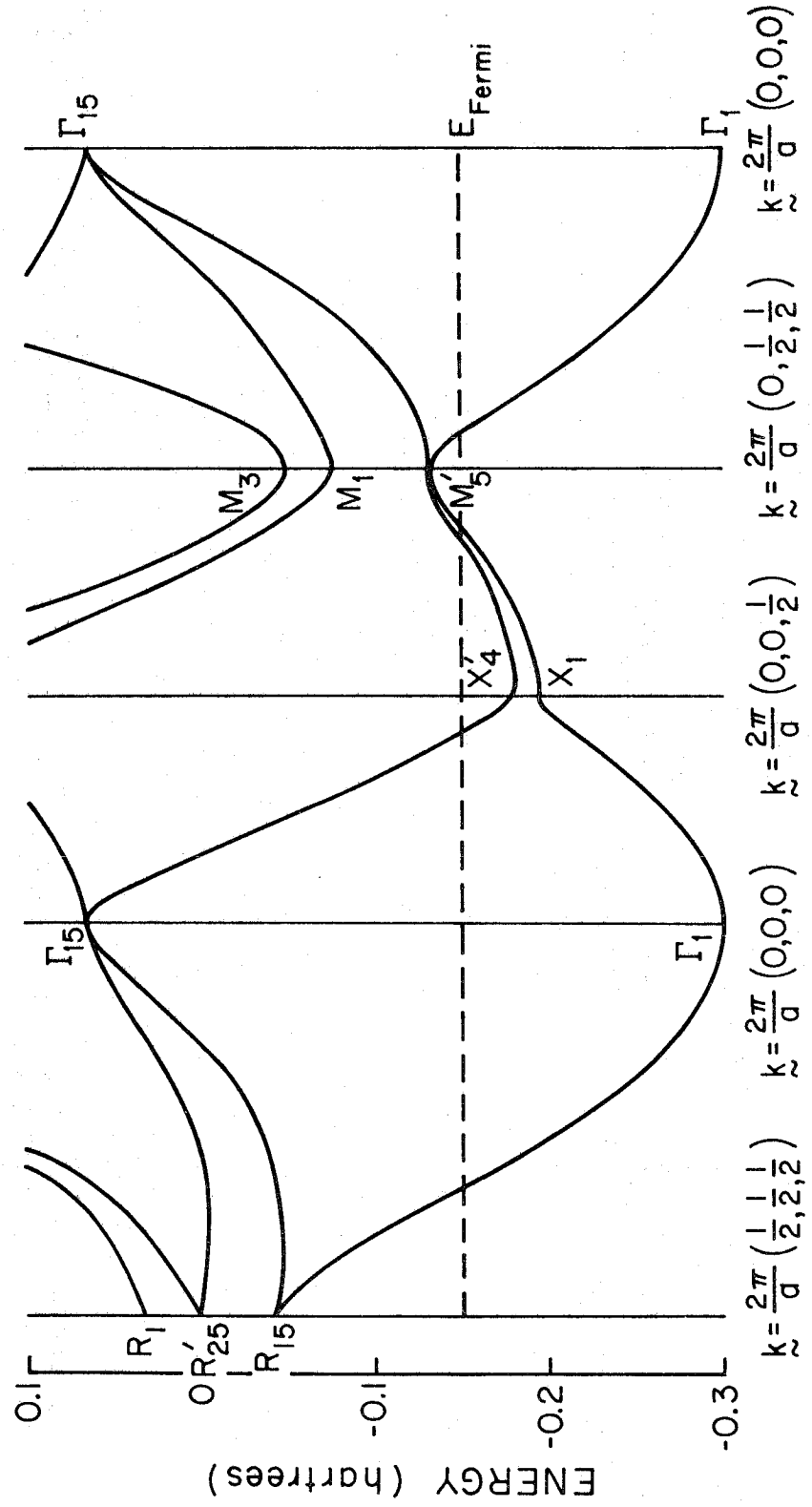
ENERGY (hartrees)
0.1
0
-0.1
-0.2
-0.3
R_1
R'_{25}
R_{15}
Γ_{15}
Γ_1
X_1
X'_4
M_3
M_1
M'_5
E_{Fermi}
$k=\frac{2\pi}{a}\left(\frac{1}{2},\frac{1}{2},\frac{1}{2}\right)$
$k=\frac{2\pi}{a}(0,0,0)$
$k=\frac{2\pi}{a}(0,0,\frac{1}{2})$
$k=\frac{2\pi}{a}(0,\frac{1}{2},\frac{1}{2})$
$k=\frac{2\pi}{a}(0,0,0)$

Fig. 6 Illustration of the types of optical transitions which can occur in HF and the new transitions permitted in GI corresponding to indirect transitions in HF.

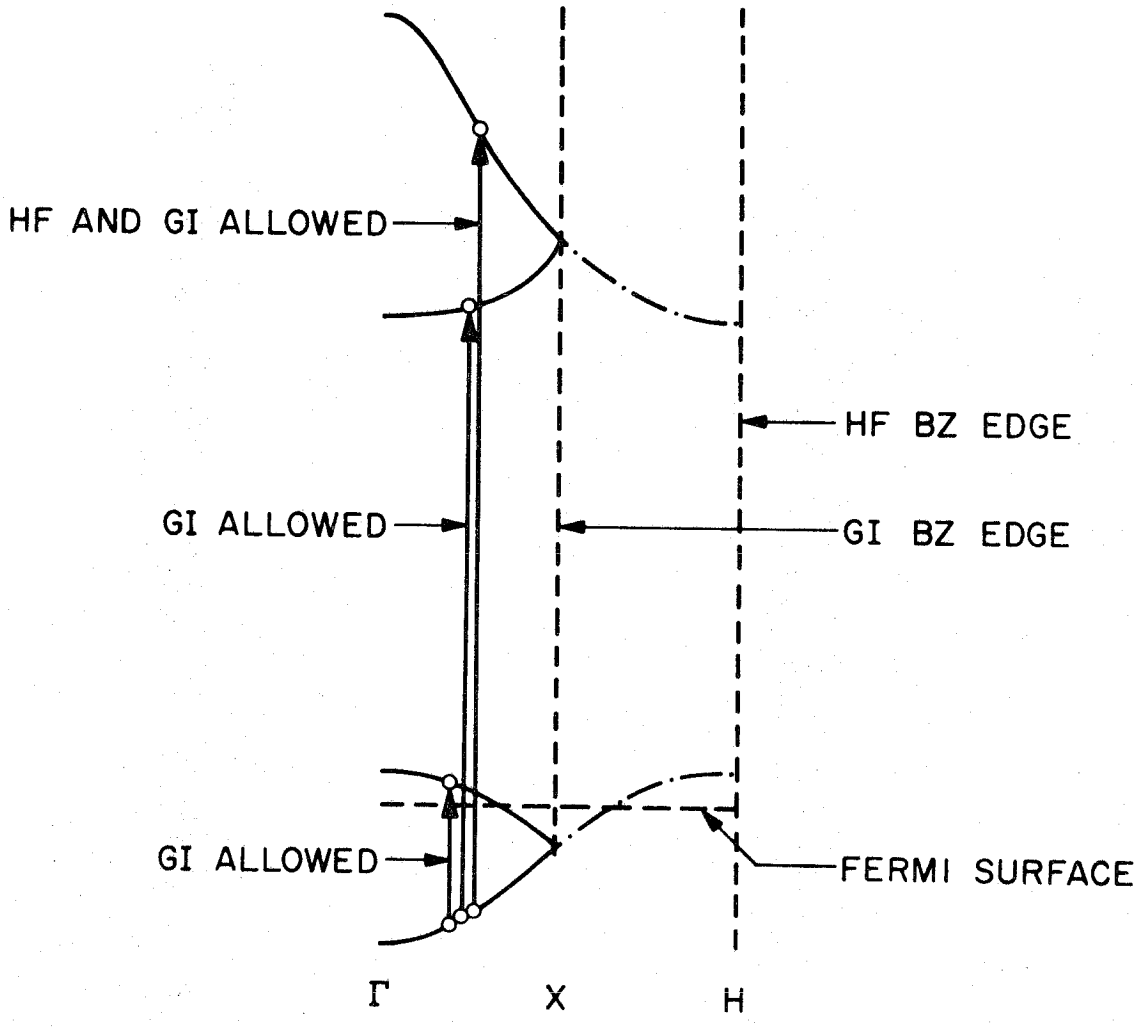
HF AND GI ALLOWED
HF BZ EDGE
GI ALLOWED
GI BZ EDGE
GI ALLOWED
FERMI SURFACE
Γ
X
H

Fig. 7 The experimental soft X-ray emission spectrum for Li and a HF calculated curve reported by Parmenter (1952).

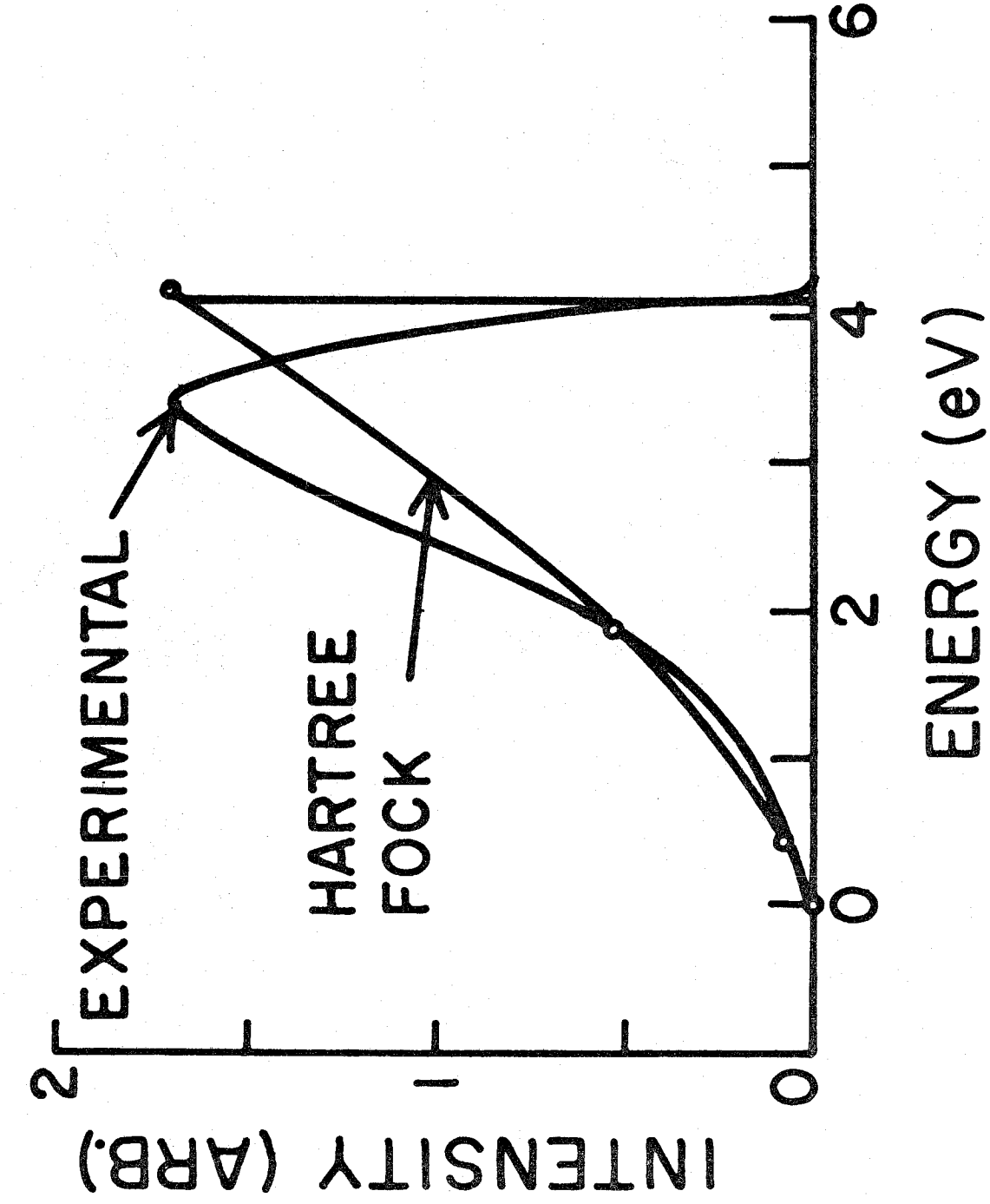
INTENSITY (ARB.)
2
1
0
EXPERIMENTAL
HARTREE
FOCK
0
2
4
6
ENERGY (eV)

Fig. 8 The experimental soft X-ray emission spectrum for Na (taken from Skinner, 1940).

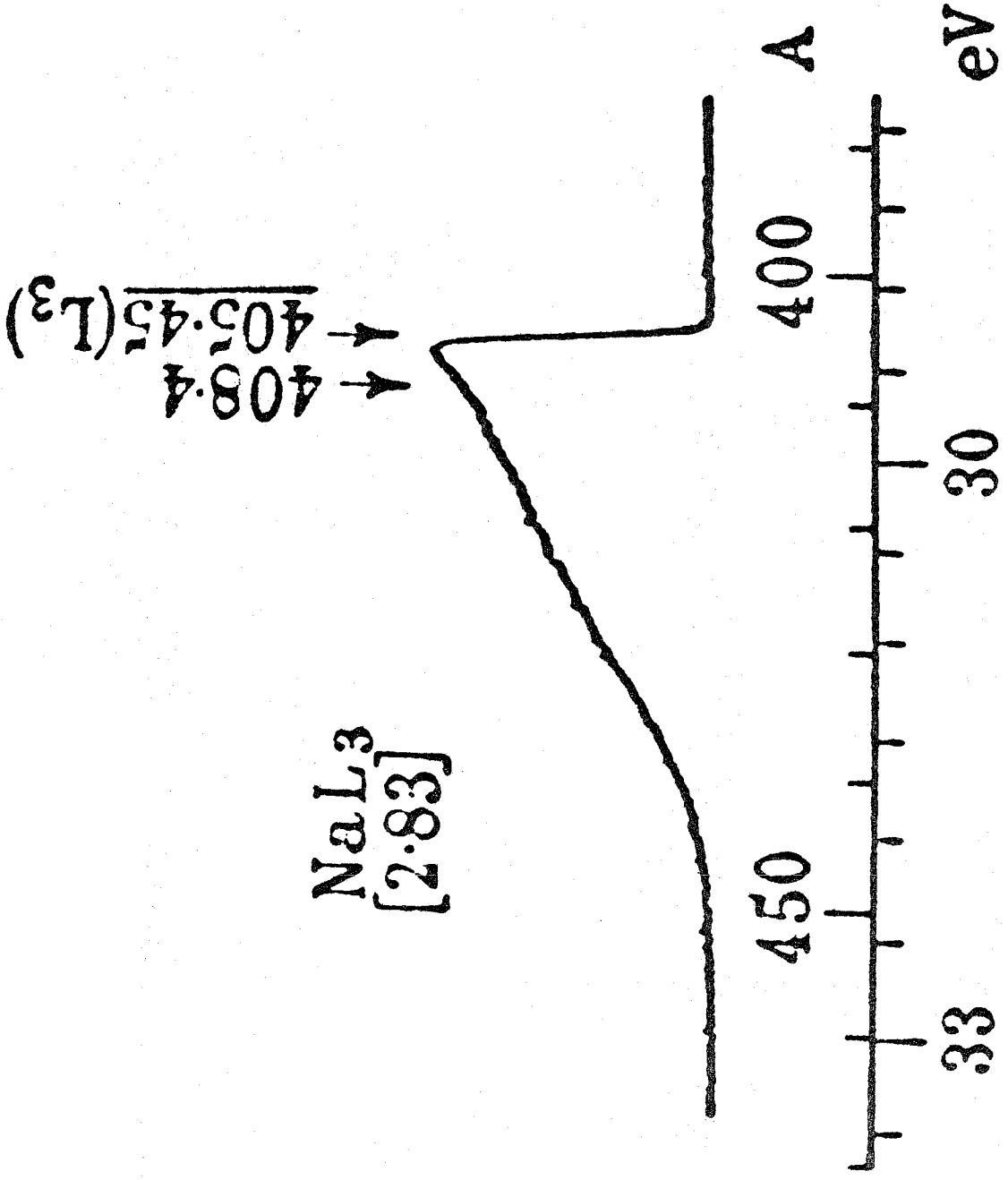
Na L3
[2.83]
408.4
405.45 (L3)
400
450
30
33
A
eV

Fig. 9 The orientation dependence of the cross sectional area in K (reported by Shoenberg and Stiles, 1964).

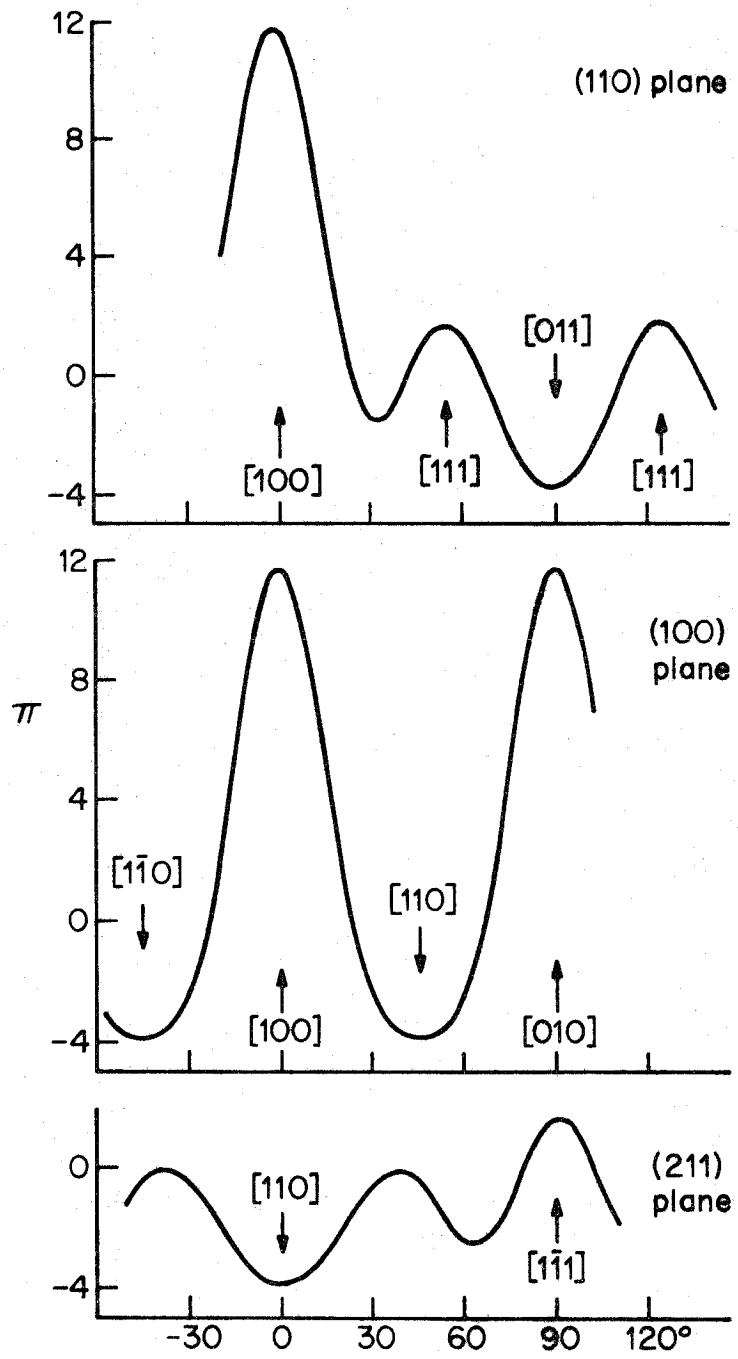
12
8
4
0
-4
(110) plane
[011]
[100]
[111]
[111]
12
8
4
0
-4
π
(100)
plane
[1$\bar{1}$0]
[110]
[100]
[010]
0
-4
(211)
plane
[110]
[1$\bar{1}$1]
-30
0
30
60
90
120°

Fig. 10 Illustration of the types of planar configurations which could lead to cross sectional area extrema in GI.

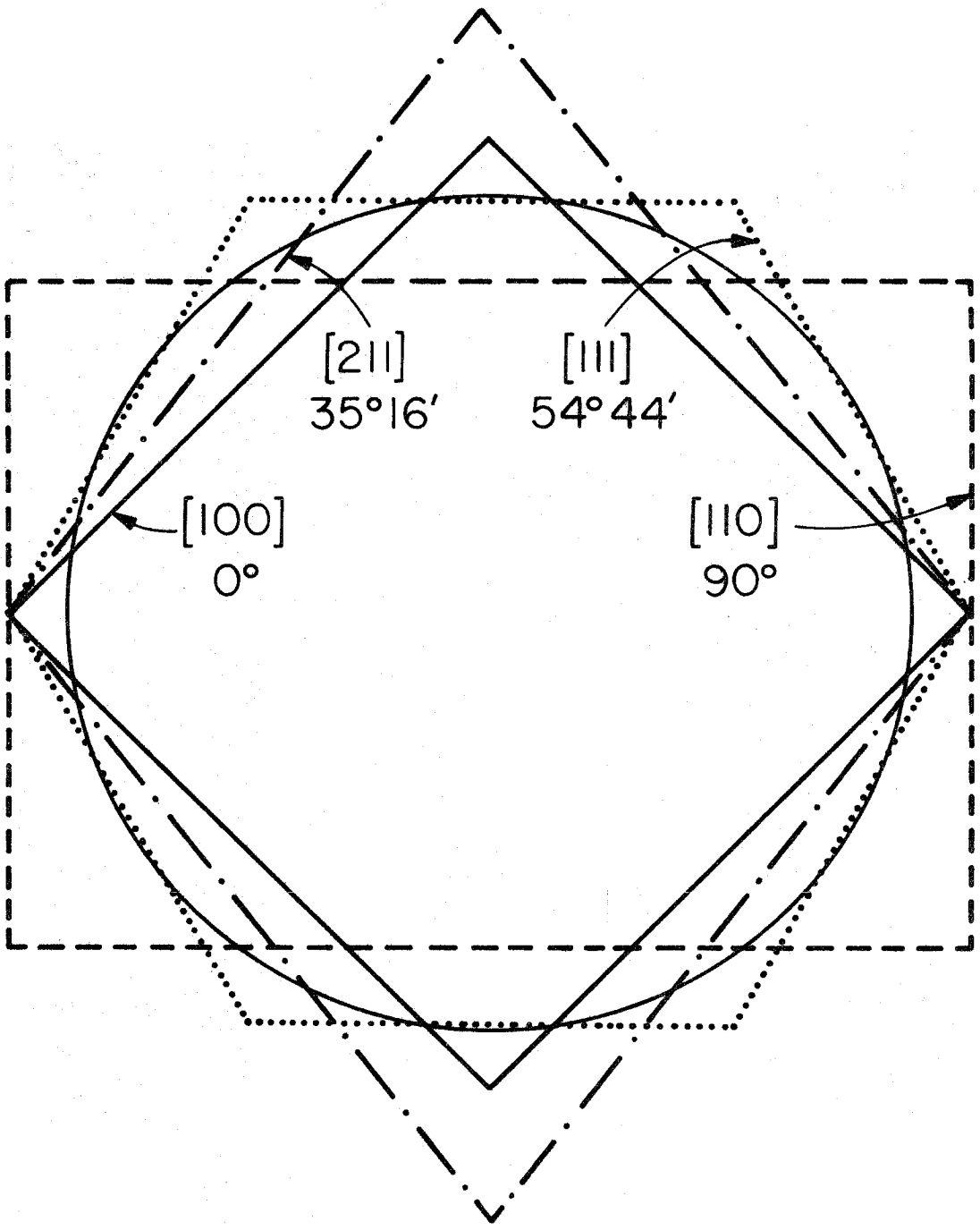

(110) Plane

Fig. 11 Form factors (Fourier transforms) for Li based on integrations over the correct surfaces and over spheres having the same volume. The abscissa is in units of $q/2\,k_f$.

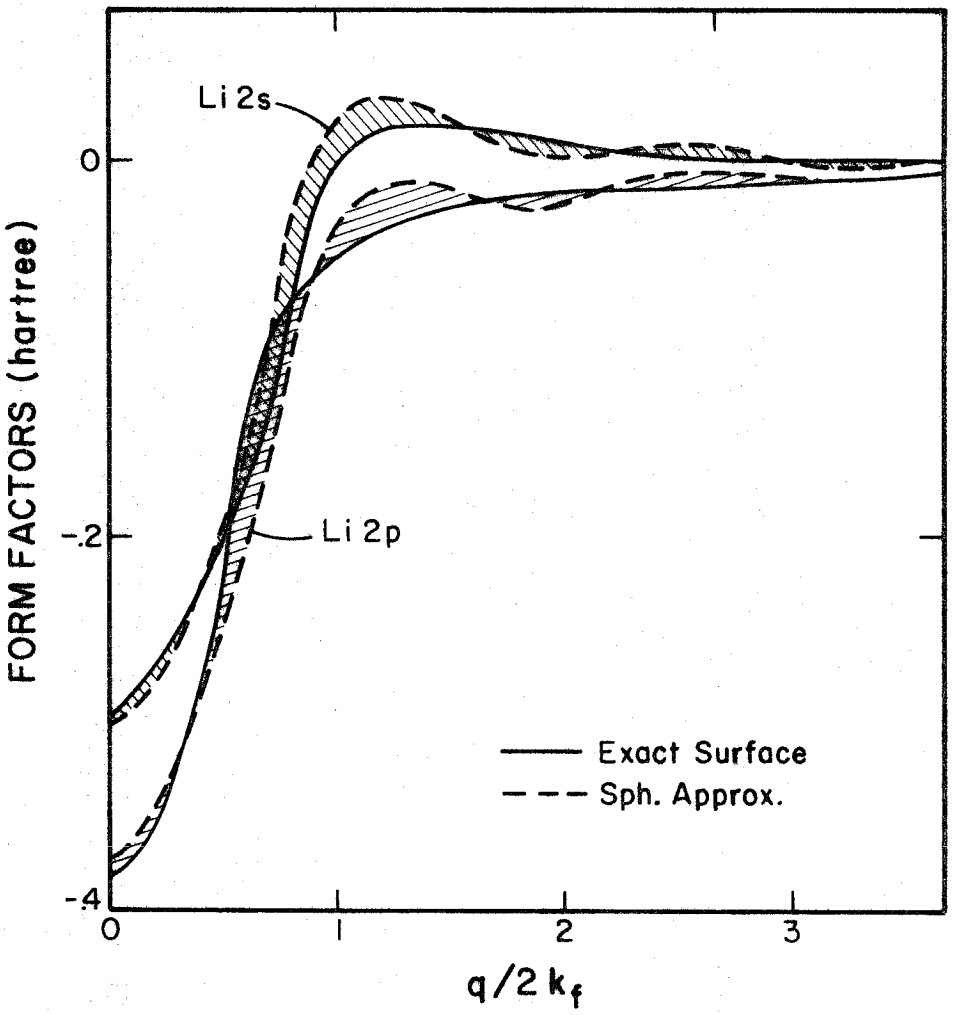
Li 2s
Li 2p
0
-.2
-.4
0
1
2
3
FORM FACTORS (hartree)
q/2 k_f
Exact Surface
Sph. Approx.

II. THEORETICAL EXPLANATION OF THE ANOMALOUS MAGNETORESISTANCE AND HALL EFFECT OF THE ALKALI METALS

A. INTRODUCTION

The behavior of the transverse magnetoresistance (hereafter simply referred to as the magnetoresistance) of the alkali metals has been the subject of some controversy in past years. Numerous experimental studies[1-6] have repeatedly demonstrated a linearity in the magnetoresistance up to fields as large as 60 to 100 kG. However, in the traditional theoretical framework (Hartree-Fock) the Fermi surface is closed and nearly spherical for these metals, and as a result the magnetoresistance should saturate at low fields (since only closed orbits can occur).

In recent years the GI method[7] has been developed for going beyond Hartree-Fock (i.e., including many-body effects) while retaining the convenient orbital interpretation of the wavefunction. This method has been applied to a number of molecules and atoms, in order to study molecular excited states,[8] chemical reactions,[9] and such properties as the hyperfine structure.[10]

We find that the application of this method to body centered cubic alkali metals leads to a splitting of the usual band into two overlapping bands. As a result the Fermi surface is no longer closed and upon applications of magnetic fields unusual magnetic transport properties can result. We find that the resulting behavior of the magnetoresistance and Hall coefficient is in qualitative agreement with the experimental results.

In section B we review some relevant aspects of the GI method and its applications to band structures. In section C we discuss the

calculation of the magnetoresistance and Hall effect including inter-band transitions (magnetic breakdown). In section D we review the experimental results and compare with the theoretical results.

B. THE GI METHOD

In the Hartree-Fock method the total wavefunction is taken as the Slater determinant

$$\mathcal{A}[\phi_1\phi_2\cdots\phi_m\phi_1\phi_2\cdots\phi_m\ \alpha\alpha\cdots\alpha\ \beta\beta\cdots\beta] \qquad (1)$$

with each orbital doubly occupied (once with each spin). In (1) $\mathcal{A}$ is the antisymmetrizer (the determinant operator), electron number is devoted by positions in the product, and α and β are the usual one-electron spin functions. The orbitals in (1) are required to be the best ones, resulting in the variational condition

$$H^{HF}\ \phi_k = \epsilon_k \phi_k\ , \qquad (2)$$

where H^{HF} is the usual Hartree-Fock Hamiltonian (containing Coulomb and exchange operators). For the ground state of an alkali metal H^{HF} has the full translational symmetry of the lattice (body-centered cubic, bcc) and hence the Hartree-Fock orbitals are Bloch functions for all translations R^{bcc} in the bcc space group,

$$R^{bcc}\ \phi_{\underset{\sim}{k}}(r) = e^{i\underset{\sim}{k}\cdot\underset{\sim}{R}^{bcc}}\ \phi_{\underset{\sim}{k}}(r)\ . \qquad (3)$$

One can generally improve upon the Hartree-Fock wavefunction (1) by allowing the up spin orbitals to be different from the down spin orbitals to obtain the unstricted Hartree-Fock (UHF) wavefunction

$$\mathcal{A} \mid \phi_{1a}\, \phi_{2a} \cdots \phi_{ma}\, \phi_{1b}\, \phi_{2b} \cdots \phi_{mb}\, \alpha\alpha \cdots \alpha\beta\beta \cdots \beta \mid . \quad (4)$$

However, even for the ground state, (4) does not describe a pure spin state (eg singlet) unless

$$\phi_{ia} = \phi_{ib}$$

for all i. In order to obtain pure spin states and yet allow the orbitals to split, we must replace the $\mathcal{A}$ (which takes care of the Pauli principle but <u>not</u> the spin symmetry) by the group operator,[11] G_i^{γ}, which has the property that for <u>any</u> set of orbitals

$$G_i^{\gamma} \left[\phi_{1a} \phi_{2a} \cdots \phi_{ma}\, \phi_{1b} \phi_{2b} \cdots \phi_{mb}\, \alpha\alpha \cdots \alpha\beta\beta \cdots \beta\right] \quad (5)$$

it is a pure spin state and satisfies Pauli's principle. The orbitals of (5) are required to be optimum, resulting in self consistent equations similar to (2) but with more complicated exchange terms in the one-electron operators. These optimum orbitals are referred to as the GI orbitals.[7] This method is discussed in more detail elsewhere.[7] It is sufficient to note several points, however.[12, 13, 14]

(1) For Li metal there are two self consistent field equations to solve

$$H_a\, \phi_{ka} = \epsilon_{ka}\, \phi_{ka} \quad (6)$$

$$H_b\, \phi_{kb} = \epsilon_{kb}\, \phi_{kb}$$

(2) The one-electron operators of (6) are expected to have only simple cubic (sc) symmetry and hence the GI orbitals should be Bloch functions only for translations of the simple cubic subgroup of the usual bcc space group. However, translations interchanging corner and center lattice

sites take H_a into H_b and vice versa so that the ϕ_{ka} orbitals are symmetrically related to the ϕ_{kb} orbitals. Consequently, the total many electron wavefunction (5) for the ground state still retains the correct bcc symmetry.

(3) Because of (2) the eigenvalue spectrum of H_a is the same as that of H_b and only one (say the H_a spectrum) need be discussed.

(4) Since H_a has only sc symmetry the Brillorium zone (BZ) for the orbitals is sc and of half the size of the usual bcc BZ.

(5) The energy spectrum of (6) is similar to that of (2), but because of (4) there are two partially occupied bands rather than one as in Hartree-Fock. This is illustrated in Fig. 1 which shows the band structure for k-vectors in the [001] direction. Note that the second GI band has been mapped into the second sc BZ in order to compare with the Hartree-Fock band. The major difference here is an energy gap within the first bcc BZ.

The differences in the Fermi surfaces for the Hartree-Fock (HF) and GI bands are illustrated in Fig. 2 and Fig. 3, which show the cross-sections in the (001) and (110) planes. At low fields the semi-classical descriptions of the motion of a wavepacket in k-space would in each case be essentially a closed circle for the Hartree-Fock band structure. However for the GI band structure and B ||[001] we obtain closed hole orbits and closed electron orbits. For B || [110] we obtain closed electron orbits and an open orbit. Thus, these band structures should lead to drastically different magnetic properties as will be discussed in the next sections.

Before proceeding we should note that since the spin symmetry is correctly taken into account there are no spin density waves as would occur in the UHF method.

C. MAGNETORESISTANCE AND MAGNETIC BREAKDOWN

As was noted from Fig. 2 and 3 the classical orbitals in the presence of small magnetic fields are quite different for Hartree-Fock and GI. Further differences arise from GI because of the small energy gaps (~ 0.1 eV) separating the first and second occupied bands. As a result magnetic breakdown (interband transitions) become important even for small fields, (e.g., 2 kG). Because of magnetic breakdown the closed orbits of Fig 2b become extended at intermediate fields and eventually at sufficiently high fields the orbits are effectively as in Fig. 2a. Similarly, for even small fields the open orbits in Fig. 3b are made finite and eventually for sufficiently large fields the orbits become circular as in Fig. 3a.

1. The Semi-classical Description

The semi-classical (LAK) description[15] derives from the assumptions that the electrons behave classically and can be treated by Fermi Dirac statistics. That is, there is no restriction on the type of dispersion relation followed. Thus the results should be quite general. Nevertheless in the high field limit when the electrons are confined to single orbits only two types of behavior are expected. For the case where only (uncompensated) closed orbits exist, saturation to a constant resistivity is the expected high field behavior. If open orbits or compensated ($n_e = n_h$) closed

orbits are present then the transverse component is predicted to exhibit a quadratic field dependence. Similarly the Hall resistivity should be linear with field, with a Hall coefficient $1/[(n_e-n_h)ec]$ for uncompensated closed orbits.

This theory has had some success in explaining the transverse behavior of the high field magnetoresistance for many metals, (e. g., the anisotropy exhibited by the noble monovalent metals Cu, Ag, Au, and numerous divalent and trivalent metals),[16] but has been conspicuously inept in accounting for the observed linearity of the magnetoresistance of the alkali metals, often thought to be the simplest of metals. It has, however, been shown[17] that other types of behavior can result when small energy gaps are present to allow magnetically induced interband transitions (hereafter called magnetic breakdown). In the HF band description of the alkali metals there is only one partially occupied band, and hence magnetic breakdown is not relevant. However, these effects can be quite important for the GI band scheme.

We will briefly review the semi-classical theory of magnetoresistance and the modifications resulting from the incorporation of magnetic breakdown. From the equations of motion of an electron in a magnetic field.

$$\dot{\underset{\sim}{k}} = \frac{e}{\hbar c}(\underset{\sim}{v} \times \underset{\sim}{B}), \qquad \underset{\sim}{v} = \nabla \mathcal{E} \tag{7}$$

We can consider the electron to move along a constant energy trajectory with its momentum component in the direction of the field and its energy conserved. Inserting the electric field, the Lorentz force becomes

$$\hbar \underset{\sim}{k} = \frac{e}{c}(\underset{\sim}{v} \times \underset{\sim}{B}) + e\underset{\sim}{E} \quad . \tag{8}$$

Assuming that the system can be described in terms of an electron distribution function varying in space and time,

$$f_k(\mathcal{E}, k_B, t) = f_o(\mathcal{E}) + g_k(\mathcal{E}, k_B, t), \tag{9}$$

where f_o is the Fermi Dirac distribution function, and k_B is the wave vector in the direction of the field $\underset{\sim}{B}$, a steady state Boltzmann equation is obtained

$$\frac{g_k}{\tau} + \frac{dg_k}{dt} = -e\underset{\sim}{E} \cdot \underset{\sim}{v} \left(\frac{df_o}{d\mathcal{E}}\right) \quad , \tag{10}$$

where we have assumed an isotropic relaxation time.[7] The solution to this equation results in the conductivity tensor[18]

$$\sigma_{ij} = -\frac{e^2}{4\pi^3} \int_{\underset{\sim}{k}} v_{k_i} \frac{\partial f_o}{\partial \mathcal{E}} \, d\underset{\sim}{k} \int_{-\infty}^{t(k)} v_{k_j}(t') \exp\left(\frac{t'-t}{\tau}\right) dt' \quad , \tag{11}$$

where the volume integral is over all occupied $\underset{\sim}{k}$ states and the path integral has been converted to a time integral.

This form of the conductivity was derived assuming that the electrons were confirmed to a single orbit. If the Fermi surface touches or intersects the Brillorium zone and if the energy gaps at the point of intersection is small, we may have interband transitions (magnetic breakdown) in the presence of large magnetic fields $\underset{\sim}{B}$. It has been shown[19-21] that the probability of breakdown is significant if the interorbit energy gap satisfies the condition

$$\frac{C\mathcal{E}_g^2\, mc}{\mathcal{E}_f e B \hbar} = \frac{C\mathcal{E}_g^2}{\mathcal{E}_f \hbar\omega_c} \leq 1 \ , \tag{12}$$

where $\mathcal{E}_g$ is the energy gap, $\mathcal{E}_f$ is the Fermi energy,

$$\omega_c = \frac{eB}{mc}, \qquad C = \frac{k_f^2}{8\hat{K} \cdot (\hat{k} \times \hat{b})} \ ,$$

$\hat{b}$ is the unit vector in the direction of $\hat{B}$, $\hat{k}$ is the vector at the energy gap, and $\hat{K}$ is the reciprocal lattice vector corresponding to the energy gap. The probability of transition between orbits is

$$P = e^{-B_o/B}, \qquad \text{where } B_o = \frac{C\mathcal{E}_g^2\, mc}{\mathcal{E}_f e \hbar},$$

or defining $\omega_o = \frac{C\mathcal{E}_g^2}{\mathcal{E}_f \hbar}$ we obtain

$$P = e^{-\omega_o/\omega_c} \tag{13}$$

Thus the probability of continuing along the next segment of the same closed orbit, that is, making no transition, is given by Q = 1-P.

Falicov and Sievert[22] have developed a method for incorporating this behavior into the theory by rewriting the Chambers path integral equation (11) as

$$\sigma_{ij} = -\frac{e^2 m\omega_c}{4\pi^3\hbar^2} \sum_{\ell=1}^{n} \int_0^{\infty} \frac{\partial f_o}{\partial \mathcal{E}}\, d \int_{-\infty}^{\infty} dk_z \int_0^{t_o} v_i(t', \ell)\, I_j(t', \ell)\, dt', \tag{14}$$

Where the path has been broke into m segments, ℓ, of equal length (transit time t_o).

$$I_j(t', \ell) = e^{-t'/\tau} \{ \int_0^{t'} v_j(s', \ell)\, e^{s'/\tau}\, ds' + K_j(\ell) \} \tag{15}$$

and

$$K_j = e^{-t_o/\tau} \{ [\, I - Me^{t_o/\tau}\,]^{-1} - I \}\, V_j \tag{16}$$

where I is the identity matrix ($n \times n$), n is the total number of independent branches necessary to account for all possible paths in the reduced zone,

$$V_j(r) = \int_o^{t_o} v_j(s', r)\, e^{s'/\tau}\, ds'; \; r = 1, 2, \cdots n \qquad (17)$$

and τ is the zero field relaxation time. In (16) the ($n \times n$) matrix M determines the probability of transition to various branch points at the termination of traversal of each segment. That is, the matrix elements M_{ij} represents the probability that an electron just leaving segment j will appear in segment i. Thus, it may assume one of the values 0, 1, P, Q.

These expressions can be generalized to different length path segments by allowing the time of the $\ell^{\underline{th}}$ branch to be variable (call it $t_{o\ell}$), and multiplying each matrix element in M by the appropriate $e^{t_{o\ell}/\tau}$. If we assume that the Fermi surface is nearly spherical (as has been established experimentally and theoretically for the alkalis) and hence that we have nearly free electron behavior at the surface, then the total velocity vector will have the same magnitude at all points on the surface (except in the regions near the energy gaps which because of their small size will result in minimal distortion, here neglected). Then $\hbar \underset{\sim}{k_f} = m \underset{\sim}{v}$, implying $|v| = \frac{\hbar |k_f|}{m}$. Since electrons are driven around orbits at the frequency of the applied field, then the time for traversing one orbit segment is θ/ω_c, where θ is the angle subtended by a given branch. Having divided t into increments of $t_{o\ell}$, then we can write $\theta_\ell = \theta(t_\ell)$ and since $v_x = v_\perp \sin\theta$ and $v_y = v_\perp \cos\theta$, we can write $v_i = v(t_o, \omega_c, \theta_\ell)$. Thus the conductivity integral for any k_z (where $\underset{\sim}{B}$ is taken to be in the z direction) becomes analytic, and it is necessary only to integrate over k_z ($-k_f$ to k_f). Of course, for each slice, Δk_z, the

number of segments (i.e. the dimension ℓ), the probability matrix, and the θ_ℓ's may vary.

2. The Model

As an example of the types of orbits encountered, figures 2b and 3b illustrate the maximal orbits for the GI Brillouin zone and Fermi surface of the bcc alkali metals with the field oriented along the [001] and [110] axes,respectively.

However, the k-space orbits may have different geometries for other k_z (we must consider all k_z in the range $|k_z| \leq k_f$). The three dimensional geometries corresponding to the [001] and [110] field orientations are illustrated in Figure 4. Here we see that the various Fermi surface sections (perpendicular to the field), can be approximated by a series of cylindrical discs. Two dimensional cross sections for the various types of orbits encountered for these two orientations are shown in Figure 5.

It is to be noted that we have what would generally be considered a compensated system, that is, the "number of electrons" in the second GI zone is equal to the "number of holes" in the first zone. However, consideration of Figure 5 illustrates that in general there is a portion of the volume in the first zone which cannot be counted as contributing to the "hole volume." That is, $n_e \neq n_h$. There is a significant part of the first zone which has closed electron orbits, and this volume varies with field direction. Hence $(n_e - n_h)$ for $\underset{\sim}{B} \perp (001)$ and (110) are different (although for the (110) case the definition of such effective carriers is obscured by the presence of the open orbit section). However, the distinct difference in behavior will become apparent when the results of our calculations of

the Hall coefficient are discussed.

3. Results

We have applied the above formalism to calculations of the magnetoresistance tensor for the model described. Thus the available parameters are the lattice constant, a, the relaxation time, τ, and the energy gap, $\mathcal{E}_g$.

Lattice constants appropriate for lithium, sodium, and potassium were used.[23] GI energy band structure calculations[12] on lithium and preliminary calculations on sodium indicate that the band gaps for these metals are on the order of from .08 to .15 eV. It is anticipated from experimental properties, [24, 25] and theoretical[26] considerations that the gap in potassium is somewhat smaller. Hence, to determine the sensitivity of the magnetoresistance components to the gap size, values from 0.02 to 0.15 eV were investigated for all three lattice constants.

A study was also undertaken to test the dependence of the curves on the relaxation time. This is of particular interest since experimentally the crystals used possess a wide range of residual resistivity ratios (RRR), and any significant dependence on this quantity should be reflected in the experiments. Actually the longitudinal component should be more directly related to the relaxation time, but this quantity is not so directly relatable to the topology of the Fermi surface and the theory has not been fully explored.

In Figure 6a we show the transverse components for lithium with the field oriented in the [001] direction, using four energy gaps 0.02, 0.04, and 0.1 and 0.15 eV, while Fig. 6b shows the corresponding

curves for the field along the (110) axis. In Fig. 6a the diagonal components, ρ_{11} and ρ_{22}, are equal. As can be seen, the gap size determines the field at which onset of breakdown occurs and the breath of the field range over which extended orbits predominate (leading to the observed pseudo-linearity). It is important to notice that saturation does occur, but not until quite high fields when the gaps are large. The larger the energy gap, the greater will be the percentage change in resistance relative to zero field at saturation. Another important feature is the behavior of ρ_{22} with the field in the [110] direction (Fig. 6b). The field dependence of this component deviates markedly from the behavior observed in the others. As we saw in Fib. 3b this direction has a maximal open orbit in the first zone. Hence ρ_{22} exhibits an initial quadratic behavior. However, the onset of interband transitions leads to finite sized orbits so the resistivity cannot go asymptotically to infinity, but begins to drop off as electron paths are randomized, and finally for larger fields, ρ_{22} saturates. Again the gap size controls how far the resistivity increases before the onset of breakdown. In lithium the resistance peak for the 0.1 eV gap exceeds that corresponding to the 0.02 eV gap by a factor of 140.

The similar plots for lattice constants appropriate to sodium and potassium are shown in Figures 7 and 8. The general features are the same as seen in lithium, but since the lattice constants of Na and K are larger, we find that larger fields are required to obtain the same effects as in Li (for the same $\mathcal{E}_g$). Thus in potassium a gap of .02 eV corresponds roughly to a gap of .04 eV in lithium. In potassium

a gap of .04 leads to an approximately linear field dependence from 15 → 50 kG for all components except ρ_{22} (110).

Now we will consider the dependence on the relaxation time, τ. Throughout the calculations we have assumed that τ is isotropic, the same for small orbits as for the large post breakdown orbits. We have looked at the magnetoresistance tensor using relaxation times appropriate to the experimentally studied specimens of these alkalis. In Figure 9 a, b, we show the τ dependence of lithium for $\mathcal{E}_g$ = .04 eV using τ = 0.05, 0.3, 0.7, and 1.3 (in units of 10^{-10} sec). Similar behaviors are seen for the other tensor components and other gap sizes. Corresponding curves for potassium are shown in Figure 10 a, b. We see that for relatively large relaxation times, little difference among the curves is observed. However, as the relaxation time decreases to a value such that $\omega_c\tau \lesssim 1$, differences in the behavior become apparent. This is because $\omega_c\tau$ (B) does not attain a value of 1 until fields which are already in the extended orbit region. That is, an electron cannot complete transversing an orbit before it is scattered and thus may not have an opportunity to undergo breakdown. For high τ, as long as $\omega_c\tau \gtrsim 1$ before the onset of breakdown, the resistivities are similar. The only component which demonstrates a significant sensitivity to τ is ρ_{22} (110) for which the open-orbit quadratic field dependence enhances the τ dependence, showing that the onset of the extended orbit region is slightly different for different τ.

The remaining tensor component to consider is the Hall resistivity (proportional to ρ_{21}). This is shown for lithium in Figure 11 for different gap sizes. Sodium and potassium ρ_{21} field dependences are shown in Figures 12 and 13. Here we see a low field linear region, an intermediate sloping

off, and an asymptotic linear region. The theory predicts that the Hall coefficient (the slope of ρ_{21}) should be $R_{II} = \frac{1}{ne}$ (in emu) where n is the effective number of electrons per unit volume. A simple calculation shows that the high field asymptotic slope in all the figures corresponds to n_e = 1 electron/cell volume which is the expected value for closed circular free-electron-like orbits. This is just the asymptotic condition under total magnetic breakdown. Hence, it is only in high fields (the magnitude of the required field being determined by $\mathcal{E}_g$) that the free electron value of the Hall coefficient should be observed. At low fields, the slope varies with the directional orientation of the field and should always be greater than asymptotic value. Since $n = n_e - n_h$ in the two band scheme, the first zone always has some hole orbits. Consequently $n < n_{fe}$ and for low fields R_H should be larger than the free electron value (unless n_h exceeds n_e in which case R_H is negative). Again, the low field slope depends on the topology of the surface in the particular B orientation.

D. Comparison with Experiment

1. Experimental Observations

Numerous experimental studies over the past forty years have been conducted to investigate the transverse magnetoresistance of the alkalis. Early workers[4, 5] using probe techniques and polycrystalline samples, obtained large Kohler slopes $\frac{\Delta\rho}{\rho}_{\omega_c\tau}$, a behavior inexplicable within the traditional theory. Rose[2] investigated Na, Li, and K using probeless helicon techniques and still observed a linear field dependence up to quite high fields although the slopes were somewhat smaller than

those previously obtained, perhaps implying that part of the linearity was attributable to the probes.

More recently, several experiments have been reported on potassium investigating the behavior of the magnetoresistance of single crystals and the effects of strain and inhomogeneities on the apparent transverse linearity. Penz and Bowers[1](1968) using the helicon method found that single crystal potassium exhibits a linear magnetoresistance up to 60 kG and polycrystalline samples up to very high fields (~ 110 kG) with no indication of saturation and that the Kohler slopes varied with crystal orientation. By subjecting their samples to various stresses effecting up to a 27% increase in strain, they found an enhancement of the Kohler slope by as much as a factor of 3. Since their experimental technique utilized probeless samples under minimum stress, it was concluded that these factors were not the basic cause of the anomalous behavior.

Babiskin and Siebenmann[6] (1969) studied the magnetoresistance of potassium to determine the effect of Fermi surface anisotropy. In their experiments they observed a knee in the curves at about 10 kG and attributed the large subsequent linear component to classical geometric effects and non-uniform current distribution. Upon subtracting out this presumably spurious linear component, the resulting curve exhibited saturation of the magnetoresistance at about 10 kG with a $\frac{\Delta\rho}{\rho}$ of 2.2% at 4.2°K which they interpreted as due to mean free path anisotropy resulting from Umklapp processes.[27]

However, some recent studies on potassium by Taub and Bowers[28] indicate that this interpretation may require revision. They have

investigated the effect of annealing on very pure samples and find that this leads to an increase in the Kohler slope, implying that strain actually decreases the slope. (Their $\frac{\Delta\rho}{\rho_o}$ is ~ 100% at 100 kG). They also observe a knee at about 5 kG but note that its occurrence and shape correlates with the RRR. In addition they report evidence for size effects affecting the resistance in very pure samples. Thus it would appear that the influence of size effects, inhomogeneities, and strain need to be better characterized before any unambiguous conclusions on the intrinsic behavior of the magnetoresistance of the alkalis can be made. In view of the inconclusive nature of the results thus far on K, an interpretation based on the theoretical implications as put forth in this paper can only be qualitative and postulatory. But clearly the theory does lead to a description capable of accounting for the observed behavior. We will now examine these observations in light of our theoretical results.

2. Theoretical Interpretation

We have found that going beyond HF leads to a two band scheme in which small gaps occur at the Fermi surface. In the presence of high magnetic fields, interband transitions across these gaps can occur, resulting in a markedly different field dependence than expected on the basis of the LAK theory. In particular, for the simple cubic geometry of our model, most field directions result in a large field range over which the magnetoresistance is linear. However, with the field oriented perpendicular to the (110) plane an open orbit is present which leads to a ρ_{22} component with an initial quadratic field dependence. Breakdown then leads to a decrease in ρ_{22} with field until saturation is attained.

Most of the experiments discussed in the last section used polycrystalline samples, which means that the observed behavior represents an average over the orientations of the crystallites. In this context the knee observed at ~2-7 kG could result from the contribution of the open orbit to the average. The peak is generally sharp and occurs prior to the long linear region characteristic of other orientations. When sample purity is such that $\omega_c\tau$ is $\lesssim 1$ in the region where this peak would occur, it disappears from the spectrum. (See Fig. 9-11). This means that an electron cannot complete traversing an orbit before it is scattered, and the concept of an orbit becomes obscure. The same effect occurs in the remaining components for small τ at the lower fields, but the higher field linearity is still obtained. Experimentally (for polycrystalline samples) the linear region in K extends to ~100 kG; from our calculations this would require a gap size of .05 to .06 eV (based on the [100] direction). However, as the gap increases, the field for the onset of this pseudolinearity increases. Of course, different orientations and hence different orbit geometries could lead to significant changes in the extent of this linear range. Penz and Bowers[1] in their study of single crystals observed a linearity from 10 to 60 kG for different orientations with quite different average Kohler slopes (the averages were based on widely scattered slopes). Although they did experiments with the field in the [110] direction, they reported only a linear dependence. However, the helicon technique only measures an average of ρ_{11} and ρ_{22}, and it is possible that slight misorientations could mask the quadratic dependence.

This theory does not treat the effects of strain or inhomogeneities on the magnetoresistance, but if in fact decreasing strain does increase the Kohler slope, the dramatically larger slopes which we obtain as opposed to those observed may not be unreasonable.

In this regard theoretical considerations might also be relevant. There are several approximations and assumptions inherent in the theory we have presented. It might well be the case that the relaxation time is $\underset{\sim}{k}$-dependent or that various scattering mechanisms have field dependent probabilities. These possibilities would introduce significant complexities into the theoretical description. One prime factor subject to improvement is the form of the expression for the interband transition probability. Small changes here could have large effects on the conductivity tensor. In particular, local orbit geometries in the immediate neighborhood of the gap could significantly affect the transition probability making some orientations much more favorable than others. These possibilities are under investigation.

Hence, this theory does provide a qualitative explanation of the observed behavior of the transverse magnetoresistivity. Other explanations have also been put forth to explain this behavior. Reitz and Overhauser[29] has suggested that charge density waves would produce heterdyne gaps in the band structure which would undergo magnetic breakdown, possibly accounting for this anomalous magnetoresistance. However, this description required a considerably distorted pear-shaped Fermi surface in disagreement with the de Haas van Alphen experiments[26] which indicate the surface to be quite spherical. Ashcroft[30] has also postulated a 'super lattice' possibly due to strain which would lead to a description similar

to ours. Young[27] has considered the possibility of Umklapp scattering and has parametrically included this mechanism in the theory. His model was a simple cubic lattice in which the Fermi surface was spherical and came in close enough proximity of the BZ to cause a mixing with states in the adjacent cell thus producing phonon-assisted Bragg reflections. He considered "hot spots" (points nearest the zone boundary) as the only regions where such mixing was allowed. To achieve a description approximating the experimental curves for K, he had to assume values for his parameters which implied a solid angle of "hot spot" area which was extremely small (10^{-5}) and a value for the transition probability constant,~ 10^{18}. The expression for the transition probability should contain a proportionality factor of $(K/q)^2$ where K is the smallest reciprocal lattice vector length and q is twice the distance from the surface to the nearest zone face. This implies the Fermi surface must be on the order of 10^{-9} a_o away from the zone boundary. For the body centered cubic structure of the alkalis, this would require that the Fermi surface be quite distorted, since a sphere would be 18% away from the edge. Such a surface seem unrealistic in view of band calculations[26] and other experimental evidence.[24, 25] Of course, such considerations may be pertinent in the GI band scheme since it is in direct contact with the BZ in some regions (here there is no need to resort to a non-spherical Fermi surface).

3. The Hall Coefficient - Experimental

Elementary transport theory leads to an expression for the Hall coefficient, $R = 1/ne$ (in emu), where n is the effective carrier density. Since a closed spherical Fermi surface is thought to be a good model

for the alkali metals, R is simply determined using n - 1 electron per atom. However, experimental studies have indicated that R in fact decreases in very high magnetic fields.[32, 33, 37] Chambers and Jones[31] (1962) using the helicon method also report a significant decrease (about 5%) in the Hall coefficient in the region of 3 to 7 kG. Extrapolating these values to the high field limit they obtained values of R 5% higher than for free electron value. However, Goodman[32] (1968) repeated the experiment using a more accurate treatment of the boundary value problem and found that in the range of 25-35 kG the Hall coefficients for Na and K were within 0.5% of the theoretical value. Penz[33] (1968) also studied the field dependence of the Hall coefficient of K and reported a decrease of ~5% in the field range from 20 to 100 kG. No measurement of the absolute value was made.

The above measurements were all conducted at about 4°K, and for Li and Na are complicated by the martenistic transformation which they undergo at low temperatures. However, measurements of the Hall coefficients of the alkalis have been made between liquid nitrogen and room temperatures and a study of their pressure dependence was carried out by Deutsch, Paul, and Brooks[34] (1961). At room temperature they reported that the number of effective charge carriers, n*, decreased by 5% for Li, 6% for Na, 6-8% for K, and 8% for Rb as the pressure is increased to 15,000 kg/cm^2. For Cs n* passed through a 7% minimum at 5000 kg/cm^2 to increase to a value 20% higher at 15,000 than at atmospheric pressure. They also reported Hall coefficients at room temperature (at ~6 kG) which were higher than the free electron values by 15%, 5%, and 5% for Li, Na, and K, respectively. Their temperature dependence study showed an increase in R by 37% in Li, 3% in Na,

and 2% in K upon decreasing the temperature to 77° K.

4. Theoretical Hall Field

All of these observations are in sharp contradiction with theoretical predictions based on a closed Fermi surface, and nearly free electrons. Within this model the Hall coefficient should be a constant independent of temperature or field, the pressure dependence should be small, and based on band structure calculations using the HF theory would lead to changes in the direction opposite to that observed.[34] Only an assumption of a strongly anisotropic relaxation time[34] would appear to be capable of accounting for the effect within the HF model.

We have seen, however, that the gaps which occur on the Fermi surface in the GI zone lead to a smaller number of effective electrons in low fields than normally expected, and only in the high field limit where total breakdown has occurred is the expected free electron value achieved. Thus the Hall coefficient should be a constant in low fields, with a value higher than the free electron value, should undergo a sloping off in intermediate fields, and should attain the free electron value in very high fields. (If τ is small enough that $\omega_c\tau$ is $\sim$1 in the region where saturation occurs, the low field slope will be closer to the free electron value). This description agrees with the reported experimental field dependences. The field range over which the decrease would be observed is dependent on the size of the energy band gap and hence may vary among the alkalis.

Hence we would expect a temperature dependent Hall coefficient at constant field if the temperature is in the range where thermal breakdown could be occurring. If the energy gap is of the order kT (0.026 eV at room temperature) then such behavior would be expected and lowering the temperature would cause a decrease in the number of effective electrons and hence an increase in the Hall coefficient. This in in agreement with the observed behavior.

It has been shown[13] that the GI bands for Li change significantly as the lattice constant is increased or decreased from equilibrium. Therefore the size of the band gaps at the Fermi surface would also change and could actually go to zero at some point as the bands cross at the surface. Not only would distortion of the Fermi surface cause changes in the number of electrons occupying the second band, but shifts in the band gap would affect the field at which breakdown saturation would occur. Thus it is quite conceivable that this description could lead to a decrease followed by a possible increase in the Hall coefficient of the alkalis without the necessity of invoking relaxation time anisotropies into the theory.

At low fields we have seen that this description leads to Hall coefficients which are dependent on the crystallographic orientation. In particular the [110] direction has an open orbit leading to a higher slope than that found in the [100] direction in which only closed electron and hole orbits occur. Thus we would expect in low fields that the Hall field would be anisotropic.[35] A study on the same crystal over a variety

of field orientations and a wide field range would certainly be of interest.

E. CONCLUSIONS

In summary, since the GI band scheme for the alkalis allows the orbitals to have a lower than bcc symmetry and yet leads to a many-electron wave function for a pure singlet state, we obtain a band structure qualitatively capable of accounting for the observed non-saturation of the transverse magnetoresistance. In fact, magnetic breakdown leads to a broad range of approximately linear behavior into very high fields before the onset of eventual saturation. In addition the Hall coefficient decrease with field is accounted for and a possible explanation of its pressure dependence is afforded by the description.

References

[1] P. A. Penz and R. Bowers, Phys. Rev., 172, 991 (1968).

[2] F. E. Rose, Ph.D. thesis, Cornell University (1965) unpublished.

[3] D. Gugan and B. K. Jones, Helv. Phys. Acta., 36, 7 (1963).

[4] D. K. C. MacDonald, Proc. Phys. Soc., (London) A63, 290 (1950); Phil. Mag. 2, 97 (1957).

[5] E. Justi, Ann. Physik., 3, 183 (1948).

[6] J. Babiskin and P. G. Siebenmann, Phys. Kondens. Materie., 9, 113, (1969).

[7] W. A. Goddard III, Phys. Rev., 157, 81 (1967); J. Chem. Phys., 48, 450 (1968); R. C. Ladner and W. A. Goddard III, J. Chem. Phys., 51, 1073 (1969).

[8] C. F. Melius and W. A. Goddard III, to be published; D. L. Huestis and W. A. Goddard III, to be published.

[9] W. A. Goddard III, and R. C. Ladner, Int. J. Quantum. Chem., 3S (1950); R. C. Ladner, and W. A. Goddard III, to be published.

[10] W. A. Goddard III, Phys. Rev. 157, 93, (1967); ibid., 176, 106 (1968); ibid., 182, 48 (1969).

[11] W. A. Goddard III, Phys. Rev., 157, 73, (1967).

[12] P. M. O'Keefe and W. A. Goddard III, Phys. Rev. Lett., 23, 300 (1969).

[13] P. M. O'Keefe and W. A. Goddard, to be published.

[14] W. A. Goddard III and P. M. O'Keefe in Computational Methods in Band Theory, ed. by P. Marcus (Plenum Press, N. Y., to be published).

[15] I. M. Lifshitz, M. Ya. Azbel, and M. I. Kaganov, J. Exptl. Theoret. Phys. (U.S.S.R.) 31, 63 (1955), (translation: Soviet Phys. JETP 4, 41 (1957).

[16] E. F. Fawcett, Adv. In. Physics, 13, 139 (1964).

[17] M. H. Cohen and L. M. Falicov, Phys. Rev. Lett., 7, 231 (1961).

[18] R. G. Chambers, Proc. Phys. Soc., A238, 344 (1956).

[19] W. A. Harrison, Phys. Rev., 126, 497 (1962).

[20] J. R. Reitz, J. Phys. Chem. Solids, 25, 53 (1964).

[21] a) E. I. Blount, Phys. Rev., 126, 1636 (1962); b) A. B. Pippard, Proc. Roy. Soc., (London), A270, 1 (1962); Phil. Trans. Roy. Soc., A256, 371 (1964).

[22] L. M. Falicov and P. R. Sievert, Phys. Rev., 138, A88 (1965).

[23] The lattice constants used are Li, 6.575 a_o; Na, 7.984 a_o; K, 9.874 a_o. (The Li values (at 4°K) are taken from W. Pearson Can. J. Phys., 32, 708 (1954) using constants reported by E. R. Cohen and J. M. W. Dumond, Rev. Mod. Phys., 37 537 (1965). Those for Na and K (at 5°K) are from C. S. Barrett, Acta. Cryst., 9, 671 (1956).

[24] D. Shoenberg and P. J. Stiles, Proc. Roy. Soc. (London), A281, 62 (1964).

[25] C. C. Grimes and A. F. Kip., Phys. Rev., 132, 1991 (1963).

[26] F. S. Ham, Phys. Rev., 128, 2524 (1962).

[27] R. A. Young, Phys. Rev., 175, 813 (1968).

[28] H. Taub and R. Bowers, private communication.

[29] J. R. Reitz and A. W. Overhauser, Phys. Rev., 171, 749 (1968).

[30] N. Ashcroft, as quoted in P. A. Penz, Ph.D. thesis, Cornell University (1967) (unpublished). p 154 .

[31] R. G. Chambers and B. K. Jones, Proc. Roy. Soc., (London), A270, 417 (1962).

[32] J. M. Goodman, Phys. Rev., 171, 641 (1968).

[33] P. A. Penz, Phys. Rev. Lett., 20, 725, (1968).

[34] T. Deutsch, W. Paul, and H. Brooks, Phys. Rev., 124, 753, (1961).

[35] Penz has reported a decrease in the Hall coefficient of K for a single crystal with the field in the (111) direction and also for a polycrystalline sample and the curves showed somewhat different decrease characteristics, but it is hard to compare the two since they were different samples with different RRR's (no absolute value measurements were made).

Figure 1. Energy bands along [001] direction in HF and GI band schemes.

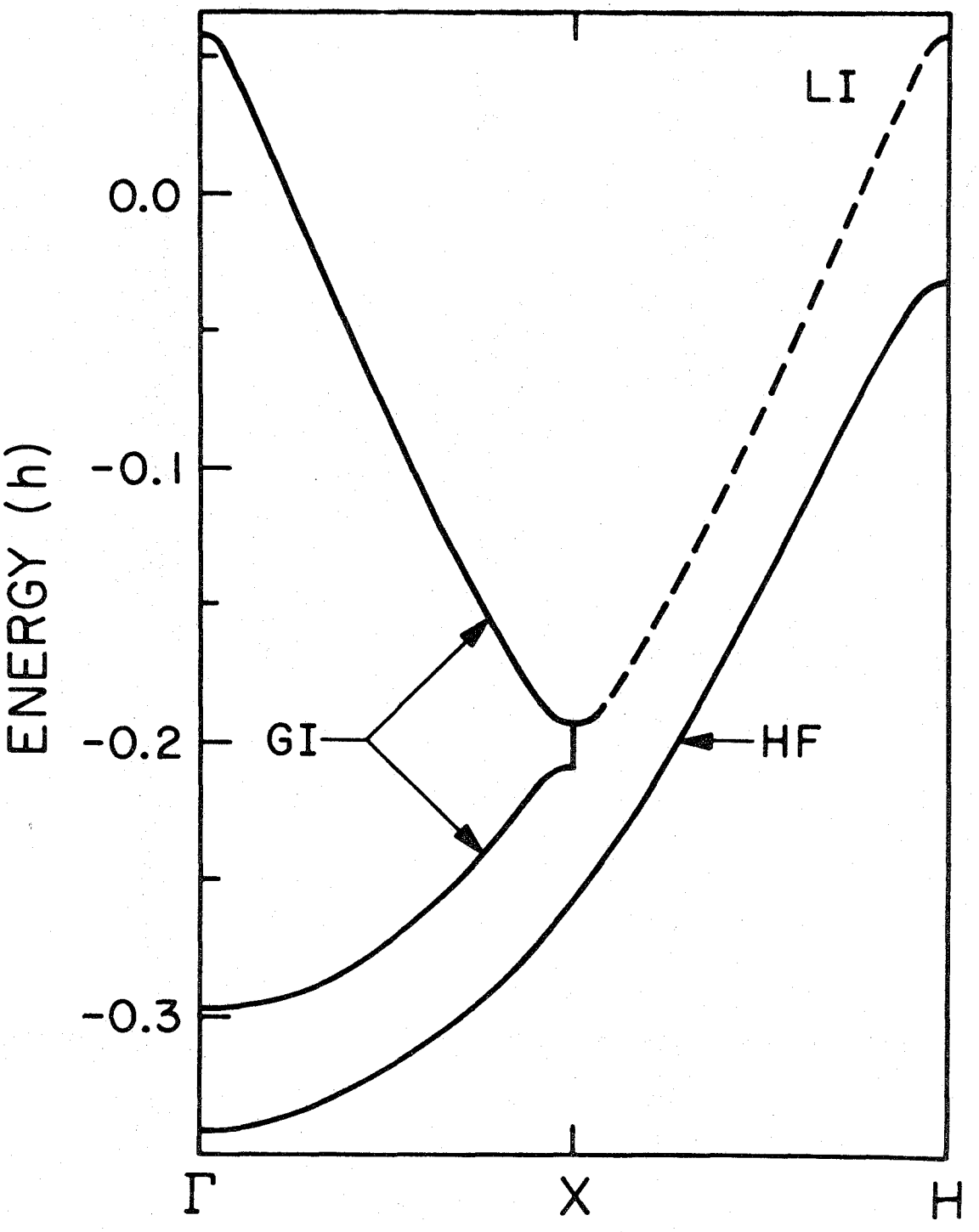
LI
0.0
-0.1
ENERGY (h)
-0.2
GI
HF
-0.3
Γ
X
H

Figure 2. Central cross sections in the (001) plane of (a) the HF and (b) the GI Fermi surface and Brillouin zone boundary.

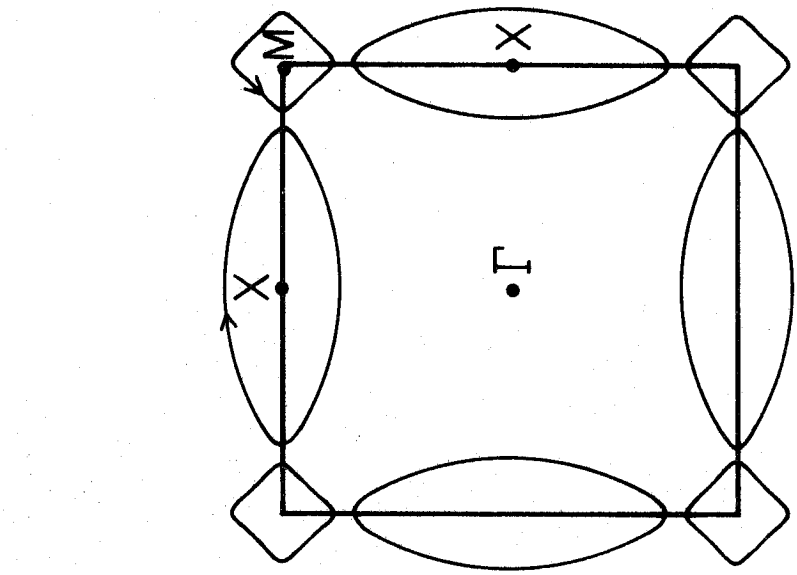

GI
(001) plane
(b)

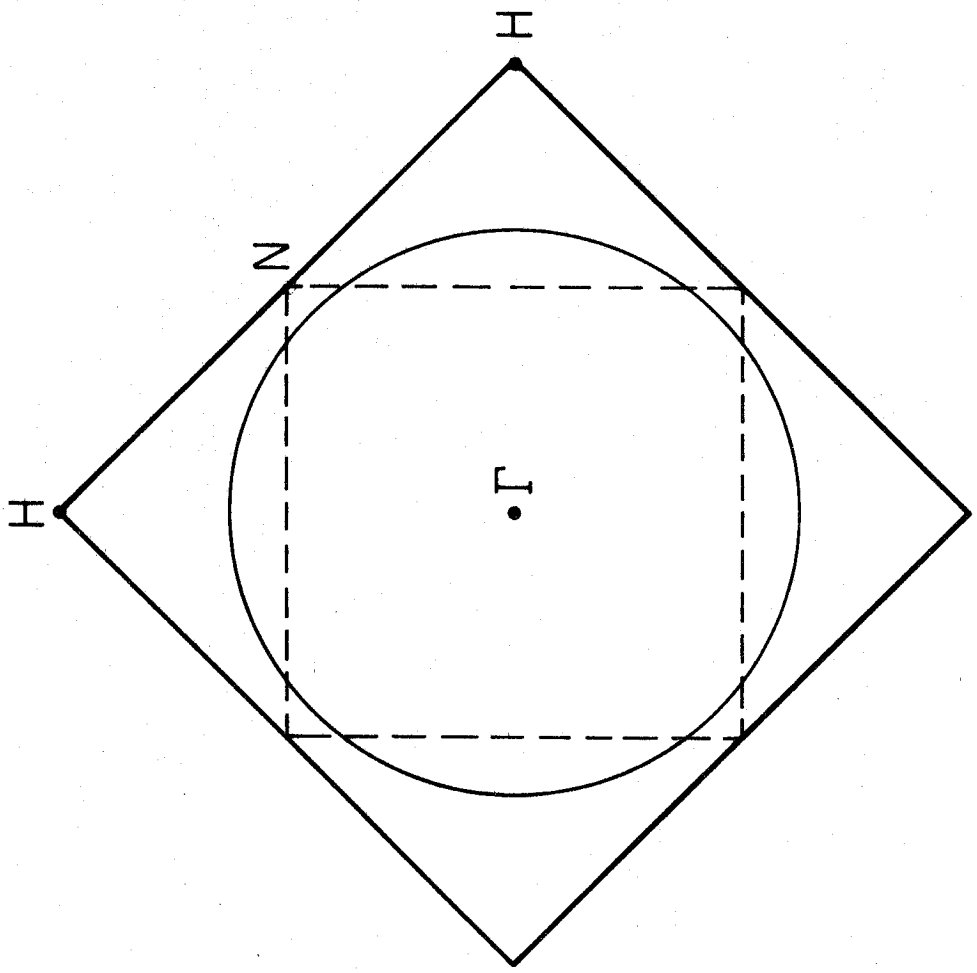

HF
(001) plane
(a)

Figure 3. Central cross section in the (110) plane of (a) the HF and (b) the GI Fermi surface and Brillouin zone boundary.

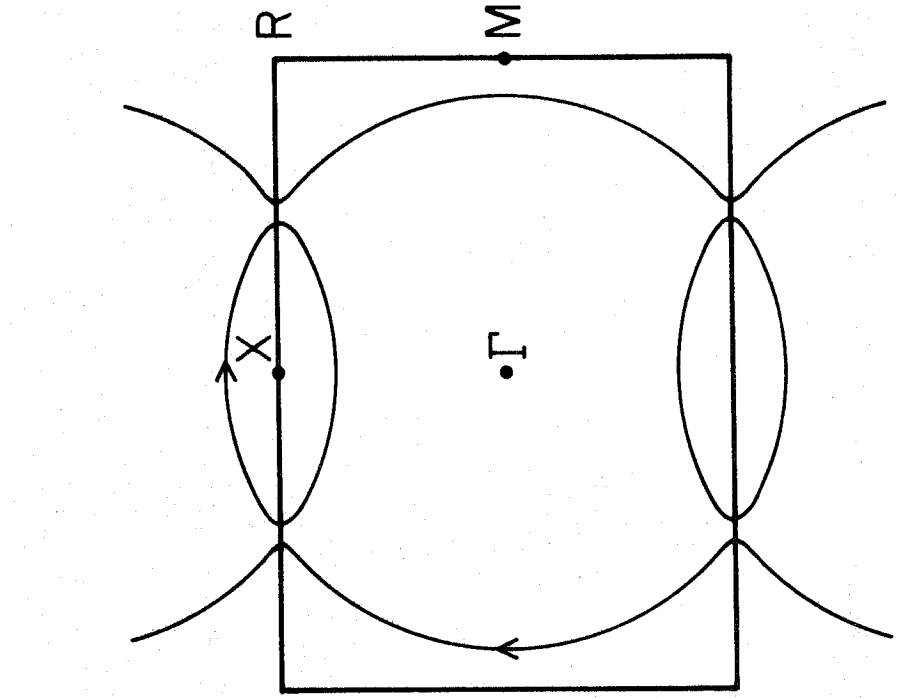

GI
(110) plane
(b)

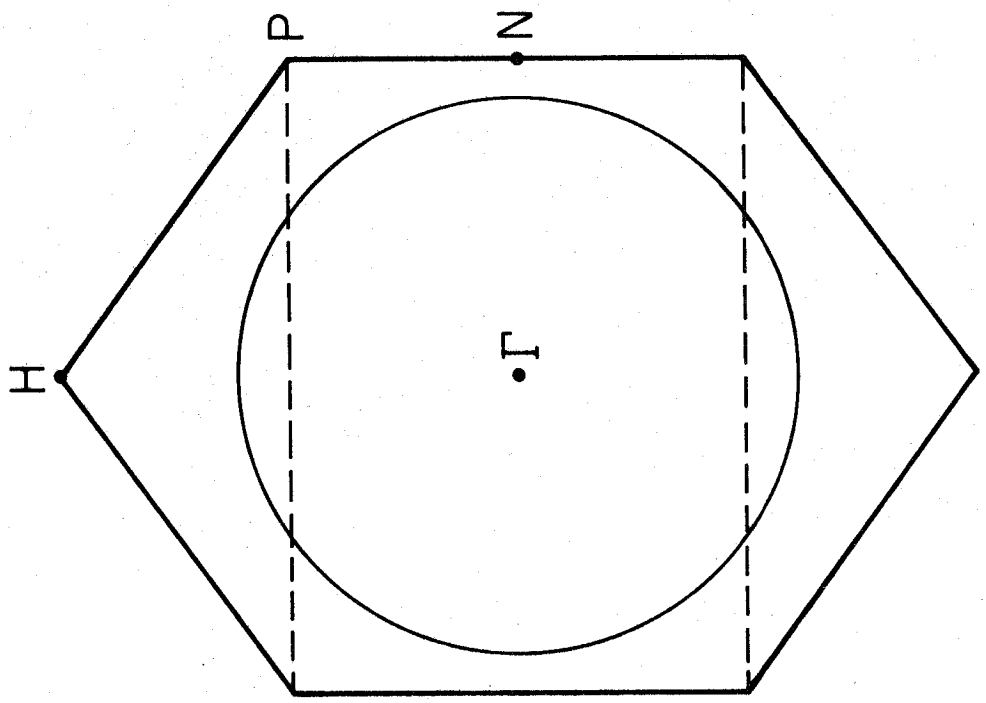

HF
(110) plane
(a)

Figure 4. The top half of the Brillouin zone showing the Fermi surface intersection for the field $\hat{B}$, oriented in (a) the [001] direction, and (b) the [110] direction.

B
B⊥ (110)
(b)
B⊥ (001)
(a)

Figure 5. (a)-(e) The various types of orbits contributing to the transverse magnetoresistance with the field oriented in the [110] direction.

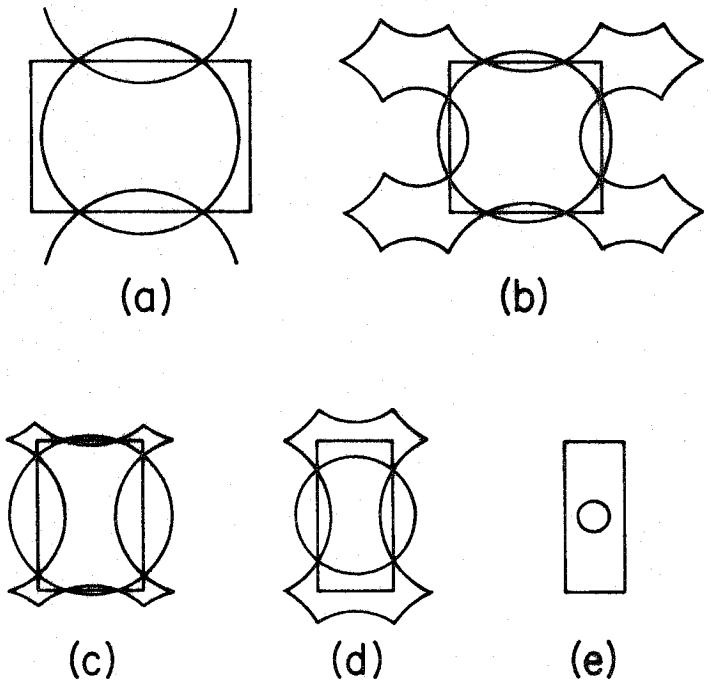
(a)
(b)
(c)
(d)
(e)

Figure 6. The transverse components, $\rho_{11} = \rho_{22}$, for lithium with the field perpendicular (a) to the (001) plane and (b) to the (110) plane. The behavior for four energy gaps $\mathcal{E}_g$ = .02, .04, .1, and .15 eV are given for $\tau = 0.7 \times 10^{-10}$ sec. (1 abohm = 10^{-9} ohms).

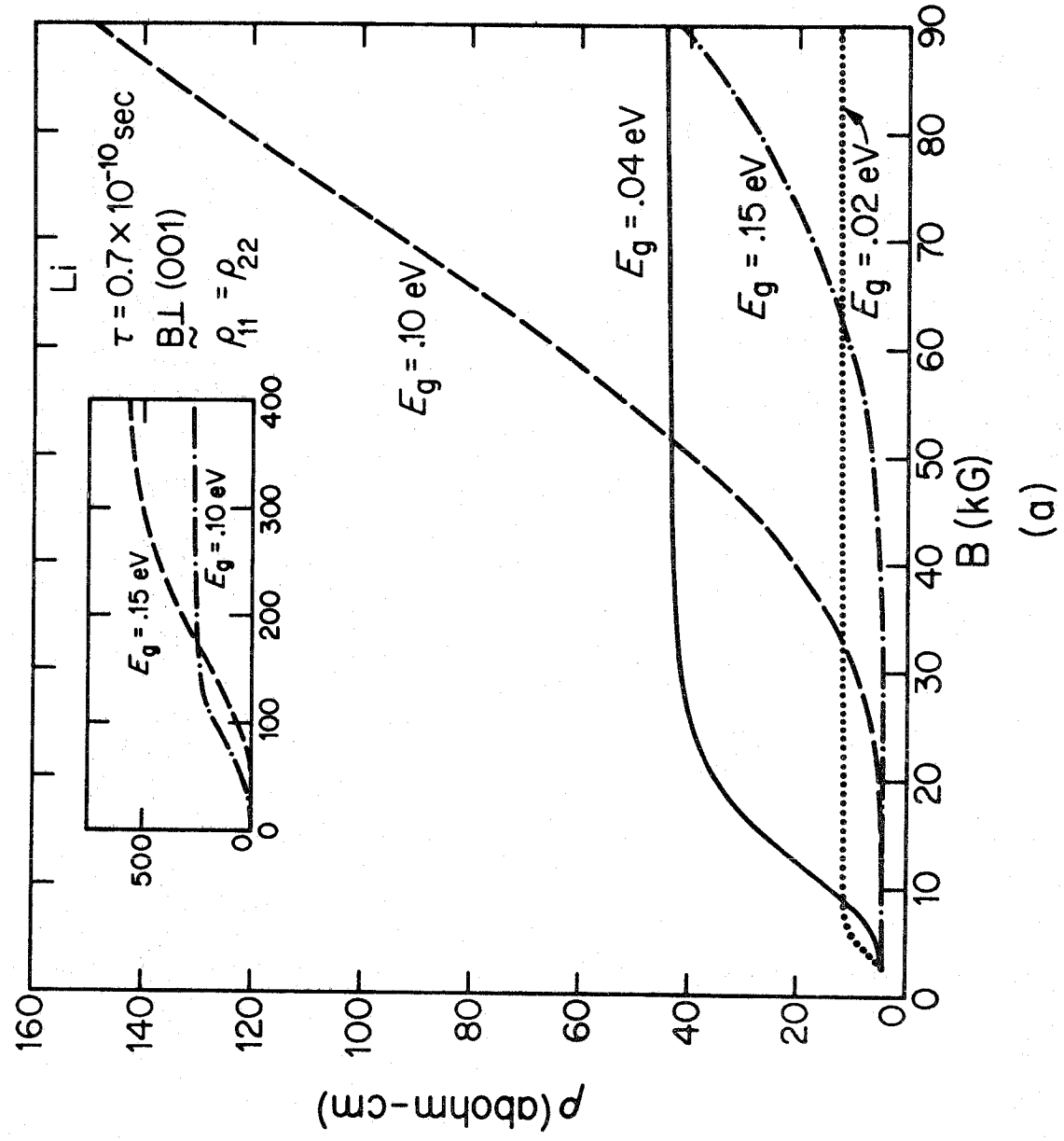
Li
τ = 0.7 × 10⁻¹⁰ sec
B⊥ (001)
ρ11 = ρ22
Eg = .10 eV
Eg = .04 eV
Eg = .15 eV
Eg = .02 eV
ρ (abohm-cm)
B (kG)
(a)

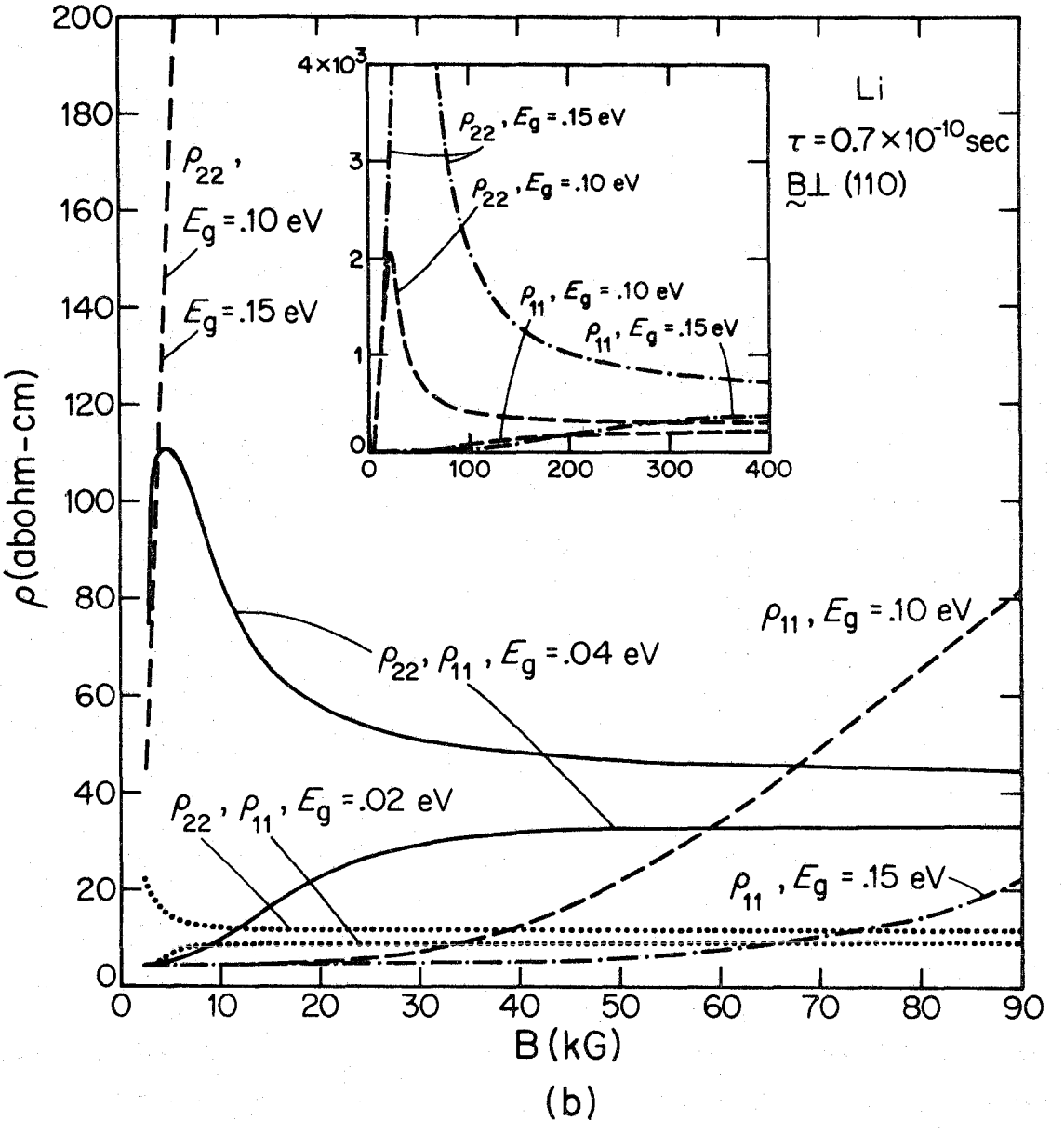
Li
τ = 0.7×10⁻¹⁰ sec
B⊥ (110)
ρ22, Eg = .15 eV
ρ22, Eg = .10 eV
ρ11, Eg = .10 eV
ρ11, Eg = .15 eV
ρ22, ρ11, Eg = .04 eV
ρ22, ρ11, Eg = .02 eV
ρ11, Eg = .10 eV
ρ11, Eg = .15 eV
ρ (abohm-cm)
B (kG)
4×10³
(b)

Figure 7. The transverse components, $\rho_{11} = \rho_{22}$, for sodium, with the field perpendicular (a) to the (001) plane and (b) to the (110) plane. The behavior for four energy gaps $\mathcal{E}_g$ = .02, .04, .1, and .15 eV are given for $\tau = 0.7 \times 10^{-10}$ sec.

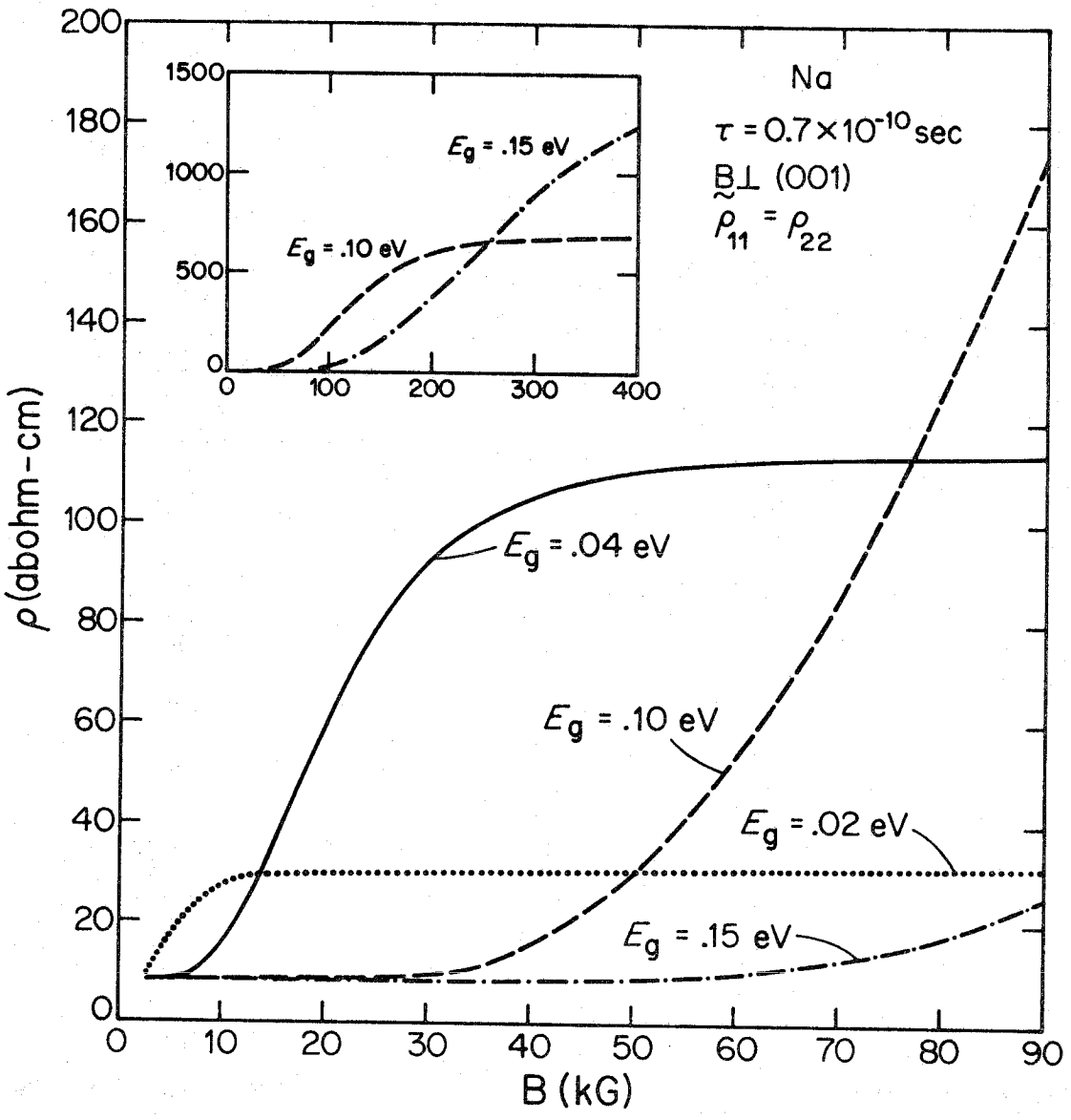
Na
$\tau = 0.7 \times 10^{-10}$ sec
B⊥ (001)
$\rho_{11} = \rho_{22}$
E_g = .04 eV
E_g = .10 eV
E_g = .02 eV
E_g = .15 eV
ρ (abohm-cm)
B (kG)
0
20
40
60
80
100
120
140
160
180
200
10
30
50
70
90
1500
1000
500
100
200
300
400

(a)

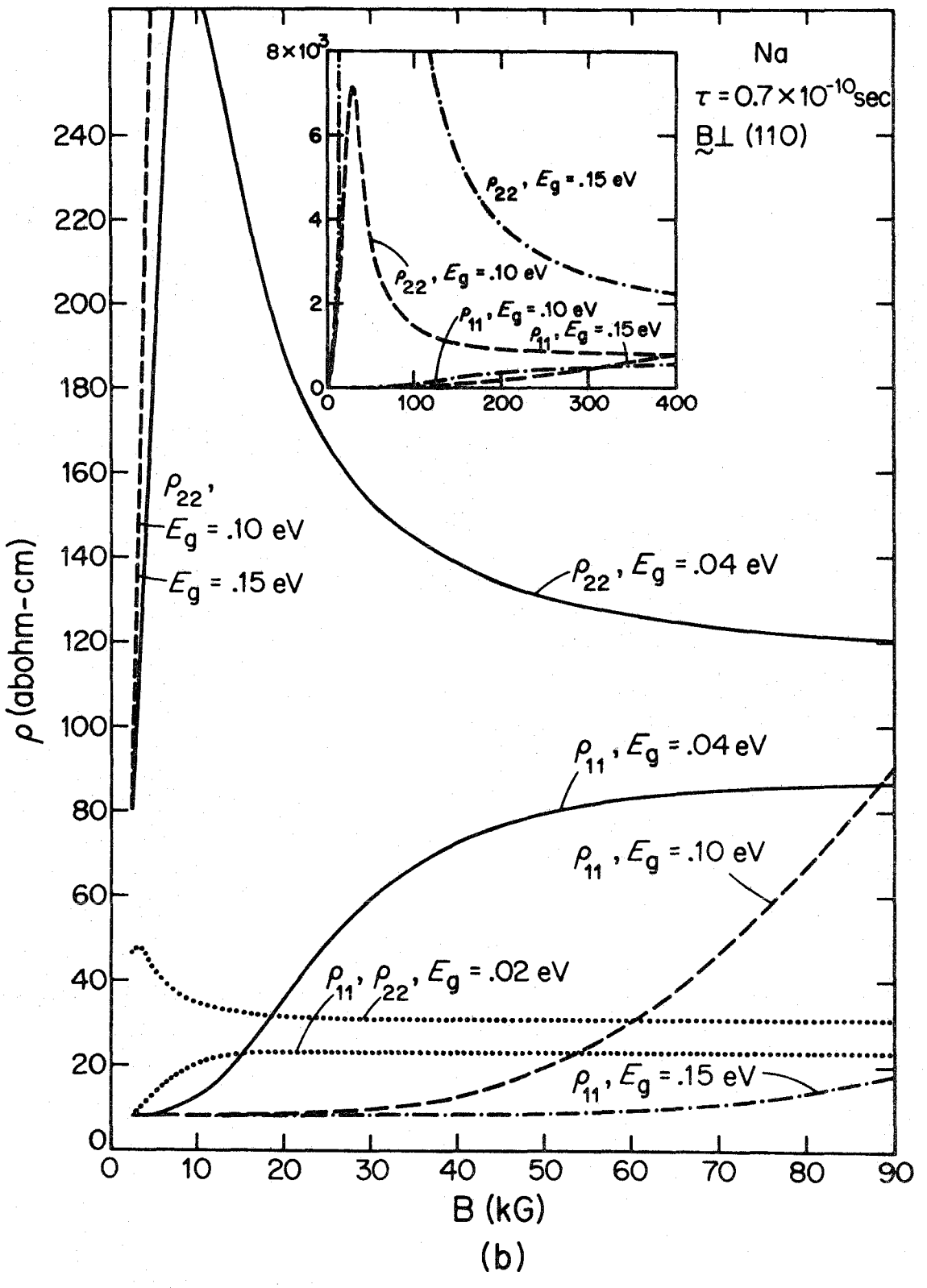
Na
τ = 0.7×10⁻¹⁰sec
B⊥ (110)
8×10³
ρ22, Eg = .15 eV
ρ22, Eg = .10 eV
ρ11, Eg = .10 eV
ρ11, Eg = .15 eV
ρ22, Eg = .04 eV
ρ22, Eg = .10 eV
Eg = .15 eV
ρ11, Eg = .04 eV
ρ11, Eg = .10 eV
ρ11, ρ22, Eg = .02 eV
ρ11, Eg = .15 eV
ρ (abohm-cm)
B (kG)
(b)

Figure 8. The transverse components, $\rho_{11} = \rho_{22}$, for potassium, with the field perpendicular (a) to the (001) plane and (b) to the (110) plane. The behavior for four energy gaps $\mathcal{E}_g = .02,\ .04,\ .1,$ and $.15$ eV are given for $\tau = 0.7 \times 10^{-10}$ sec. (1 abohm = 10^{-9} ohms).

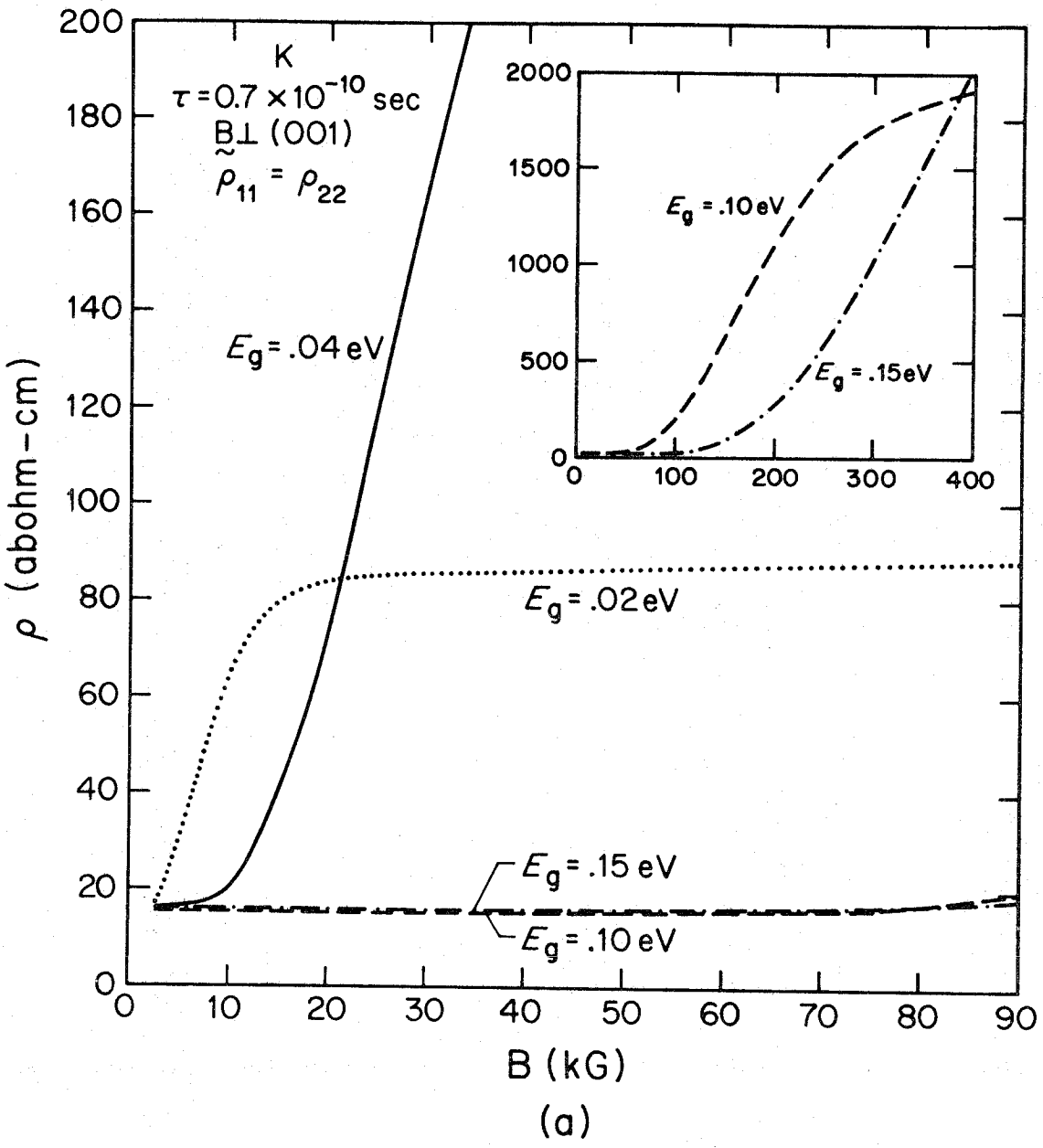
K
$\tau = 0.7 \times 10^{-10}$ sec
$\underset{\sim}{B} \perp$ (001)
$\rho_{11} = \rho_{22}$
$E_g = .04$ eV
$E_g = .02$ eV
$E_g = .15$ eV
$E_g = .10$ eV
$E_g = .10$ eV
$E_g = .15$ eV
ρ (abohm-cm)
B (kG)
0
20
40
60
80
100
120
140
160
180
200
10
30
50
70
90
500
1000
1500
2000
100
200
300
400

(a)

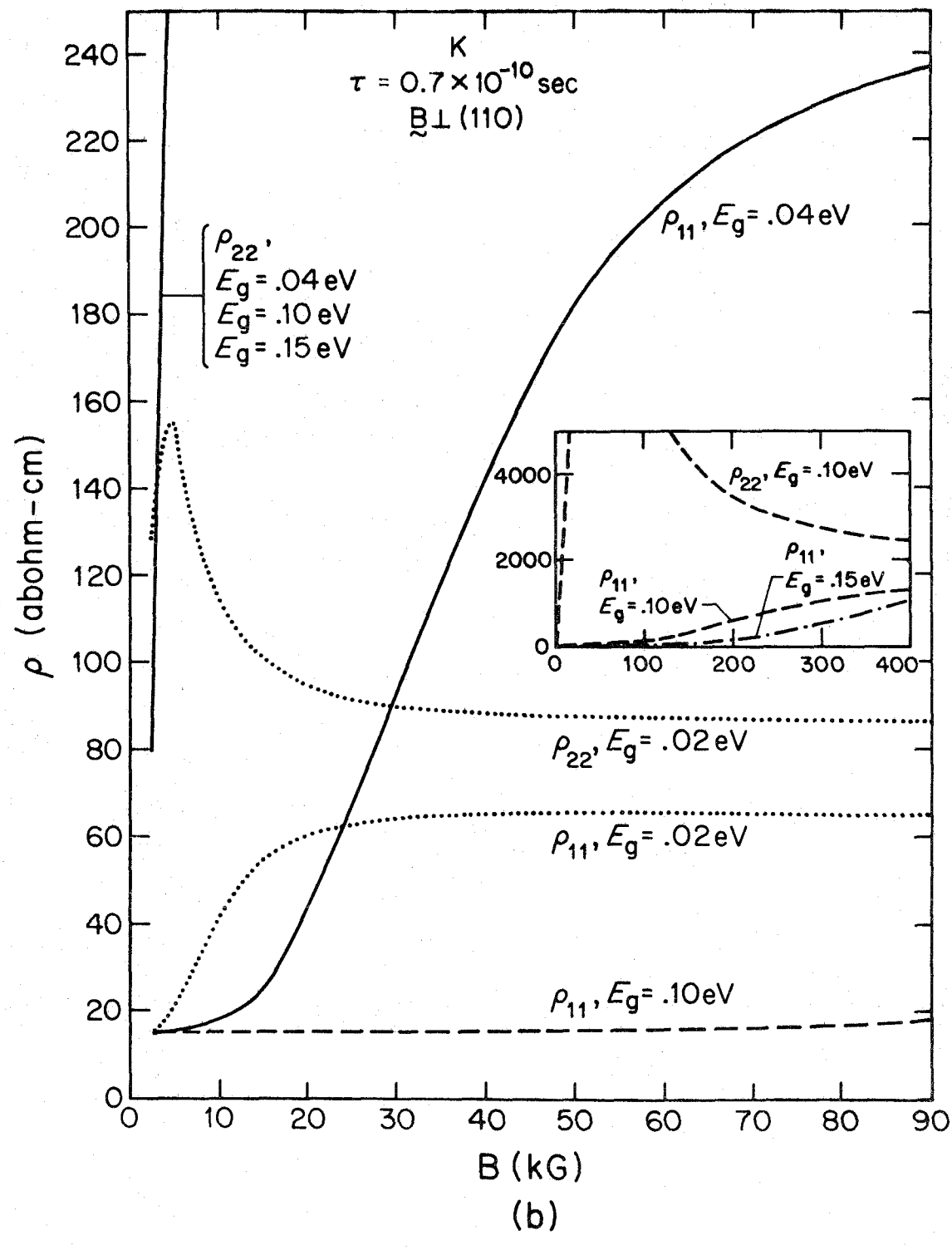
K
$\tau = 0.7 \times 10^{-10}$ sec
$\underset{\sim}{B} \perp (110)$
ρ_{22},
$E_g = .04$ eV
$E_g = .10$ eV
$E_g = .15$ eV
$\rho_{11}, E_g = .04$ eV
$\rho_{22}, E_g = .02$ eV
$\rho_{11}, E_g = .02$ eV
$\rho_{11}, E_g = .10$ eV
$\rho_{22}, E_g = .10$ eV
ρ_{11}, $E_g = .15$ eV
ρ_{11}, $E_g = .10$ eV
ρ (abohm-cm)
B (kG)
(b)

Figure 9. The relaxation time (τ) dependence of the transverse components for lithium. (a) for $\underset{\frown}{B} \perp (001)$ and $\mathcal{E}_g = 0.04$ and 0.1 eV's (b) for $\underset{\frown}{B} \perp (110)$ and $\mathcal{E}_g = 0.04$ eV.

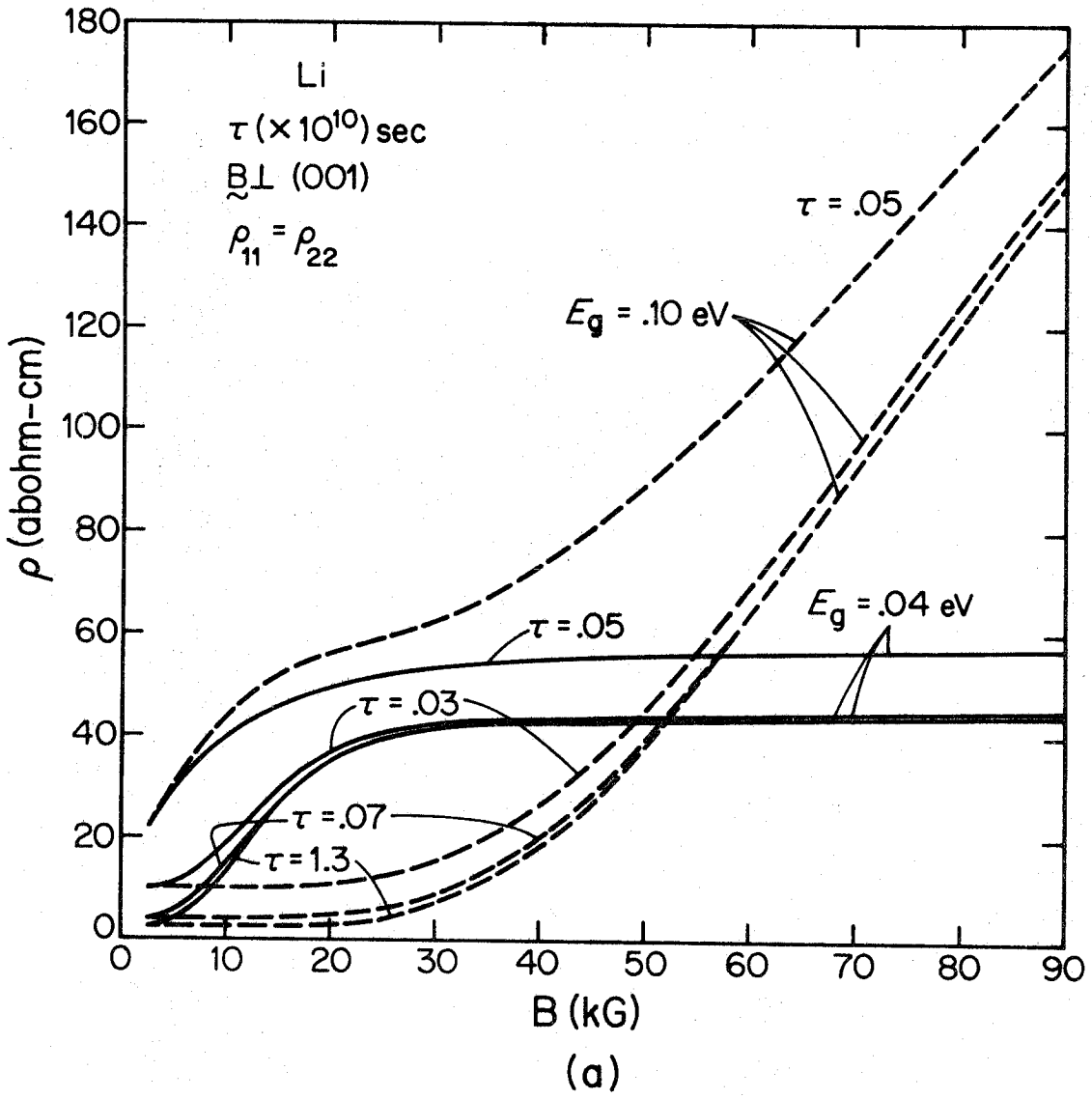
Li
τ (×10^10) sec
B⊥ (001)
ρ11 = ρ22
τ = .05
Eg = .10 eV
τ = .05
Eg = .04 eV
τ = .03
τ = .07
τ = 1.3
ρ (abohm-cm)
B (kG)
0
10
20
30
40
50
60
70
80
90
0
20
40
60
80
100
120
140
160
180

(a)

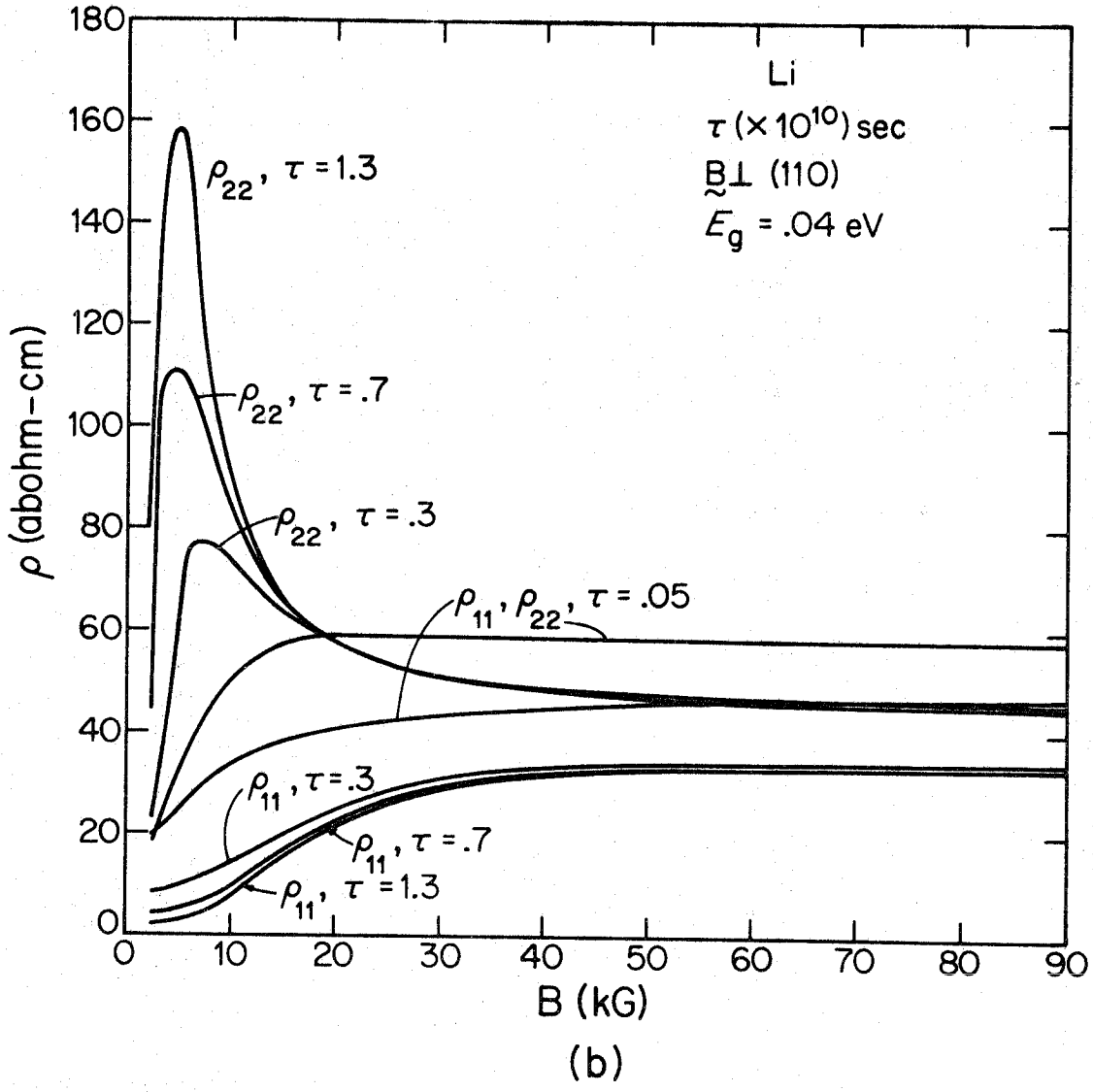
Li
τ (×10^10) sec
B⊥ (110)
E_g = .04 eV
ρ_22, τ = 1.3
ρ_22, τ = .7
ρ_22, τ = .3
ρ_11, ρ_22, τ = .05
ρ_11, τ = .3
ρ_11, τ = .7
ρ_11, τ = 1.3
ρ (abohm-cm)
B (kG)
0
10
20
30
40
50
60
70
80
90
0
20
40
60
80
100
120
140
160
180

(b)

Figure 10. The relaxation time (τ) dependence of the transverse components for potassium. (a) for $\underset{\frown}{B} \perp (001)$ and $\mathcal{E}_g = 0.04$ and 0.1 eV's (b) for $\underset{\frown}{B} \perp (110)$ and $\mathcal{E}_g = 0.04$ eV.

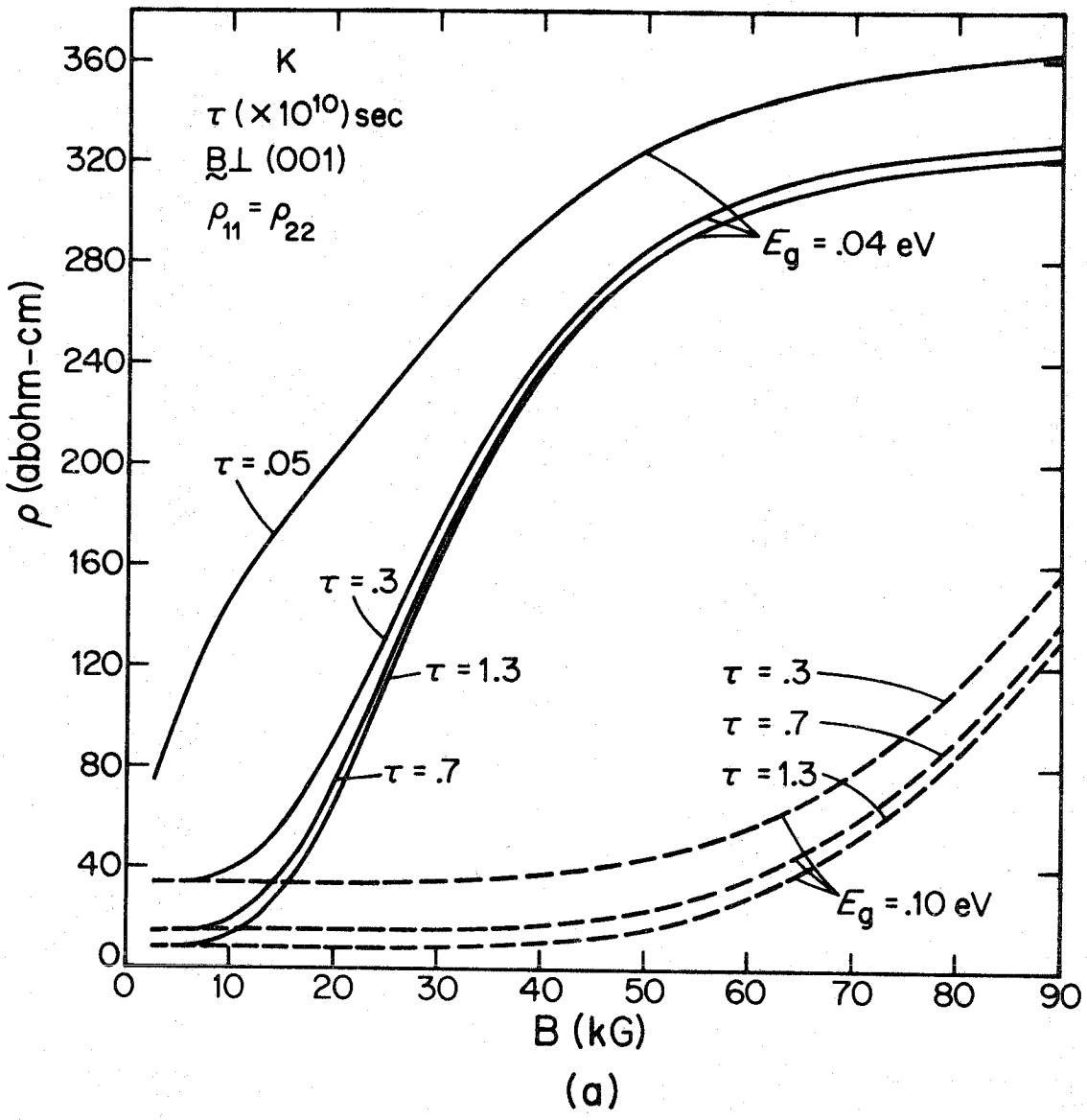
K
τ (×10^10) sec
B⊥ (001)
ρ11 = ρ22
Eg = .04 eV
τ = .05
τ = .3
τ = 1.3
τ = .7
τ = .3
τ = .7
τ = 1.3
Eg = .10 eV
ρ (abohm-cm)
B (kG)
0
40
80
120
160
200
240
280
320
360
0
10
20
30
40
50
60
70
80
90

(a)

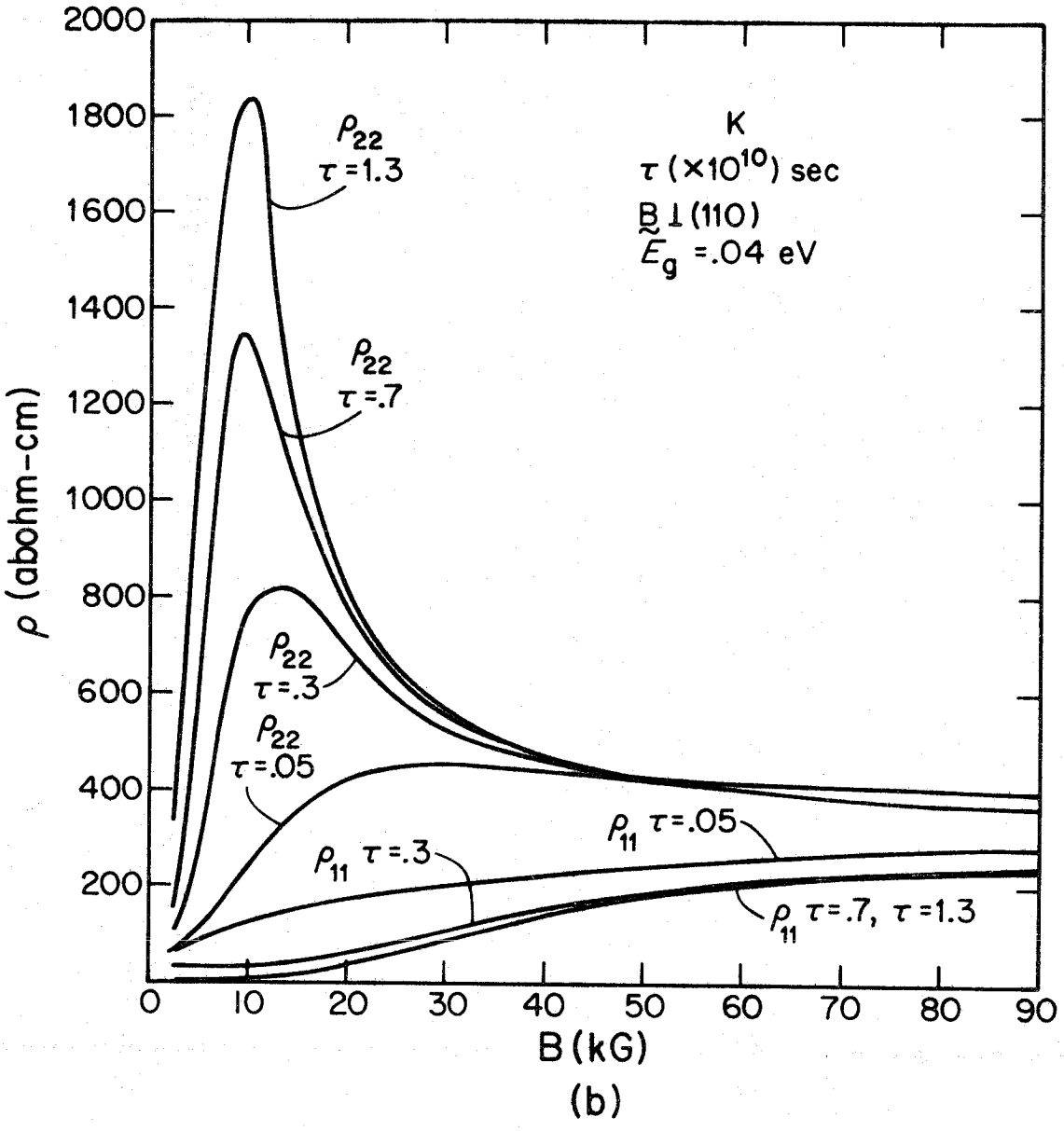
2000
1800
1600
1400
1200
1000
800
600
400
200
ρ (abohm-cm)
0
10
20
30
40
50
60
70
80
90
B (kG)
K
τ (×10^10) sec
B̲ ⊥ (110)
E_g = .04 eV
ρ22 τ=1.3
ρ22 τ=.7
ρ22 τ=.3
ρ22 τ=.05
ρ11 τ=.05
ρ11 τ=.3
ρ11 τ=.7, τ=1.3

(b)

Figure 11. The Hall resistivity (ρ_{21}) of lithium for the indicated energy gaps with $\tau \geq 0.3 \times 10^{-10}$ sec. The curves are identical. The dotted line indicates the type of behavior resulting whom $\tau = 0.05 \times 10^{-10}$ sec.

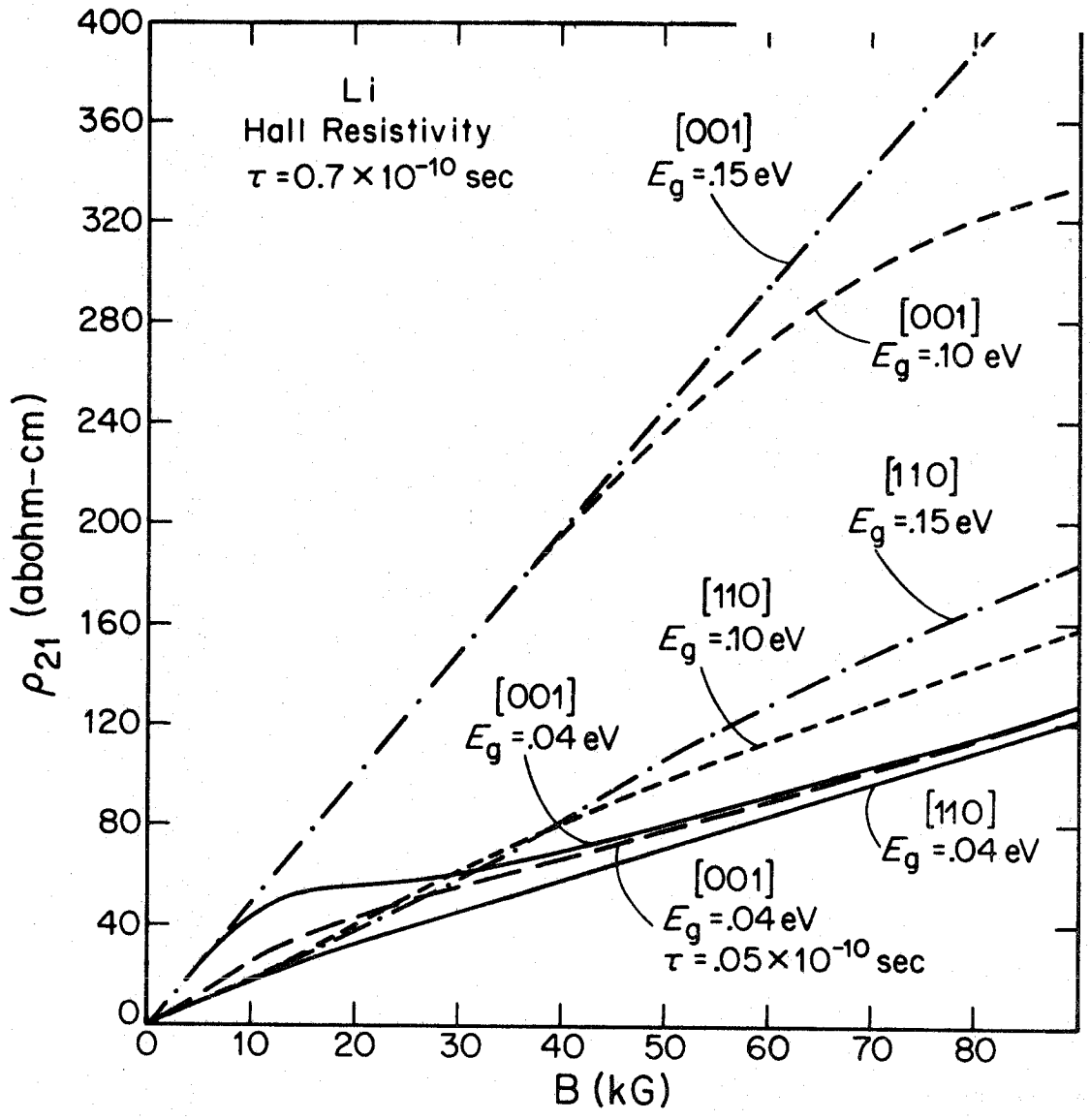
Li
Hall Resistivity
$\tau = 0.7 \times 10^{-10}$ sec
[001]
E_g = .15 eV
[001]
E_g = .10 eV
[110]
E_g = .15 eV
[110]
E_g = .10 eV
[001]
E_g = .04 eV
[110]
E_g = .04 eV
[001]
E_g = .04 eV
$\tau = .05 \times 10^{-10}$ sec
ρ_{21} (abohm-cm)
B (kG)
0
40
80
120
160
200
240
280
320
360
400
0
10
20
30
40
50
60
70
80

Figure 12. The Hall resistivity (ρ_{21}) of sodium for the indicated energy gaps with $\tau = 0.7 \times 10^{-10}$ sec.

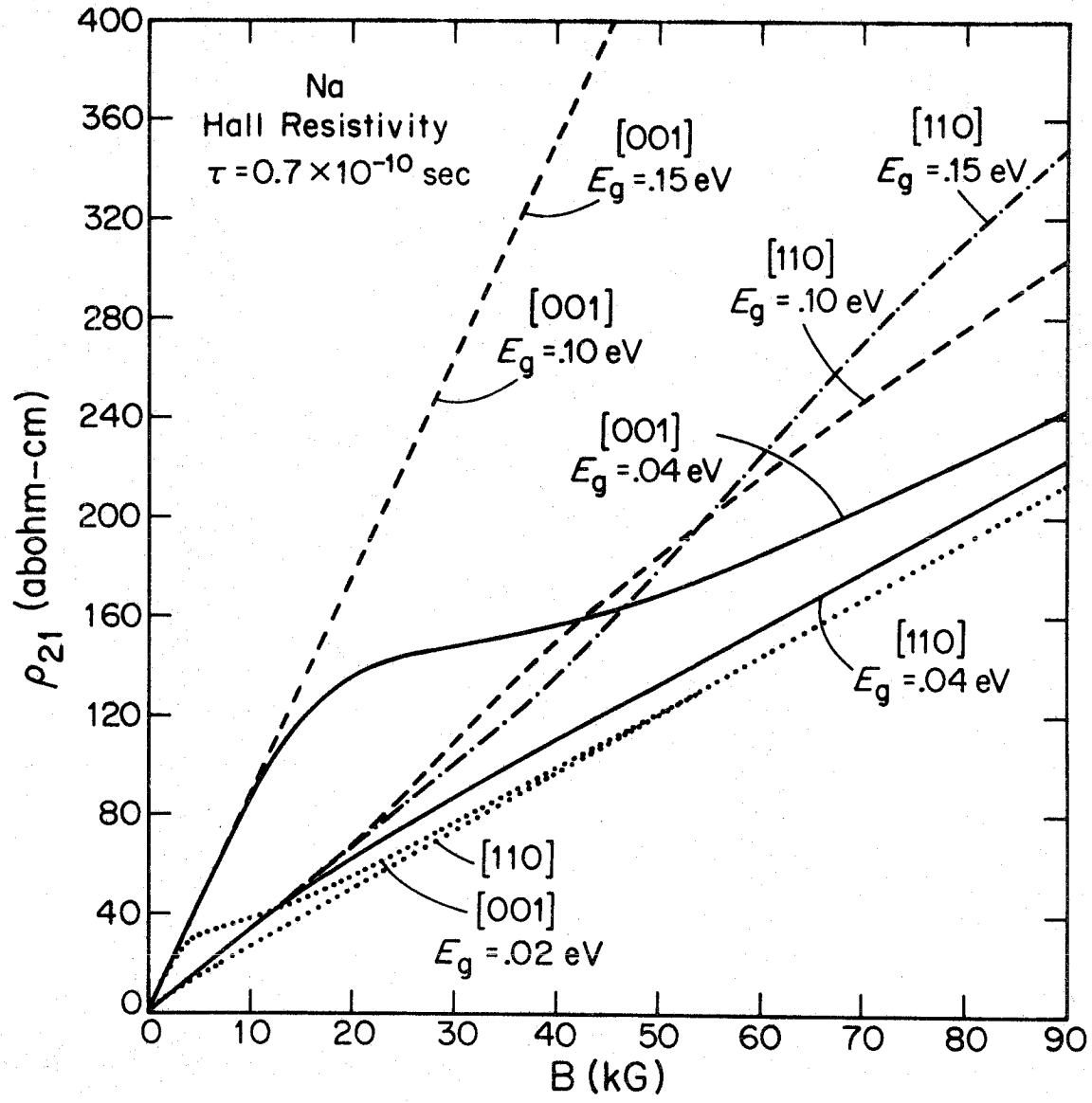
Na
Hall Resistivity
$\tau = 0.7 \times 10^{-10}$ sec
[001]
E_g = .15 eV
[110]
E_g = .15 eV
[110]
E_g = .10 eV
[001]
E_g = .10 eV
[001]
E_g = .04 eV
[110]
E_g = .04 eV
[110]
[001]
E_g = .02 eV
ρ_{21} (abohm-cm)
B (kG)
0
40
80
120
160
200
240
280
320
360
400
0
10
20
30
40
50
60
70
80
90

Figure 13. The Hall resistivity (ρ_{21}) of potassium for the indicated energy gaps with $\tau = 0.7 \times 10^{-10}$ sec. (The dotted line indicates the type of behavior resulting when $\tau = 0.05 \times 10^{-10}$ sec, the longer τ's all shows the same behavior as $\tau = 0.7 \times 10^{-10}$ sec.).

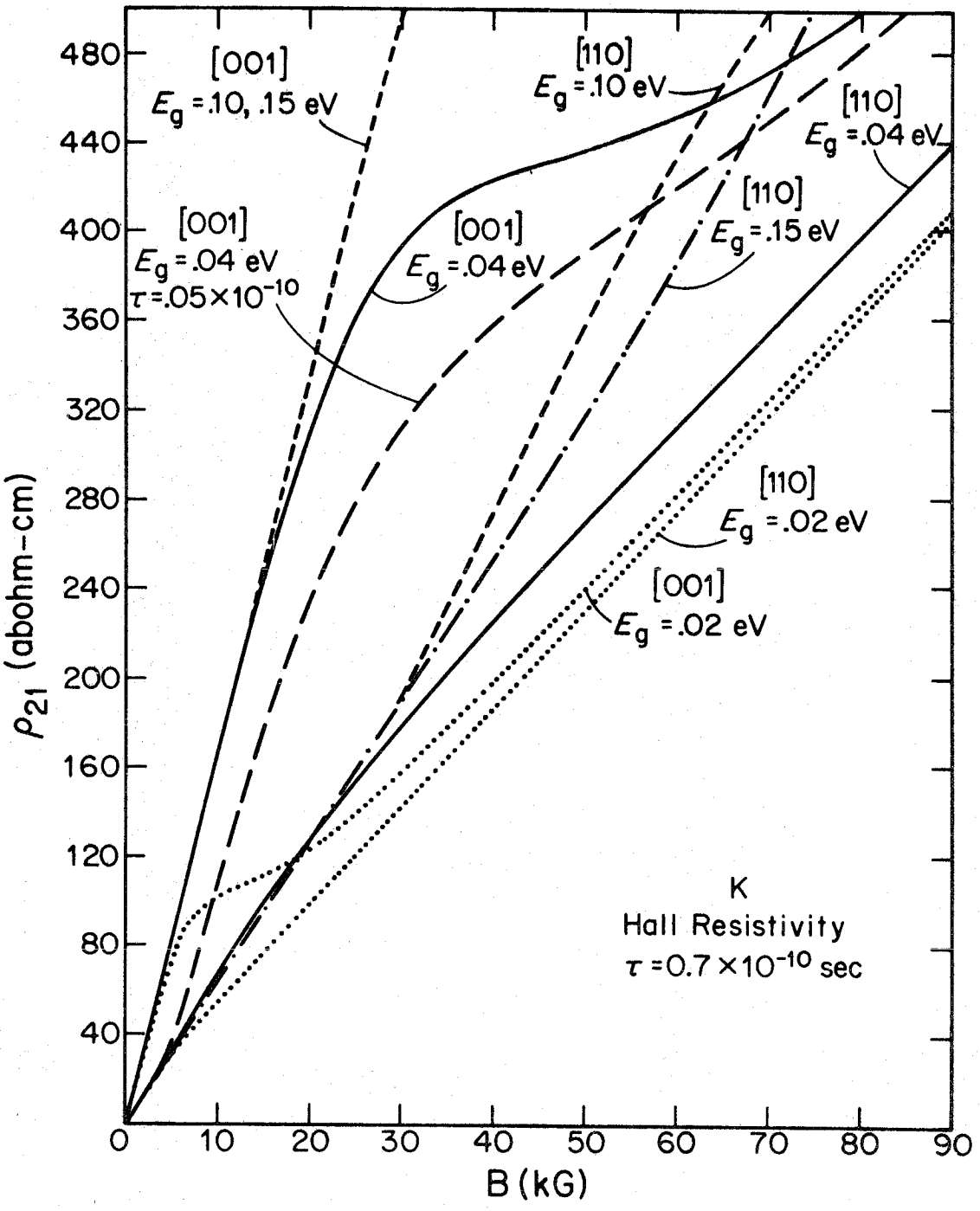
[001]
E_g = .10, .15 eV
[110]
E_g = .10 eV
[110]
E_g = .04 eV
[110]
E_g = .15 eV
[001]
E_g = .04 eV
τ = .05×10^{-10}
[001]
E_g = .04 eV
[110]
E_g = .02 eV
[001]
E_g = .02 eV
K
Hall Resistivity
τ = 0.7 ×10^{-10} sec
ρ_{21} (abohm-cm)
B (kG)
480
440
400
360
320
280
240
200
160
120
80
40
0
10
20
30
40
50
60
70
80
90

III. RESOLUTION OF THE MOTT PARADOX

A. INTRODUCTION

The usual band description of metals often leads to a poor description of the system as the crystal is pulled apart.[1,2] For example consider a body centered cubic alkali metal such as sodium. If there are N lattice sites,[3] there are N states in the first Brillouin zone (BZ). Thus, if each orbital in the conduction band were doubly occupied, the band would contain 2N electrons. But sodium is monovalent so that there are only N electrons in the band therefore filling only N/2 of the states. Hence, we would correctly expect the system to be a metal (since there are many empty orbitals with energies infinitesimally close to the occupied states). Thus, this band description would lead to the idea that sodium is a metal even for infinite lattice constant ($a = \infty$). However, at $a = \infty$ the ground state of the system should have every isolated Na atom in its ground state; hence in order to obtain conduction we must move an electron from one sodium atom to another which requires an energy of 4.6 eV. Thus, for $a = \infty$ sodium should be an insulator and the usual band description is clearly inappropriate. This result that the band picture implies a metal for a system which clearly must be an insulator is sometimes called the Mott Paradox.[2]

Mott considered a system with a large lattice constant, a, in which the valence orbitals were localized at the various lattice sites. He proposed that as a decreases and the orbitals start overlapping, eventually a point is reached at which each orbital is shielded from its own nucleus sufficiently to delocalize over the various sites and thus help shield other orbitals from their sites

leading to more delocalized orbitals, etc. Consequently, there should be some critical a at which the system changes discontinuously from an insulator to a metal. Such a transition from localized to delocalized valence states is called a Mott transition, and has been used to discuss metal semiconductor transitions in V_2O_3 and similar systems.

However, the difficulty for a system such as sodium just results from the double-occupation restriction in Hartree-Fock. For $a = \infty$ we require N singly-occupied orbitals each localized in its own region of space. However, we saw that the HF wavefunction contains N/2 doubly-occupied valence orbitals and, thus, cannot correctly describe the separated atoms limit [this same problem also occurs in the HF description of many diatomics (e.g., H_2, Li_2, LiH, N_2, etc.) resulting in improper dissociation].

In this paper we will be concerned with the consequences of the removal of the double-occupation restriction in HF. We find that proper band calculations with this restriction removed correctly lead to a metal for equilibrium and an insulator for large internuclear distances.

B. WAVEFUNCTIONS

We will first consider a simple molecular system, H_2, and see what problems are encountered in removing the double-occupation restriction from the HF wavefunction. Here the HF wavefunction is given by

$$\mathcal{A}[\phi(1)\phi(2)\alpha(1)\beta(2)] = \phi(1)\phi(2)[\alpha(1)\beta(2) - \beta(1)\alpha(2)] \quad (1)$$

where $\mathcal{A}$ is the antisymmetrizer, ϕ is a spacial orbital and α and β designate spin up and spin down orbitals respectively. We take ϕ as doubly-occupied and functionally optimize (1) to minimize the total energy. The resulting orbital[4] is shown in Fig. 1b and is seen to have σ_g symmetry, even for large internuclear distances. We can separate ϕ into components localized on the left and right protons,

$$\phi = \chi_\ell + \chi_r \quad (2)$$

such that χ_ℓ and χ_r have essentially no overlap for large internuclear distances. Thus, the spacial part of (1) becomes

$$\phi(1)\phi(2) = [\chi_\ell(1)\chi_r(2) + \chi_r(1)\chi_\ell(2)] + [\chi_\ell(1)\chi_\ell(2) + \chi_r(1)\chi_r(2)]. \quad (3)$$

But for well separated nuclei the spacial wavefunction should be just a product of separated atomic functions (properly symmetrized),

$$\chi_\ell(1)\chi_r(2) + \chi_r(1)\chi_\ell(2). \quad (4)$$

The spurious ionic terms in (3) cause the HF wavefunction to behave poorly at large distances, as shown in Fig. 2.[7] These terms arise because the orbital ϕ is forced to be doubly-occupied. If we allow the orbitals to be different (obtaining the Unrestricted Hartree-Fock or UHF wavefunction), (1) becomes

$$\mathcal{A}[\phi_a(1)\phi_b(2)\alpha(1)\beta(2)] = \phi_a\phi_b\alpha\beta - \phi_b\phi_a\beta\alpha. \quad (5)$$

Now as we separate the system, ϕ_a becomes an orbital localized on say the left center (χ_ℓ) and ϕ_b an orbital on the right (χ_r) and the molecule dissociates correctly. However, the ground state should be a singlet state; thus, applying the spin raising operator, S^+, to (5) should give zero. But,

$$S^+\mathcal{A}[\phi_a\phi_b\alpha\beta] = \mathcal{A}[\phi_a\phi_b\alpha\alpha] = (\phi_a\phi_b - \phi_b\phi_a)\alpha\alpha \quad (6)$$

yields zero only if ϕ_a is proportional to ϕ_b. Thus, to obtain the correct spin symmetry the orbital must be doubly occupied. But as we saw this leads to incorrect dissociation. In order to circumvent this problem and obtain both the correct spin symmetry and dissociation properties, we replace the antisymmetrizer by a more general operator, the Group Operator G_i^γ [10] to obtain wavefunctions of the form $G_i^\gamma\,\phi_a\phi_b\alpha\beta$. The Group Operator has the property that the resulting many-electron wavefunction is an eigenfunction of $\hat{S}^2$ and satisfies Pauli's Principle;[10] thus, no restriction need be imposed on ϕ_a and ϕ_b. For a two-electron singlet state the resulting wavefunction is

$$G_i^\gamma[\phi_a\phi_b\alpha\beta] = (\phi_a\phi_b + \phi_b\phi_a)(\alpha\beta - \beta\alpha). \quad (7)$$

Applying the variational principle, we functionally optimize the orbitals of (7) to obtain a pair of coupled integro-differential equations[11]

$$h_a\phi_a = \mathcal{E}_a\phi_a$$

$$h_b\phi_b = \mathcal{E}_b\phi_b. \tag{8}$$

The resulting optimum orbitals[6] for H_2 at equilibrium ($R = 1.4\ a_0$) are shown in Fig. 1a.

We see that not only are ϕ_a and ϕ_b different but they have a lower symmetry than that of the molecule. They belong to $C_{\infty v}$, while the molecule has $D_{\infty h}$ symmetry. But if we apply the inversion operator i to the orbitals (thus interchanging the nuclei), we obtain

$$i\phi_a = \phi_b$$

$$i\phi_b = \phi_a. \tag{9}$$

Hence, under this operation, the many-electron wavefunction is unchanged,

$$i(\phi_a\phi_b + \phi_b\phi_a) = \phi_a\phi_b + \phi_b\phi_a \tag{10}$$

and is correctly a $^1\Sigma g^+$ state of $D_{\infty h}$ symmetry.

Now as the nuclei are separated to large distances, the orbitals become more and more like H 1s functions and, hence, they dissociate correctly as shown in Fig. 2.[7]

For more than two electrons, the wavefunction[6,10] cannot be factored into spacial and spin parts as in (7). In the G_i^γ operator for a given system there may be several operators which one can

construct. γ represents the total spin projection and the index i designates the particular spin coupling to be used (there are in general several independent ways of coupling the spins of the N electrons to obtain some total spin, S). This spin coupling must be optimized along with the orbitals to obtain the spin-coupling optimized GI or SOGI wavefunction.[12] We will now discuss the GI description of two molecular systems, square planar H_4 and hexagonal H_6.

The resulting wavefunction for H_4 yields the orbitals shown in Fig. 3. The optimum spin coupling for this system is extremely close to what is generally referred to as f-type coupling.[6,10,14] Here half the spins are coupled to maximum spin, the other half are coupled to maximum spin, and these two sets are coupled together to give minimum spin. For this description the many-electron wavefunction for singlet H_4 is

$$G_f^{\gamma}[\phi_{1a}\phi_{2a}\phi_{1b}\phi_{2b}\alpha\alpha\beta\beta]$$

$$= \mathcal{A}\{\phi_{1a}\phi_{2a}\phi_{1b}\phi_{2b}[2\alpha\alpha\beta\beta - (\alpha\beta + \beta\alpha)(\alpha\beta + \beta\alpha)$$

$$+ 2\beta\beta\alpha\alpha]\}. \qquad (11)$$

It is clear in this expansion that ϕ_a and ϕ_b are not uniquely associated with any given spin and yet it is exactly a singlet state. The orbitals in (11) are determined by applying the variational principle to minimize the energy of (11) which leads to the following set of simultaneous equations:

$$h_a\phi_{ka} = \varepsilon_{ka}\phi_{ka}, \quad k = 1, 2$$

$$h_b\phi_{kb} = \varepsilon_{kb}\phi_{kb}, \quad k = 1, 2. \qquad (12)$$

In (11) it is no restriction to take the a orbitals to be mutually orthogonal and similarly to take the b orbitals as orthogonal; however, in general the a orbitals do not have any special relationship to any of the b orbitals. We see in Fig. 3 that the one-electron orbitals of H_4 are symmetry functions of D_{2h} rather than D_{4h}. Thus, just as in H_2, the orbitals have symmetry lower than that of the full spatial symmetry group. Even so the many-electron wavefunction still has the full symmetry of the molecule. For example, consider the effect of the operation C_4 on the wavefunction of (11). Since

$$C_4\phi_{1a} = \phi_{1b}; \quad C_4\phi_{1b} = \phi_{1a}$$

$$C_4\phi_{2a} = \phi_{2b}; \quad C_4\phi_{2b} = -\phi_{2a}$$

(see Fig. 3), we have that $C_4G_f\Phi\chi = -G_f\Phi\chi$. Similarly, considering the other operations of $\underset{\sim}{D}_{4h}$, we find that the wavefunction (11) correctly possesses $^1B_{1g}$ symmetry. Note that this symmetry reduction is not forced on the orbitals. We solve for the variationally optimum orbitals which are found to have D_{2h} symmetry; they could have had D_{4h} symmetry if this would have lowered the energy.

We now examine H_6 with D_{6h} symmetry [a regular hexagon of H atoms ($R=2\,a_o$)].[15] (This can be considered a molecular prototype to a one dimensional crystal). As in H_4 the optimum spin coupling is found to be very near the f-spin coupling. The resulting H_6 orbitals[16] are shown in Fig. 4. Once again, we find that the orbitals have a reduced symmetry, here they belong to D_{3h} rather than the D_{6h} of the molecule.

In each of these cases since our orbitals are singly-occupied, we obtain a description which is valid as the system is pulled apart. Other attempts have been made to construct useful wavefunctions which behave correctly for all internuclear distances. We have seen that the UHF wavefunction has incorrect spin symmetry. To circumvent this difficulty, it is necessary to project out the desired spin component. But then the spin projected orbitals are not optimized in the new description. Actually the GF method[11] discussed above can be shown to be equivalent to spin-polarized UHF in which the orbitals are optimized after spin projection.

Numerous schemes using alternate molecular orbital (AMO)[17,18,19] have been developed. This treatment couples ground state HF orbitals to their corresponding excited state orbital in symmetric and antisymmetric combination. A parameter determining the degree of localization is optimized to minimize the total energy. However, this approach is applicable only to the ground state of a system and the orbitals are parametrically, not functionally, optimized so that an independent particle interpretation is not obtained.

Another attempt to describe electron correlation in a consistent manner utilizes Heitler London pairwise coupling of the orbitals, but attempts to extend the application to highly resonating structures and metals involves many equivalent pairs which render the calculation impractical, if not impossible. In addition, the model implies localized spatial orbitals with strong spin coupling between nearest neighbors which has been shown to be applicable only to low electron density systems.

It should be noted that the GF orbitals are not strongly coupled with neighboring orbitals. Such a description involves a quite different spin representation generally referred to as G1, the use of which corresponds to a generalization of the valence bond method and will not be considered here.

C. APPLICATION OF THE GI METHOD TO METALS

We will now consider how this method might be applied to an alkali metal such as lithium. The many electron wavefunction can be written as

$$G_f^{\gamma}\,[\phi_{1a}\phi_{2a}\cdots\phi_{na}\phi_{1b}\phi_{2b}\cdots\phi_{nb}\alpha\alpha\cdots\alpha\beta\beta\cdots\beta] \tag{14}$$

where we are considering only the conduction orbitals. As before, these sets of orbitals $\{\phi_a\}$ and $\{\phi_b\}$ are solutions of two equations,

$$h_a\phi_{ka} = \mathcal{E}_{ka}\phi_{ka} \qquad k = 1, 2, \cdots, n$$

$$h_b\phi_{kb} = \mathcal{E}_{kb}\phi_{kb} \qquad k = 1, 2, \cdots, n \tag{15}$$

where here k denotes a particular wave vector. These orbitals are all singly occupied and, as per previous considerations, would be expected to have higher amplitude on alternate sites in the bcc lattice and thus to have simple cubic symmetry. That is, if $\underset{\sim}{R}$ is a symmetry operation belonging to the simple cubic (sc) subgroup of the bcc space group, then the orbitals transform as

$$\underset{\sim}{R}\, \phi_{ka}(\underset{\sim}{r}) = e^{i\underset{\sim}{k}\cdot\underset{\sim}{R}}\, \phi_{ka}(\underset{\sim}{r}) \tag{16}$$

with a similar relation holding for the $\{\phi_{kb}(\underset{\sim}{r})\}$. That is, these operations produce two sc sublattices. The operations of the bcc group not contained in this set are those translations interchanging corner and center atoms, or those which map one substructure into the other, denoted by $\underset{\sim}{R}_{ab}$, and yielding

$$\underset{\sim}{R}_{ab}\, \phi_{ka}(\underset{\sim}{r}) = e^{i\underset{\sim}{k}\cdot\underset{\sim}{R}_{ab}}\, \phi_{kb}(\underset{\sim}{r})$$

$$\underset{\sim}{R}_{ab}\, \phi_{kb}(\underset{\sim}{r}) = e^{i\underset{\sim}{k}\cdot\underset{\sim}{R}_{ab}}\, \phi_{ka}(\underset{\sim}{r}). \tag{17}$$

Thus, these orbitals are Bloch functions only for the sc subgroup, a condition equivalent to that found in (9) and (13). Therefore, for a lattice constant, a, the set of inequivalent k-vectors can be taken to be:

$$-\frac{\pi}{a} < k_x, k_y, k_z \leq \frac{\pi}{a} \tag{18}$$

which defines the first Brillouin zone (BZ), a simple cube. This cube occupies half the volume of the usual bcc dodecahedral BZ (which in this case is just the second BZ). We now have two sets of orbitals localized on different sublattices and equivalent except for a spacial translation. For N conduction electrons there are N/2 singly occupied conduction orbitals in each set and these are sufficient to just fill the first BZ. In fact, this is exactly what occurs for large lattice constants, but near equilibrium the Fermi surface

is very nearly a sphere and, hence, intersects the zone boundary, introducing new gaps into the usual band scheme.[22] Thus, both the first and the second band are only partially filled and we have a conductor. Since both of these sublattice sets yield exactly the same band structure, it suffices to treat just one of them.

For our one-electron Hamiltonian we have (in Hartree atomic units[24])

$$h_a = -\tfrac{1}{2}\nabla^2 + U_a \tag{19}$$

where U_a is a nonlocal operator somewhat more complicated than that appropriate in HF representing the interaction of the electron with N-1 other conduction electrons and the core electrons. Since ab-initio GI calculations on Li atom lead to nodeless valence orbitals,[20] weak effective potentials[21] derived from these calculations can be used to construct an effective U_a. In this context plane wave expansions of the orbitals are found to converge rapidly, and, hence, there is no need to orthogonalize the conduction orbitals to the core. A description of the construction of the potential is lengthy and will be given in a subsequent paper.

D. RESULTS AND DISCUSSION

We have used this approach to calculate the band structure of Li metal at the high symmetry points Γ, X, M, and R[23] of the GI Brillouin Zone for lattice constants ranging from 5.48 a_0 to 18 a_0. The resulting energy bands[24] as a function of $2\pi/a$ are reported in

Fig. 5.[26] The equilibrium lattice constant is a_e[25] = 6.575 a_0 (3.48 Å) and the two adjacent values correspond to ±15% volume changes. At equilibrium the first two bands overlap significantly and the system is clearly metallic. However, as the lattice constant is increased, the bands gradually separate until at 10.3 a_0 (5.45 Å) the overlap between the bands goes to zero. For larger a the first BZ is full and the second BZ is completely empty (since as we have seen we have just enough occupied states to fill the first zone) and there is an energy gap separating all the states in the first band from those in the second. Hence, the system is an insulator. Further increase in the lattice constant leads to a continuous separation of the bands toward the atomic limits until at $a = 18\ a_0$ the first band (2s) is completely flat, the 2p band is quite narrow, and the higher bands are likewise merging. This is more clearly shown in Fig. 6. To the right of the figure are the atomic valence orbital energies obtained from self-consistent GI calculations on the respective atomic states of lithium using large basis sets. For the calculation of the band states an expansion of 81 plane waves using all reciprocal lattice vectors up to and including $2\pi/a(2,1,1)$ was used. This basis set was tested at a_e where we found that an increase to 93 plane waves [up to $2\pi/a(2,2,0)$] decreased the energy of Γ by 0.001 and decreased the energy of X_4' by 0.002. Such accuracy is quite adequate for illustrating the effects of lattice parameter on the band structure.

As seen in Fig. 6 the first energy gap corresponds to the energy required for a 2s → 2p atomic transitions. However, to

obtain conduction, the required energy should be larger than this since an electron must be transferred from one neutral atom to another to create an ion pair $Li^+ Li^-$. For atoms far enough distant so that they have no overlap, this energy should be about 0.179 h = 4.9 eV [the ionization potential of Li (0.198 h) minus the electron affinity (0.019 h)].

A crude estimate of the transition point to go from an insulator to a metal can be made in the following way. We assume that the atoms do not overlap so that the energy of the normal covalent state is essentially independent of a. The energy of the state with one $Li^+ Li^-$ pair will drop as - 1/R where R is the nearest neighbor distance, $\sqrt{3}/2$ a. Thus, the ionic state will cross the covalent state at $2/\sqrt{3a} = 0.179$ or a = 6.8 a_0. Actually, the crossing point is at a = 10.3 a_0 indicating that the no overlap assumption is rather poor (there is an overlap of 0.02 between two ground state valence orbitals of Li even at 15 a_0).

The dotted-dashed line in Fig. 5 corresponds to the free electron Fermi energy for the various lattice constants. We see that this line passes through the point at which the two bands separate. This is no doubt just a coincidence since a free electron type of dispersion relation is certainly inappropriate when the bands have distorted to the extent shown at 10.3 a_0. Even at equilibrium the approximate Fermi level as indicated is well below the free electron value, that is, the dispersion relation leads to a higher density of states in the occupied part of the band than would be predicted on the basis of the face electron model.

Thus, the GI band model leads to a description which changes smoothly and continuously from a metal near the equilibrium lattice separation to an insulator at large distances and no Mott paradox is encountered. We see that the problem arises solely from the HF restriction that the orbitals be doubly occupied which in the case of odd electron systems cannot correctly describe the dissociated system. However, Mott's physical discussion of the reason that a system can be an insulator at large distances and a metal at short distances remains valid, and may be applied directly to interpret the changes which occur in the GI band description.

One aspect of considerable importance in considering the changes which a system undergoes in the transition from a metal to an insulator is the drastic change which must occur in the resistivity. Our band calculations suggest a rather continuous change in the resistivity with dilation rather than the sharp first-order transition proposed by Mott. Considering again Fig. 5, the amount of Fermi surface overlap into the second zone for large lattice constants is determined by the proximity of the point X_4' (at the center of the cube face) to the Fermi level above it (or alternatively $E_{R_1} - E_{Fermi}$). The fact that these energy changes are quite smooth indicates that the occupied volume in the second zone quite continuously goes to zero, in turn implying that no first-order transition occurs. However, in the neighborhood of 10 a_0 there must be a functional change in the temperature dependence of the lattice contribution to the resistivity, from αT as is characteristic of good metals to an $e^{\beta T}$ dependence appropriate for semiconductors. A theoretical calculation

of the resistivity in this region would be of interest to clarify this point.

There is an alternative consideration which might prove to be pertinent to the description of lattice dissociation. We have stated that in the GI method the spin coupling as well as the orbitals must be optimized. Although the coupling appropriate to a metal at equilibrium is predominantly f-type coupling, we have no assurance that this assumption is valid for spanning the range of internuclear distances through a semiconductor to an insulator. If significant coupling changes are found to be important in this region, it is quite possible that Mott's conjecture of a discontinuous change in the bands at some critical distance could be the case.

Although there is no physical means of dilating lithium metal through the range considered here, there may be other systems which would exhibit similar changes and for which a_e is above the transition point. In such a system a could be decreased by compression and could perhaps undergo an insulator to metal transition as indicated in Fig. 5. In fact, there are a number of transition metal oxides (e.g., V_2O_3 and VO_2)[27] which undergo metal-insulator transitions and are thought[28] to perhaps be examples of the kind of transitions discussed by Mott. In these transition metal oxides the GI band scheme would again lead to lower symmetries for the orbitals. Thus, it could well be that these systems just correspond to cases in which $a_t \approx a_e$ in which case the GI band scheme might well provide a convenient basis for discussing the transitions.

We will now consider the changes which occur in Li as the lattice is compressed. We see that the point X which is within the Fermi surface is split at equilibrium into two states, X_1 and X_4'. The X_1 state here lies below the X_4' state, although there is no a priori restriction that this be so. As the lattice constant is decreased, the gap between these states decreases until at 6.1 a_0 the two states coalesce. Further compression leads to a crossing and again the states separate, now with X_4' lower. A similar crossing of states occurs between M_3 and M_1, but since these states lie significantly above the Fermi level, this behavior is of little physical significance. However, the behavior exhibited by the X-states could be physically relevant if detectable changes occur in a region which can be experimentally reached by pressure or temperature changes. Of course, the critical feature here is the gap at the Fermi surface, but the behavior of the X states implies that the gap might be undergoing strong modification in this region. In this event considerations discussed elsewhere lead us to expect significant changes in the galvanomagnetic properties and in the Hall coefficient as the lattice is compressed. Such effects have been observed in the latter property[25] for the alkalis, but more careful study of the surface gap is required before any theoretical conclusions can be made.

E. CONCLUSIONS

The Mott Paradox for a system such as an alkali metal is due solely to the double-occupation restriction in the Hartree-Fock method. Relaxation of this restriction and incorporation of the correct spin symmetry leads to a band structure for a conductor at equilibrium and which changes continuously to lead to an insulator at large distances.

REFERENCES

[1]N. F. Mott, Proc. Phys. Soc. (London) A62, 416 (1949); Can. J. Phys. 34, 1356 (1956); Phil Mag 6, 287 (1961); Rev. Mod. Phys. 40, 677 (1968).

[2]J. M. Ziman, Principles of the Theory of Solids (Cambridge University Press, 1964).

[3]By N sites we refer to a perfectly ordered lattice with Born-von Karman boundary conditions.

[4]The HF orbital in Fig. 1 is from Ref. 5 and the GI orbitals are from Ref. 6.

[5]S. Fraga and B. J. Ransil, J. Chem. Phys. 35, 1967 (1961).

[6]W. A. Goddard III, Phys. Rev. 157, 81 (1967).

[7]In Fig. 2 the HF energy curve is from Ref. 5, the GI energy curve is from Ref. 8, and the exact energy curve is from Ref. 9.

[8]R. C. Ladner and W. A. Goddard III, J. Chem. Phys., to be published.

[9]W. Kolos and L. Wolniewicz, J. Chem. Phys. 41, 3663 (1964).

[10]W. A. Goddard III, Phys. Rev. 157, 73 (1967).

[11]W. A. Goddard III, J. Chem. Phys. 48, 1008 (1968).

[12]R. C. Ladner and W. A. Goddard III, J. Chem. Phys. 51, 1073 (1969).

[13]This distance is nearly the optimum distance for square H_4.

[14]W. A. Goddard III, J. Chem. Phys. 48, 450, 5337 (1968).

[15]This is close to the equilibrium internuclear separation (see L. F. Mattheiss, Phys. Rev. 123, 1209 (1961).

[16]P. M. O'Keefe and W. A. Goddard, to be published; HF, GF, and SOGI calculations were carried out using 12 (contracted Gaussian) basis functions. The distance $R = 2\ a_0$ is known to be near equilibrium reported CI calculations.[a] We obtained for our energies (values from published results are also given)

HF	-3.23186 h
GF	-3.29024 h
SOGI	-3.29491 h
CI[a]	-3.24961 h
AMO[19]	-3.21303 h

(our energies are lower than CI since we have not used a minimum basis set). [a]See L. F. Mattheiss, Phys. Rev. 123, 1209 (1961).

[17]R. Paunz, J. DeHeer, and P. O. Lowdin, J. Chem. Phys. 36, 2247, 2257 (1962).

[18]E. G. Larson and W. R. Thorson, J. Chem. Phys. 43, 3832 (1965); Ibid. 45, 1539 (1966).

[19]J. W. Moskowitz, J. Chem. Phys. 38, 677 (1963).

[20]W. A. Goddard III, Phys. Rev. 169, 120 (1968).

[21]W. A. Goddard III, Phys. Rev. 174, 659 (1968); L. R. Kahn

and W. A. Goddard III, Chem. Phys. Lett. 2, 667 (1968).

[22]P. M. O'Keefe and W. A. Goddard III, Phys. Rev. Lett., 23, 300, (1969).

[23]These symmetry points are $\Gamma = 2\pi/a(0,0,0)$, $X = 2\pi/a(0,0,\frac{1}{2})$, $M = 2\pi/a(\frac{1}{2},\frac{1}{2},0)$, and $R = 2\pi/a(\frac{1}{2},\frac{1}{2},\frac{1}{2})$, where a is the lattice constant.

[24]We use Hartree atomic units, in which $\hbar = 1$, $|e| = 1$, $m_e = 1$. Thus, the unit of length is the Bohr, 1 a_0 = 0.52917 Å and the unit of energy is the Hartree, 1 h = 27.2107 eV = 2 Rydbergs.

[25]This value is for 4°K as obtained from W. Pearson, Can. J. Phys. 32, 708 (1954) using conversion constants from E. R. Cohen and J. M. W. Dumond, Rev. Mod. Phys. 37, 537 (1965).

[26]For the larger lattice constants, the set of higher lying states (e.g., f, g, ··· and excited states of those shown) which could have been included is much greater than those shown, but states above the 3d level contribute little to the description and are less well converged.

[27]F. J. Morin, Phys. Rev. Lett. 3, 34 (1959); International Conference on the Metal-Nonmetal Transitions, Rev. Mod. Phys. 40, 677-879 (1968); A. Jayaraman and J. P. Remeika, Bull. Amer. Phys. Soc. II, 15, 386 (1970).

[28]See for example Ref. 1, N. F. Mott, Rev. Mod. Phys., (1968).

[29]T. Deutsch, W. Paul, and H. Brooks, Phys. Rev. 124, 753 (1961).

Fig. 1 (a) The GI and (b) the HF orbitals for H_2 at equilibrium.

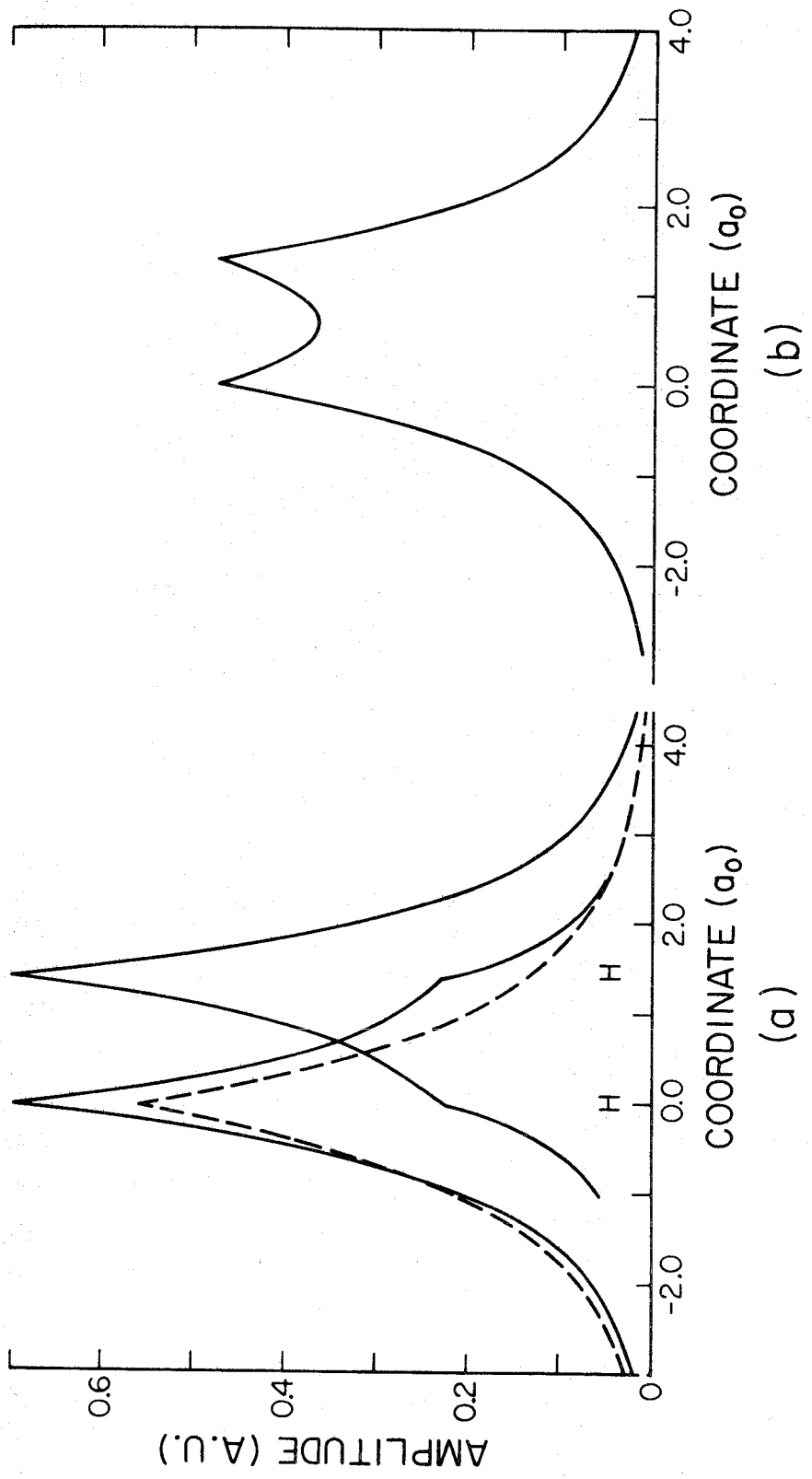
AMPLITUDE (A.U.)
0.6
0.4
0.2
0
-2.0
0.0
2.0
4.0
H
H
COORDINATE (a_o)
(a)
-2.0
0.0
2.0
4.0
COORDINATE (a_o)
(b)

Fig. 2. The energy of H_2 as a function of the internuclear distance for the HF, GI, and CI descriptions.

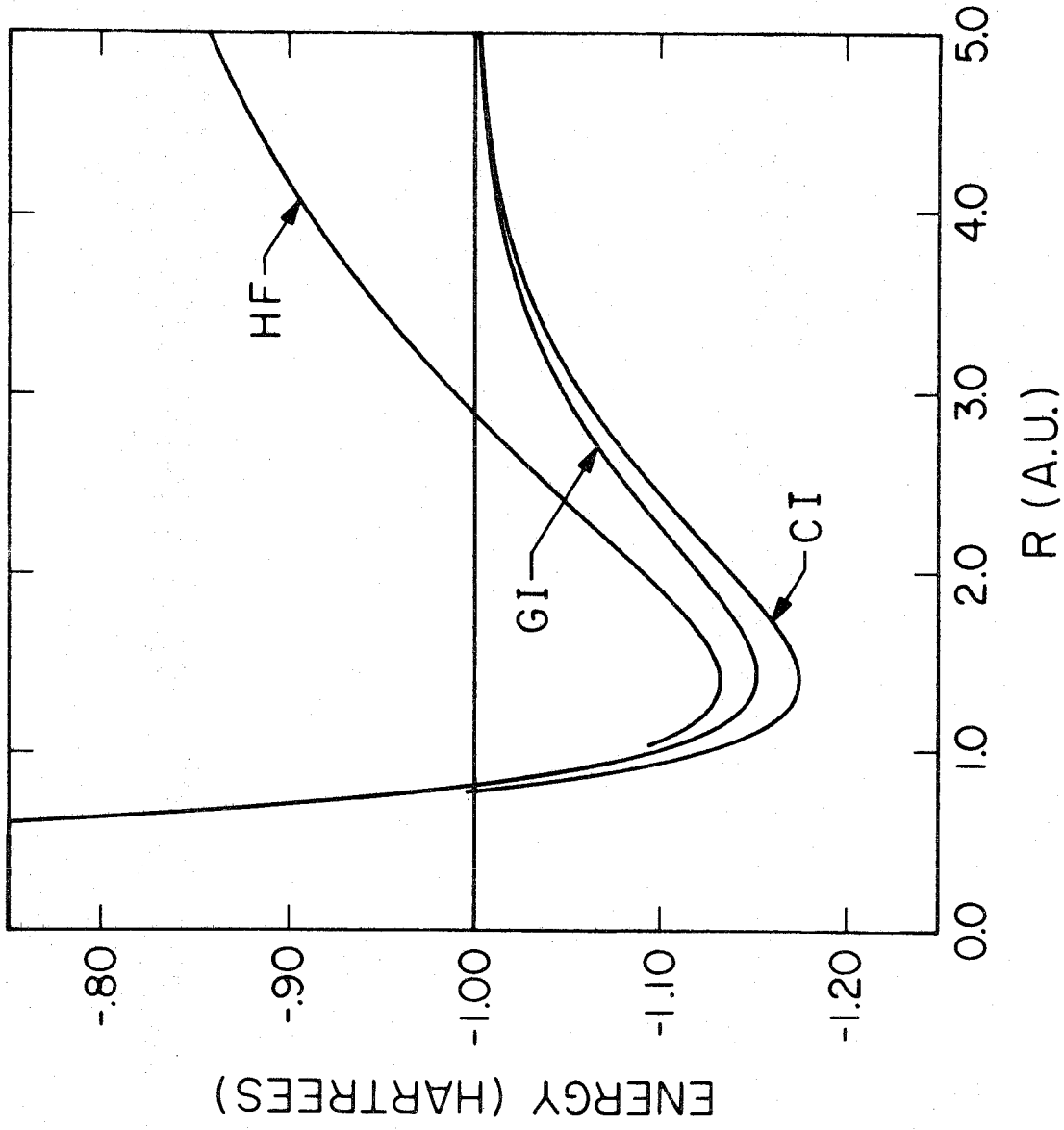
HF
GI
CI
-.80
-.90
-1.00
-1.10
-1.20
ENERGY (HARTREES)
0.0
1.0
2.0
3.0
4.0
5.0
R (A.U.)

Fig. 3. The GF orbitals for H_4 at the equilibrium separation (2.54 a_0).

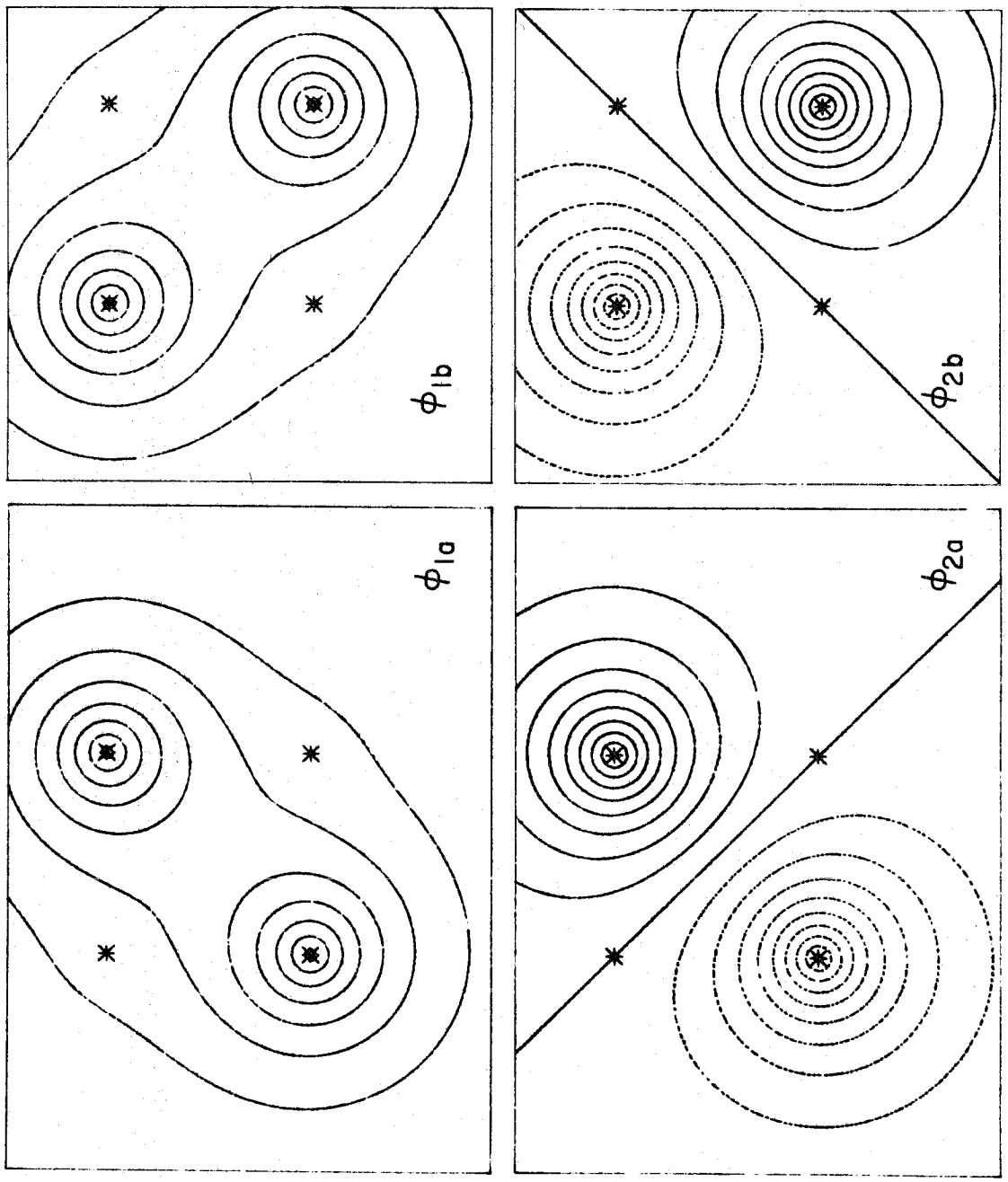
ϕ_{1b}
ϕ_{2b}
ϕ_{1a}
ϕ_{2a}

Fig. 4. Three of the GF orbitals for H_6 near the equilibrium. The remaining three orbitals are mirror images of these.

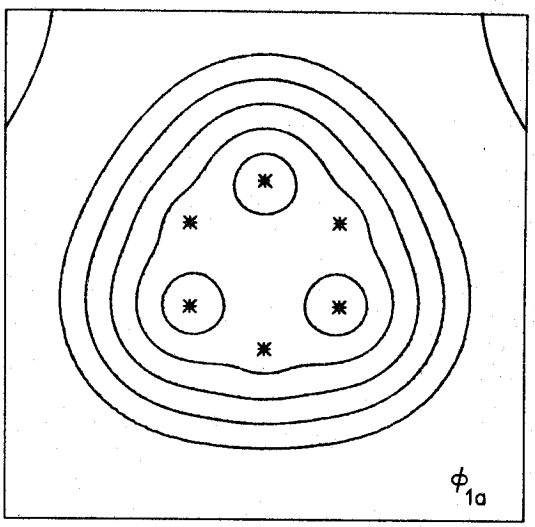
ϕ_{1a}

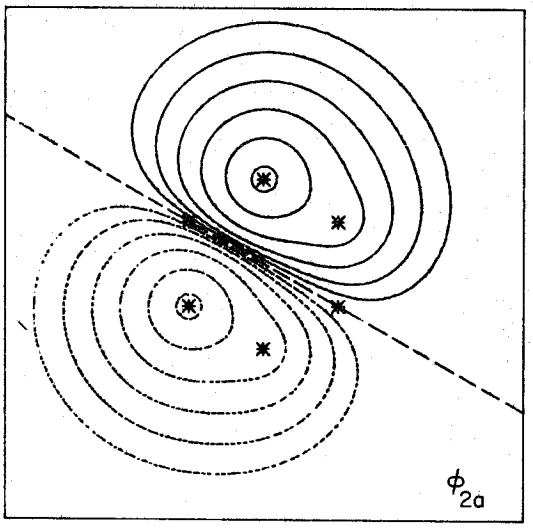
ϕ_{2a}

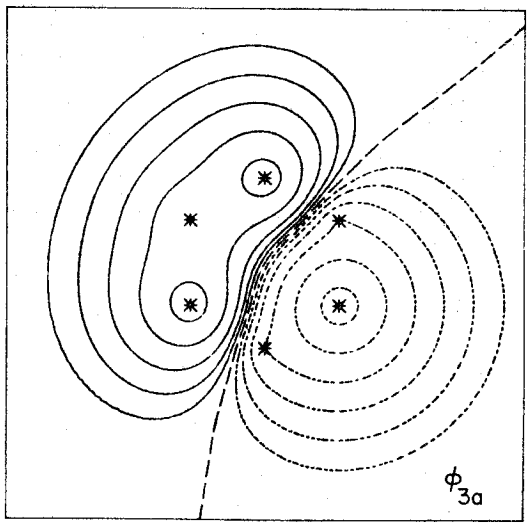
ϕ_{3a}

Fig. 5. Energies at high symmetry points in the GI band scheme as a function of the lattice constant. The lines on either side of equilibrium (6.575 a_0) are for a = 6.25 a_0 and 6.90 a_0, respectively.

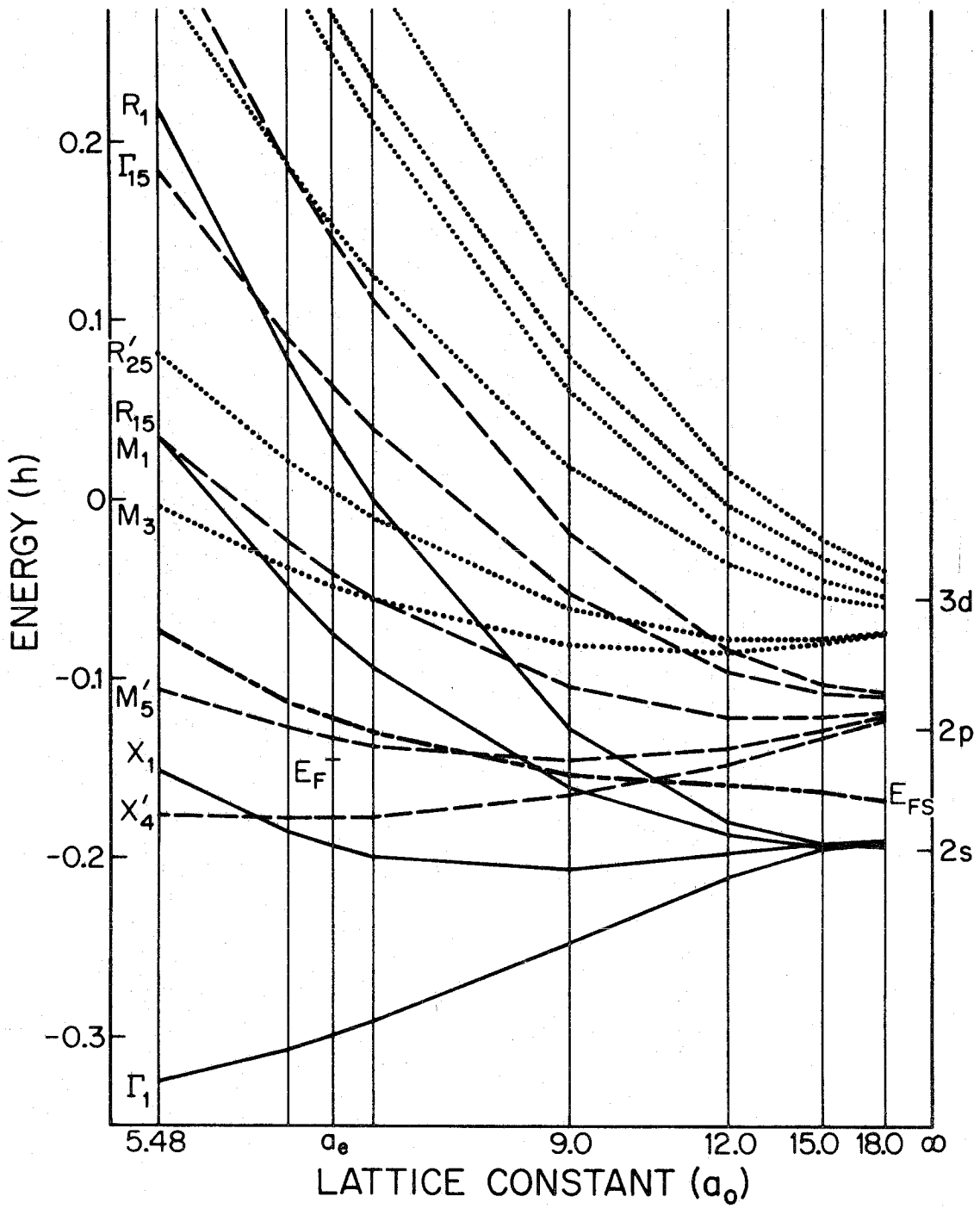
R1
Γ15
R'25
R15
M1
M3
M'5
X1
X'4
Γ1
E_F
E_FS
3d
2p
2s
0.2
0.1
0
-0.1
-0.2
-0.3
ENERGY (h)
5.48
a_e
9.0
12.0
15.0
18.0
∞
LATTICE CONSTANT (a_0)

Fig. 6. The energies at the high symmetry points in the Brillouin Zone at a = 18 a_0. The levels indicated to the right of the figure are the orbital energies from GI calculations of the indicated atomic states.

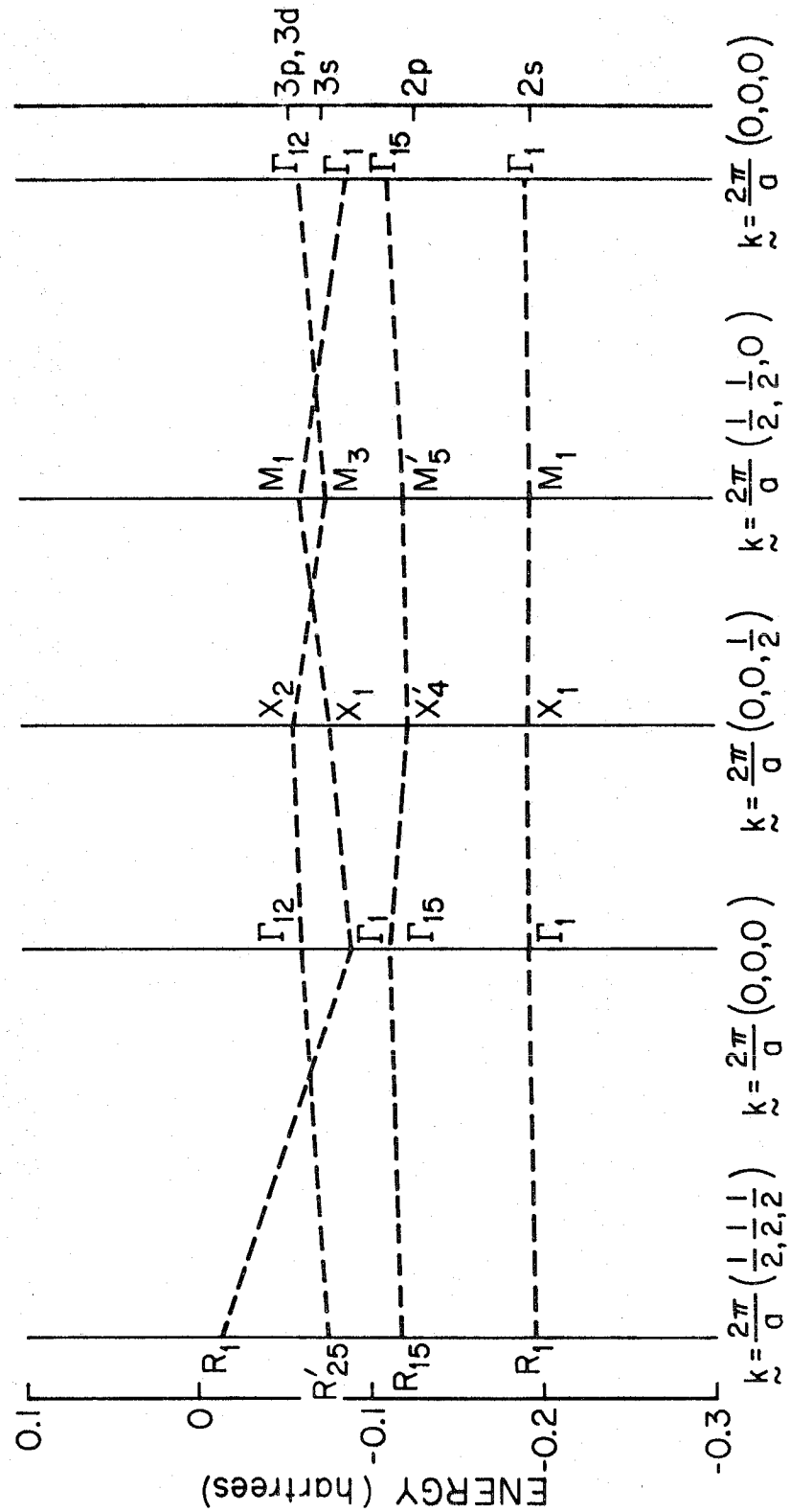
ENERGY (hartrees)
0.1
0
-0.1
-0.2
-0.3
3p, 3d
3s
2p
2s
R1
R'25
R15
R1
Γ12
Γ1
Γ15
Γ1
X2
X1
X'4
X1
M1
M3
M'5
M1
Γ12
Γ1
Γ15
Γ1
k = 2π/a (1/2, 1/2, 1/2)
k = 2π/a (0,0,0)
k = 2π/a (0,0,1/2)
k = 2π/a (1/2, 1/2,0)
k = 2π/a (0,0,0)

IV. PUBLICATIONS

Reprinted from THE PHYSICAL REVIEW, Vol. 180, No. 3, 747–749, 15 April 1969

Lithium Energy-Band Structure Calculations Using *Ab Initio* Pseudopotentials*

PATRICIA M. O'KEEFE† AND WILLIAM A. GODDARD, III‡
Arthur Amos Noyes Laboratory of Chemical Physics, California Institute of Technology, Pasadena, California 91109
(Received 7 October 1968)

A recently suggested method for constructing *ab initio* pseudopotentials has been applied to Li and used to calculate the energies at high-symmetry points of the Brillouin zone for lithium metal. This potential is unique, local, and Hermitian and is much weaker than the Hartree-Fock potential. As a result of the weakness of the potential, the conduction-band orbitals are smooth in the core regions, and plane-wave expansions are found to converge rapidly. (There is no restriction that the conduction orbitals be made orthogonal to the core orbitals.) The lowest energy band has character similar to the band obtained from orthogonalized planes-wave calculations using the Seitz empirical potential.

INTRODUCTION

SIGNIFICANT progress has been made in elucidating the electronic band structure of metals.[1] Although it has not been possible to carry out *ab initio*[2] calculations for solids, techniques have been developed for estimating the crystal potential.[3–7]

Once one has an approximate Hartree-Fock crystal potential in a metal, it is necessary to solve for the conduction orbitals in this potential. Orthogonality restrictions imposed by the Hartree-Fock method result in rapid oscillation of the conduction orbital near the atomic cores, so that plane-wave expansions converge extremely slowly here, requiring high momentum waves.[1] This behavior is incorporated in the basis set by orthogonalizing the plane waves[8] to the core functions. Expansion of the conduction orbitals in these orthogonalized plane waves (OPW) then converges rapidly.[8,9]

In recent years a different approach, using pseudopotentials,[10,11] has received much attention. In this approach one deals not with Hartree-Fock states but rather with pseudo-orbitals which are "smoothed" Hartree-Fock orbitals. These pseudo-orbitals are eigenstates of a pseudopotential which is the sum of the Hartree-Fock potential and a repulsive potential. Such an approach has several distinct advantages. Since the pseudopotential is much weaker than the Hartree-Fock potential, perturbation theory may be used in describing scattering due to impurities or electron-phonon interactions.[12,13] In addition, since the orbitals are smooth, plane-wave expansions are rapidly convergent.[10,11]

However, as has long been recognized,[10,12] the fundamental foundation for pseudopotentials is tenuous in that the pseudopotential is not unique,[14] is not Hermitian,[10,15] and, within the Hartree-Fock framework, has not been derived from *ab initio*[2] calculations.

It has been shown elsewhere[16] that an alternative approach, the G1 method, for electronic-wave functions automatically leads to a smooth, nodeless valence

TABLE I. Band energies (Ref. 19) in hartree atomic units (Ref. 20) for the lowest state Γ_1 in the lowest band, and for another low-lying state N_1', calculated using basis-set sizes as indicated. The lowest energies calculated in the same way using the Seitz Fourier coefficients (Ref. 9) are included for comparison.

	Original plane-wave set	Size of reduced matrix	Lowest energy	Next lowest energy	Lowest Seitz value
	1	1	−0.3220		−0.5011
	7	2	−0.3239		−0.5035
Γ_1	19	3	−0.3275	0.7876	−0.7291
	43	4	−0.3296	0.7683	−0.8420
	51	5	−0.3296	0.7679	−0.8767
	75	6	−0.3297	0.7648	−0.9532
	123	7	−0.3297	0.7644	−1.024
	2	1	−0.1821		−0.1823
	6	2	−0.1852	0.7321	−0.1915
	14	3	−0.1946	0.7145	−0.2049
N_1'	16	4	−0.1973	0.7111	−0.2074
	20	5	−0.1977	0.7102	−0.2075
	24	6	−0.1986	0.7052	−0.2076
	32	7	−0.1988	0.7041	−0.2076
	36	8	−0.1990	0.7032	−0.2078
	44	9	−0.1993	0.6980	−0.2079
	52	10	−0.1993	0.6972	−0.2080

* Partially supported by Grant No. GP-6965 from the National Science Foundation.
† NDEA Fellow.
‡ Alfred P. Sloan Research Fellow.
[1] J. C. Slater, *Quantum Theory of Molecules and Solids* (McGraw-Hill Book Co., New York, 1965), Vol. 2.
[2] By an *ab initio* wave function, we mean one obtained directly from the many-electron Schrödinger equation with no restrictions except on the functional form of the many-electron wave function (e.g., a Slater determinant or G1-type function). Thus, calculations which make use of classical approximations such as using Poisson's equation, or of such approximations as the Slater exchange approximation, we would consider to be *a priori* (not empirical) but not *ab initio*.
[3] R. H. Parmenter, Phys. Rev. **86**, 552 (1952).
[4] F. Seitz, Phys. Rev. **47**, 400 (1935); corrected values are reported by W. Kohn and N. Rostoker, *ibid.* **94**, 1111 (1954).
[5] B. Segall, Phys. Rev. **125**, 109 (1962).
[6] F. Herman and S. Skillman, *Atomic Structure Calculations* (Prentice-Hall, Inc., Englewood Cliffs, N. J., 1963).
[7] E. C. Snow and J. T. Waber, Phys. Rev. **157**, 570 (1967).
[8] C. Herring and A. G. Hill, Phys. Rev. **58**, 132 (1940); C. Herring, *ibid.* **57**, 1169 (1940).
[9] M. L. Glasser and J. Callaway, Phys. Rev. **109**, 1541 (1958).
[10] W. A. Harrison, *Pseudopotentials in the Theory of Metals* (W. A. Benjamin, Inc., New York, 1966).
[11] J. C. Phillips and L. Kleinman, Phys. Rev. **116**, 287 (1957); **116**, 880 (1957).
[12] J. M. Ziman, Advan. Phys. **13**, 89 (1964).
[13] L. J. Sham and J. M. Ziman, Solid State Phys. **15**, 221 (1963).
[14] M. H. Cohen and V. Heine, Phys. Rev. **125**, 1821 (1961).
[15] B. J. Austin, V. Heine, and L. J. Sham, Phys. Rev. **127**, 276 (1962).
[16] W. A. Goddard, III, Phys. Rev. **174**, 659 (1968).

TABLE II. Band energies (Ref. 19) in hartree atomic units (Ref. 20) based on G1 pseudopotentials. The two lowest values are reported for each state (Ref. 21). OPW results are included for comparison.

State	Type	Lowest solution G1(exact)	G1(sph.)	OPW[a]	Second lowest solution G1(exact)	G1(sph.)	OPW[a]
Γ_1	s	−0.3296	−0.3353	−0.3432	0.7683	0.8022	0.9393
Γ_{15}	p	0.3083	0.3085	0.3085	1.346	1.334	1.355
Γ_{25}'	d	0.4778	0.4196	0.427	2.178	2.142	2.175
Γ_{12}	d	0.5242	0.5633	0.573	1.365	1.396	1.42
Γ_{25}	f	0.5471	0.5680	0.578	2.330	2.384	2.425
Γ_2'	f	2.222	2.213	2.245	5.128	5.121	5.09
N_1'	p	−0.1990	−0.2021	−0.202	0.7032	0.7120	0.7165
N_1	s	−0.0890	−0.1001	−0.088	0.4025	0.4189	0.4355
N_3'	p	0.1515	0.1293	0.137[b]	1.064	1.003	1.055[b]
N_4'	p	0.2115	0.2263	0.2375[b]	0.6174	0.6401	0.685[b]
N_2	d	0.2841	0.2653	0.262	1.150	1.128	1.22
N_4	d	0.7198	0.7220	0.7385	1.181	1.221	1.245
N_3	d	1.092	1.087	1.105	1.650	1.646	1.675
N_2'	f	1.224	1.198	1.20	3.448	3.402	...
H_{15}	p	−0.0170	−0.0431	−0.046	0.8568	0.8949	0.8695
H_{12}	d	0.0805	0.1133	0.1135	1.754	1.785	1.76
H_1	s	0.2066	0.2104	0.2855	1.154	1.195	1.30
H_{25}'	d	0.9233	0.9095	0.92	1.824	1.785	1.855
H_2'	f	0.9535	0.8492	0.865	3.562	3.528	3.59
H_{25}	f	1.816	1.818	1.85	1.930	1.964	2.00
P_4	p	−0.0882	−0.0901	−0.0945	0.6410	0.6502	0.669
P_1	s	0.0538	0.0296	0.165	1.090	1.042	1.375
P_3	d	0.7924	0.7845	0.8015	1.756	1.748	1.785
P_5	f	0.8893	0.9089	0.930	1.738	1.758	1.825

[a] Glasser and Callaway (Ref. 9).
[b] These values may be incompletely converged.

orbital for the lithium atom and consequently a weak effective potential $V_{\text{atom}}^{\text{G1}}$ for this orbital. This G1 potential (being Hermitian, unique, and local) possesses all of the properties required for pseudopotentials, and *is* derived from *ab initio* calculations.[16]

Making use of this *ab initio* pseudopotential, we present here the initial results of band calculations which we are carrying out on lithium metal.

CALCULATIONS AND DISCUSSION

For the crystal potential V, we make the common approximation[1,9] that within any one Wigner-Seitz cell $V=V_{\text{atom}}^{\text{G1}}$,[17] with the origin taken to be the center of the cell. Since $V_{\text{atom}}^{\text{G1}}$ is weak, the orbitals ϕ_k were expanded in simple plane waves. In this case, the solution of the G1 wave equation for ϕ_k requires only the Fourier transform of $V_{\text{atom}}^{\text{G1}}$ over the Wigner-Seitz cell.

In order to test the rapidity of convergence of the plane wave expansion, we considered the low-lying states Γ_1 and N_1'.[18] All orders of the reduced matrix were considered up to the set based on 123 and 52 plane waves, respectively. These energies are reported in Table I. We see that the plane-wave expansion does indeed lead to rapid convergence for the G1 functions, whereas in the Hartree-Fock case it shows extremely slow convergence for the Γ_1 state. In Table II we report the calculated energies[19,20] for many of the lower states[21] at the center (Γ) and at several points on the surface of the Brillouin zone (N,H,P).[18] These values are compared to those for an OPW calculation[9] utilizing the empirical Seitz potential.[4] We see that the G1 energies and those obtained from OPW's agree to about 10% in most cases, indicating that either method yields a qualitatively correct band structure. However, the G1 results are based on *ab initio* pseudopotentials and lead to smooth conduction orbitals and, as such, are more likely to be useful for scattering calculations and other considerations.[12,13]

In the past, it has been a common practice to calculate the Fourier transforms over the Wigner-Seitz cell by assuming the bcc cell to be spherical.[9] Although this greatly simplifies the calculations, we have found the resulting coefficients to often be in poor agreement with the exact values (obtained by numerical integration[22]) as is shown in Table III. We note several cases (e.g., $n^2=4$, 8, 10, 14, 18) in which the spherical-cell approximation leads to sizeable errors in the Fourier coefficients. Since the spherical approximation was used

TABLE III. Fourier coefficients[a] for the s and p potentials[b] as calculated exactly using the spherical approximation

n^2	$(a/2\pi)\mathbf{K}$	Exact	Spherical s	Exact p	Spherical p
0	(0,0,0)	−0.32197	−0.32342	−0.49122	−0.48996
2	(1,1,0)	0.01957	0.01435	−0.08086	−0.08611
4	(2,0,0)	0.02427	0.04861	−0.04328	−0.01832
6	(2,1,1)	0.01888	0.02101	−0.02945	−0.02734
8	(2,2,0)	0.01223	0.00165	−0.02425	−0.03514
10	(3,1,0)	0.00658	0.00191	−0.02214	−0.03075
12	(2,2,2)	0.00287	0.00197	−0.02021	−0.02103
14	(3,2,1)	0.00142	0.00574	−0.01717	−0.01285
16	(4,0,0)	0.000765	0.00624	−0.01456	−0.00900
18	(3,3,0)	−0.000557	0.00366	−0.01358	−0.00902
18	(4,1,1)	−0.000768	0.00366	−0.01334	−0.00902
20	(4,2,0)	−0.00157	−0.000324	−0.01196	−0.01102
22	(3,3,2)	−0.00185	−0.00401	−0.01096	−0.01311
24	(4,2,2)	−0.00274	−0.00633	−0.01070	−0.01412
26	(4,3,1)	−0.000888	−0.00701	−0.00999	−0.01368
26	(5,1,0)	−0.00107	−0.00701	−0.01010	−0.01368

[a] Defined by $V_{FT}(\mathbf{K})=(1/\Omega_0)\int_{\Omega_0}e^{i\mathbf{K}\cdot\mathbf{r}}V(r)d\mathbf{r}$, where Ω_0 is the atomic volume and $\mathbf{K}$ is a reciprocal-lattice vector.
[b] All values are in hartree atomic units (Ref. 20).

[17] The pseudopotential derived for the $2s$ valence orbital of Li atom was used for the s symmetry states in the metal and the corresponding $2p$ potential was used for the p, d, and f states. Since the s pseudopotential is quite different from the p pseudopotential, it would approximate the p states poorly (see Ref. 1). However, the d and f potential are rather similar, so that the p potential leads to a good approximation for d states. Of course, all of these atomic pseudopotentials are spherically symmetric.

[18] For a bcc lattice, Γ, H, P, and N represent, respectively, the reciprocal vectors $(a/2\pi)\mathbf{k}=(0,0,0)$, $(1,0,0)$, $(\frac{1}{2},\frac{1}{2},\frac{1}{2})$, and $(\frac{1}{2},\frac{1}{2},0)$.

[19] We have used a lattice constant of $a=6.575a_0$ corresponding to an atomic volume of $142.12068a_0^3$ (see Ref. 16).

[20] The units used throughout are hartree atomic units; thus the unit of energy is the hartree or 27.2107 eV.

[21] A basis set of 43 plane waves was used in the calculations of these energies. This corresponds to using all reciprocal-lattice vectors up to $(a/2\pi)\mathbf{K}=(2,1,1)$.

[22] A Riemann integration was performed under the exact surface. For choosing the optimum integration points, we used the technique of H. Conroy, J. Chem. Phys. 47, 5307 (1967).

in the OPW calculation on lithium, we have also included in Table II the energies corresponding to the use of this approximation for the G1 potential.

SUMMARY

We have found that band calculations using *ab initio* pseudopotentials on lithium metal are simple and lead to reasonable energies. The resulting conduction orbitals are smooth and may be useful for considering various properties of metals. Because the orbitals are smooth, plane-wave expansions are found to converge rapidly. Band calculations to further characterize the electron-band structure of lithium for points within the Brillouin zone are currently in progress.

NEW APPROACH TO ENERGY-BAND CALCULATIONS WITH RESULTS FOR LITHIUM METAL*

Patricia M. O'Keefe† and William A. Goddard, III‡
Arthur Amos Noyes Laboratory of Chemical Physics,
California Institute of Technology, Pasadena, California 91109
(Received 23 June 1969)

A new method, the GI method, for electronic wave functions has been applied to the study of energy bands in bcc lithium metal. The GI method leads to energy bands for lithium comparable with the Hartree-Fock bands except that small gaps occur within the first Hartree-Fock Brillouin zone. This leads to a compelling interpretation of several anomalous experimental properties of alkali metals (such as the very low optical absorption threshold and the lack of saturation of the transverse magnetoresistance).

Band structures for solids have usually been calculated using the Hartree-Fock (HF) method.[1] In this method the total wave function is a Slater determinant of spin orbitals,

$$\alpha\Psi, \tag{1}$$

where Ψ is a product of spin orbitals and α is the antisymmetrizer. For a singlet state, the spin orbitals are required to occur in pairs which involve the same spatial orbitals but different spins, say $\varphi_i\alpha$ and $\varphi_i\beta$ (i.e., the orbitals φ_i are doubly occupied) in order that the total wave function have the correct spin symmetry. One of the most valuable features of the HF method is that each orbital can be interpreted as the eigenstate of an electron moving in the average field due to the other electrons.

Recently it has been shown that it is possible to go beyond the HF framework while retaining an independent particle interpretation.[2] In the GI method[2] the antisymmetrizer in (1) is replaced by the group operator[3] G_i^{γ}, which ensures that

$$G_i^{\gamma}\Psi \tag{2}$$

is an eigenfunction of $\hat{S}^2$ and satisfies the Pauli principle for all choices of orbitals in Ψ. Thus every spatial orbital is allowed to be different (no double occupation). This method has been applied to a number of atoms and molecules, including Li[4] and Li_2,[5,6] and always leads to a better energy than HF. In calculations on Li it was found that the core orbitals could be exactly replaced by an effective local potential (the ab initio pseudopotential),[7] and it was found that this potential accurately reproduces the states of Li_2.[6] In Li_2, instead of one symmetric (σ_g) doubly occupied bonding orbital as in the HF method, we obtain two bonding orbitals, each concentrated on one of the respective Li centers.

We have now applied the GI method to studying the band structure of Li metal. Just as in the Li_2 molecule, the GI orbitals have lower symmetry than the HF orbitals. In order to describe the states of Li metal, it is convenient to view the bcc lattice in terms of the two equivalent interpenetrating simple cubic (sc) sublattices. The GI conduction orbitals divide into two sets: The

a orbitals $\{\varphi_{ia}\}$ are mutually orthogonal, are eigenfunctions of the one-electron self-consistent-field Hamiltonian H_a, and are concentrated (or localized) more on the a sublattice (sc_a); similarly the b orbitals $\{\varphi_{ib}\}$ are orthogonal, are eigenfunctions of a different Hamiltonian H_b, and are concentrated more on the b sublattices (sc_b).[8] No orthogonality conditions exist between the sets $\{\varphi_{ia}\}$ and $\{\varphi_{ib}\}$, but they are related by the translation vectors between sc_a and sc_b. The GI orbitals are Bloch functions, but only for the sc space group, not for the bcc space group; however, the many-electron wave function (2) still transforms according to the bcc space group. Hence, since the unit cell for sc is twice the volume of the bcc unit cell, the resulting sc Brillouin zone (BZ) is only half the volume of the bcc BZ and is a cube inscribed in the HF dodecahedral BZ. In terms of this reduced sc BZ each HF band becomes two bands, and in this new context it is possible for small energy-band gaps to occur on the boundary of the sc BZ. We will see below that since this first BZ has the same volume as the Fermi surface, and since the Fermi surface is roughly spherical, the Fermi surface overlaps the first two GI bands.

As discussed below, the existence of two partially filled bands seems to provide a cogent explanation of several properties observed in the alkalis which afford no natural explanation within the HF framework. These properties are the following: (1) The observed linearity of the transverse magnetoresistance[9,10] of the alkalis is in contradiction to the saturation in high fields expected for the closed orbits found in HF.[11] (2) The Hall coefficient[12] exhibits a significant decrease in increasing fields which is not expected for the HF schema. (3) The optical absorption threshold observed for alkali metals is far lower than expected from the HF energy bands.[13] (4) The soft-x-ray spectra[14] are difficult to explain for the HF energy band.

We have carried out GI calculations for band states at the center and at three symmetry points[15] on the surface of the sc BZ. The wave functions were expanded in plane waves and solved in the field of the Li atom ab initio effective potential[7,16] centered at the center of the cell. As for Li_2,[6] the potential is angular-momentum dependent (i.e., different for s and p states). The energies of the states calculated using the GI approach and the connectivity of these states are shown in Fig. 1.

We find that the splittings are small, 0.5 eV at $k=(2\pi/a)(\frac{1}{2},0,0)$ and dropping to 0.0 at $k=(2\pi/a)\times(\frac{1}{2},\frac{1}{2},0)$. Thus the Fermi surface should be nearly spherical. However, the Fermi surface overlaps the first two GI bands and intersects the sc BZ at about 0.734 of the distance from $k=(2\pi/a)(\frac{1}{2},0,0)$ to $k=(2\pi/a)(\frac{1}{2},\frac{1}{2},0)$, at which point ($k_F=0.59a_0^{-1}$) the energy gap should be about 0.08 to 0.16 eV.[17] This gap size should cause little distortion from sphericity for the Fermi surface, which is in agreement with de Haas–van Alpen,[18] cyclotron-resonance,[19] and positron-annihilation experiments,[20] and with the x-ray determination of electron moments.[21] But optical transitions are now allowed between occupied states of the first band and empty states of the second band, and thus the threshold for optical transitions

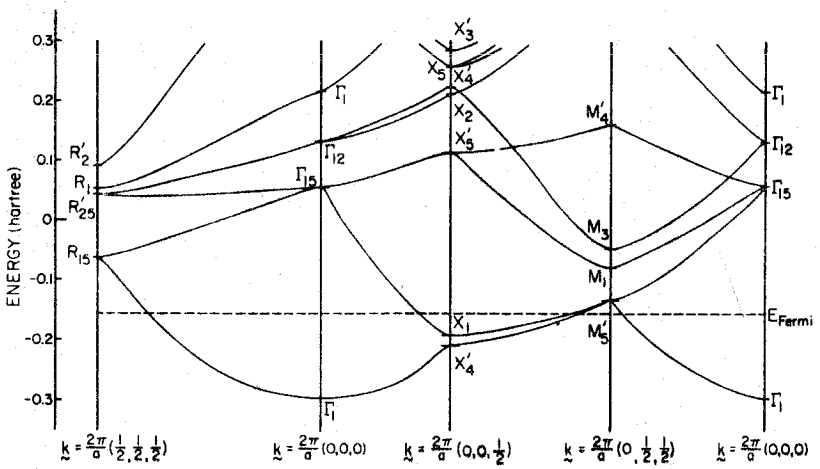

FIG. 1. GI energy-band states at the center and at high-symmetry points on sc BZ boundary for bcc lithium metal. [All quantities are in Hartree atomic units (the unit of energy is the Hartree = 27.211 eV). A lattice constant of $6.575a_0$ has been used.] Lines indicate only the connectivity of the states and the dashed line denotes the approximate location of the Fermi level.

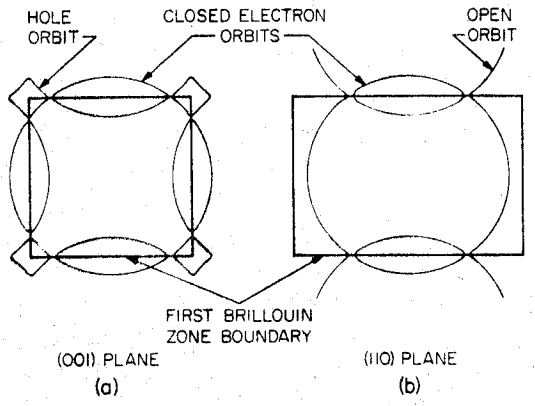

FIG. 2. Maximum orbitals in k space (Fermi-surface radius $k_F = 0.5298 a_0^{-1}$). (a) The (001) plane (appropriate for $B \parallel [001]$); $\theta = 72°$; $\theta' = 18°$; side of square $= 0.9556 a_0^{-1}$. (b) The (110) plane (appropriate for $B \parallel [110]$); $\theta = 72°$; $\theta' = 108°$; sides of rectangle $= 0.9556 a_0^{-1}$ and $1.3514 a_0^{-1}$.

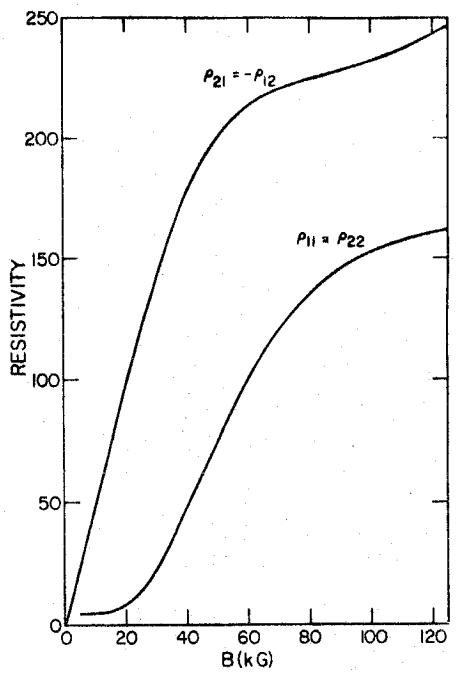

FIG. 3. The lithium-metal resistivity components $\rho_{11} = \rho_{22}$ and $\rho_{21} = -\rho_{12}$ as a function of the magnetic field (oriented in the [001] direction). Calculations were carried out allowing transitions between orbits. An energy gap of 0.08 eV = 0.002 94 Hartrees and a relaxation time $\tau = 0.7 \times 10^{-10}$ sec were used.

should be very small. These new transitions from the first to the second GI band correspond to indirect (or k-symmetry-forbidden) transitions in terms of the HF band. Such indirect transitions have also been detected in other materials[22] and it may be that GI energy bands could be used to explain these.

As shown in Fig. 2(b) it is possible to have open orbitals in some planes [e.g., (110)] whereas for other planes [e.g., (001) in Fig. 2(a)] both the electron and hole orbits are closed. The very small energy gap is expected to allow magnetic breakdown which would lead to transitions between open and closed orbits and between closed orbits. As discussed by Falicov and Sievert[23] such band-to-band transitions can lead to unusual variations in the magnetoresistance as a function of magnetic field. We have carried out similar calculations for the cases in Fig. 2 and find results similar to theirs. In order to make a relevant comparison with experimental results, we have extended the calculation to an integration over the entire Fermi surface rather than just over the maximal orbits. Our results for the field in the [001] direction are reported in Fig. 3. We find a distinctly linear behavior (20 to 80 kG) in the transverse magnetic resistance over a large part of the field range (10 to 60 kG) investigated by Penz and Bowers.[9] In addition we find that ρ_{21} (the Hall coefficient R times the magnetic field) is linear at low fields, decreases in slope at intermediate fields, and is again linear (with smaller slope) at high fields. This is consistent with the decrease in R found by Penz for intermediate fields. The large slope at small fields occurs because of the large fraction of hole orbits. On account of magnetic breakdown in the limit of high fields all orbits are electron orbits. On the basis of the band-structure calculations the ratio of these slopes is expected to be about 4:1, which is consistent with the ρ_{21} calculations for various values of the energy gap and relaxation time (τ).

The HF wave function for Li has a half-filled conduction band for all lattice constants, including $a = \infty$. However, as noted by Mott[24] this cannot be correct for large a since the system must be an insulator at sufficiently large internuclear separations. This is known as the Mott paradox[11] and has been explained in terms of electron correlation.[11,24] We have carried out GI calculations on Li at larger internuclear distances and find that the energy gap increases and the bandwidths decrease with internuclear distance until for large a ($15 a_0$) the gap corresponds approximately to the Li atom $2s$-$2p$ excitation energy and the width of the first band is negligible. Thus the first cubic BZ is completely filled and the second zone completely empty, and bcc Li is an insulator at larger distances, just as it should be. That is, for the GI band structure, bcc Li changes continuously from an insulator at large a to a

metal at small a, and we see that the Mott paradox merely arises as an artifact of the HF band scheme. (It actually results because the HF orbitals are forced to be doubly occupied which results in an incorrect dissociation of the wave function as $a \to \infty$. The analogous incorrect behavior also occurs for the HF wave function of Li_2 molecule.)[8] It may be that a study of the GI band structure of transition-metal oxides would provide an understanding of the Mott-like transitions which occur in these and related systems.[24,25]

In addition to the aforementioned properties, it may be possible to explain the anomalous soft x-ray emission spectrum[14] of Li from the GI energy bands. However, here it is essential to calculate the states within the sc BZ. We are now in the process of carrying out such calculations, which are required for a consideration of the intensities of both optical and x-ray transitions and are also necessary for a more accurate determination of the magnetoresistance.

Other attempts to explain the anomalous properties of the alkali metals have been made by Phillips and Cohen,[26] postulating a collective resonance state, and by Overhauser and co-workers,[27] postulating spin-density or charge-density waves. The GI wave function (2) for Li leads to an alternative to these explanations; however, it retains the correct bcc periodicity and is exactly a singlet state with no net spin density anywhere.

In conclusion, we find that the band structure of Li metal obtained directly from GI calculations leads to two partially filled bands and small energy gaps. The existence of these gaps leads to a direct and simple explanation of several anomalous properties of alkali metals.

---

*Work partially supported by National Science Foundation Grant No. GP-6965.

†National Defense Education Act Fellow.

‡Alfred P. Sloan Fellow.

[1]J. C. Slater, Quantum Theory of Molecules and Solids (McGraw-Hill Book Company, Inc., New York, 1965), Vol. II.

[2]See W. A. Goddard, III, Phys. Rev. 157, 81 (1967), for an explanation of this method.

[3]W. A. Goddard, III, Phys. Rev. 157, 73 (1967).

[4]W. A. Goddard, III, Phys. Rev. 169, 120 (1968).

[5]R. J. Blint, W. E. Palke, and W. A. Goddard, III, to be published.

[6]L. R. Kahn and W. A. Goddard, III, Chem. Phys. Letters 2, 667 (1968).

[7]W. A. Goddard, III, Phys. Rev. 174, 659 (1968).

[8]W. A. Goddard, III, J. Chem. Phys. 48, 450 5337 (1968).

[9]P. A. Penz and R. Bowers, Phys. Rev. 172, 991 (1968).

[10]P. Kapitza, Proc. Roy. Soc. (London), Ser. A 123, 292 (1929).

[11]J. M. Ziman, Principles of the Theory of Solids (Cambridge University Press, Cambridge, England, 1964).

[12]P. A. Penz, Phys. Rev. Letters 20, 725 (1968).

[13]H. Mayer and M. H. El Naby, Z. Physik 280, 289 (1963); H. Mayer and B. Hietel, in Optical Properties and Electronic Structure of Metals and Alloys, edited by F. Abelès (John Wiley & Sons, Inc., New York, 1966).

[14]H. W. B. Skinner, Rept. Progr. Phys. 5, 257 (1938).

[15]The energy states evaluated were Γ for $\vec{k} = (0,0,0)$, and, on the Brillouin-zone boundary, the states X at $\vec{k} = (2\pi/a)(\frac{1}{2},0,0)$, M at $\vec{k} = (2\pi/a)(\frac{1}{2},\frac{1}{2},0)$, and R at $\vec{k} = (2\pi/a)(\frac{1}{2},\frac{1}{2},\frac{1}{2})$. Here a is the cubic-lattice constant (the same for bcc and sc).

[16]A comparable calculation in the HF framework has been carried out [P. M. O'Keefe and W. A. Goddard, Phys. Rev. 180, 747 (1969)] using this Li atomic effective potential. The result was a band spectrum similar to that from previously reported orthogonalized-plane-wave [M. L. Glasser and J. Callaway, Phys. Rev. 109, 1541 (1958)] and model-potential [V. Čápek, Czech. J. Phys. B18, 313 (1968)] calculations.

[17]These numbers are estimated assuming the Fermi surface to be spherical. A more exact determination must await the completion of band calculations throughout the BZ.

[18]D. Shoenberg and P. J. Stiles, Proc. Roy. Soc. (London), Ser. A 28, 62 (1964).

[19]C. C. Grimes and A. F. Kip, Phys. Rev. 132, 1991 (1963).

[20]J. J. Donaghy and A. T. Stewart, Phys. Rev. 164, 391 (1967).

[21]W. C. Phillips and R. J. Weiss, Phys. Rev. 171, 790 (1968).

[22]W. E. Spicer, Phys. Rev. 154, 385 (1967).

[23]L. M. Falicov and P. R. Sievert, Phys. Rev. 138, A88 (1965).

[24]N. F. Mott, Proc. Phys. Soc. (London) A62, 416 (1949).

[25]F. J. Morin, Phys. Rev. Letters 3, 34 (1959).

[26]M. H. Cohen and J. C. Phillips, Phys. Rev. Letters 12, 662 (1964).

[27]A. W. Overhauser, Phys. Rev. Letters 13, 190 (1964); J. R. Reitz and A. W. Overhauser, Phys. Rev. 171, 749 (1968); A. W. Overhauser, Phys. Rev. 167, 691 (1968).